Delft University of Technology

MSc Thesis

Skin friction of Diaphragm Walls

An experimental study based on modified direct-shear tests

Author:
J.S. de Wolf

Supervisors:
Prof. dr. M.A. Hicks
Dr. ir. W. Broere
Dr. ir. C. van der Veen
ir. J.H. van Dalen
ir. R.C. van Dee

November 14, 2016

Skin friction of Diaphragm Walls

An experimental study based on modified direct-shear tests

by

J.S. de Wolf

to obtain the degree of Master of Science
at the Delft University of Technology.

Author:	J.S. de Wolf	
Student number:	4023854	
Project duration:	December, 2015 – November, 2016	
Thesis committee:	Prof. dr. M.A. Hicks,	TU Delft
	Dr. ir. W. Broere,	TU Delft
	Dr. ir. C. van der Veen,	TU Delft
	ir. J.H. van Dalen,	TU Delft, Strukton, DAED Ingenieurs
	ir. R.C. van Dee,	Strukton, DAED Ingenieurs

An electronic version of this thesis is available at `http://repository.tudelft.nl/`.

Preface

This thesis has been performed in collaboration with Strukton and DAED Ingenieurs, to conclude the MSc Geo-Engineering program at the faculty of Civil Engineering & Geo-Sciences of Delft University of Technology. With the upcoming revision of the CUR 231 (Handboek Diepwanden), the need arises for additional experimental research on the external friction angle δ of diaphragm walls to improve current recommendations. This thesis aims to analyse the conservatism in the current CUR 231 recommendations on δ by combining existing knowledge with an experimental investigation.

The experimental phase of this research proved to be very challenging and instructive. Especially the development of the new experimental set-up provided many challenges. However, to eventually getting it all to work and to obtain useful data was a very satisfying experience. During the course of this research I have received much assistance and I would like to thank everyone involved. First of all, I would like to thank ir. J.H. van Dalen, for introducing me to the subject of skin friction of diaphragm walls and for providing me with the experimental set-up he developed. Special thanks go to all other committee members; Prof. dr. M.A. Hicks, dr. ir. C. van der Veen, dr. ir. W. Broere and ir. R.C. van Dee for their guidance and support. Furthermore I would like to express my gratitude towards a number of TU Delft staff and students for their assistance:

- A. Mulder, H. de Visser, J. van den Berg (all Geotechnical Laboratory) and B. Bakker (Electronic and Mechanical Support Division of the TU Delft) for their assistance in the development and manufacturing of the new modified direct-shear set-up;
- J. van Haagen (Geotechnical Laboratory) for her assistance in preparation of the in-situ slurry samples for hydrometer testing;
- M. van Leeuwen (Stevin Laboratory, concrete specialist) for his help and advice in the application of diaphragm wall concrete during my experiments;
- dr. ir. F.J. van Leijen, dr. B. Riveiro and E. Prentice for their kind support in the execution and interpretation of the 3D laser scans of the concrete samples.

In addition, I would like to thank J. Stam from CEBO Holland BV for providing me with the bentonite (Trenchcontrol AT) I applied in my experiments, which also proved to be washed out of clothing quite easily. Finally, I would like to thank my family, friends and especially Elske for her advice and support.

J.S. de Wolf
Delft, November 2016

Soms denk ik uren na en heb ik nog niks op papier,
een andere keer bereik ik precies datzelfde in vijf minuten.
– *Herman Finkers*

Contents

List of Figures

List of Tables

Abstract

This thesis aims to analyse the conservatism in the current Dutch recommendations on the external friction angle δ of diaphragm walls: $\delta = min[\phi, 20°]$ (for curved slip surfaces) (CUR/COB, 2010), by means of an experimental investigation. Based on literature, two sources of conservatism are identified: 1) filter cake contamination by excavated soil particles is not taken into account, which can lead to an increased δ of around 30° (Day et al., 1981; Henry et al., 1998; Arwanitaki et al., 2007); 2) a continuous shear plane through the filter cake is assumed, ignoring the influence of concrete roughness and filter cake thickness. Cernak et al. (1973) and Lam et al. (2014) found that the concrete roughness causes an increased shear strength compared to the filter cake below a certain filtration time (which controls the filter cake thickness). These aspects are captured in a conceptual model (hypothesis), which predicts the development of interface shear strength as a function of filtration time for the case of a contaminated filter cake compared to a clean filter cake: For a contaminated filter cake, the lower boundary shear strength, which is that of the filter cake, is higher compared to that of a clean filter cake. However, this lower boundary is reached after a shorter filtration time for a contaminated filter cake compared to a clean filter cake, caused by the higher filter cake growth rate due to slurry contamination. The first experimental phase focusses on the filter cake shear strength. A series of small-scale direct-shear tests (Ø 67 mm) on sand/filter cake (clean)/cement-mortar samples show a linear trend of peak shear strength of 18,3° for normal pressures in the range of 200 kPa - 400 kPa at a shear rate of 1,2 mm/min. This result corresponds to the friction angle of 19,5° by Deltares (2008), which lies at the basis of the current Dutch δ recommendations. Additional tests on clean filter cakes indicate a peak shear strength around 23° at a shear rate of 0,0072 mm/min. Test series on contaminated filter cakes show an increased linear trend of peak shear strength of 25,6° for normal pressures in the range of 200 kPa - 400 kPa at a shear rate of 1,2 mm/min. The filter cake contamination is based on an analysis of an in-situ slurry sample analysis from the Spoorzone Delft project. Increased friction angles of 28,5° and 32,8° are observed at 0,0072 mm/min shear rate. In the second experimental phase, the influence of filtration time on the interface shear strength for clean and contaminated filter cakes is investigated. In total, 7 direct-shear tests have been performed on sand/filter cake/concrete samples (170 mm x 170 mm), in which a realistic diaphragm wall concrete mix is applied (max. aggregate size 16 mm, class F5). The test results (normal pressure of 200 kPa, shear rate 1,2 mm/min) show a decrease of interface shear strength with increased filtration time for both clean and contaminated filter cake samples and it is shown that for the contaminated case the filter cake shear strength is reached after a shorter filtration time (around 12 hours) compared to clean filter cakes (around 24 hours), confirming the hypothesis. An analysis of the concrete surface textures (based on 3D laser scans) indicates an increased surface roughness with increased filter cake thickness. The obtained concrete surface roughness is comparable to in-situ conditions based on an analysis of in-situ data from the Spoorzone Delft project. In this comparison the influence of macro-roughness patterns is not taken into account. The experimental results of this thesis indicate that the main source of conservatism of the current Dutch recommendations on δ is the omission of the influence of filter cake contamination on the filter cake shear strength. In addition, δ could further be optimised as a function of filtration time. However, the time frame of increased interface shear strength from the filter cake shear strength towards ϕ is limited for contaminated filter cakes (around 12 hours in this research). It is therefore concluded that the recommended δ value(s) can best be based on contaminated filter cake shear strength, omitting the time effect. It is therefore suggested that future research should focus on the lower boundary shear strength for the case of in-situ filter cake samples. For this purpose the developed direct-shear set-up can be applied. It is also suggested to further investigate the influence of macro-roughness patterns, since it can not be excluded that macro-roughness patterns do not cause an extended time frame of increased interface shear strength.

1

Introduction

1.1. Background

For the design of retaining structures, the friction angle between the retaining wall and the surrounding soil is an important parameter. This friction angle, also referred to as the 'external friction angle δ ', together with the internal friction angle of the soil ϕ, influences the magnitude of the passive resistance of the soil. For a conventional retaining structure such as a sheet pile wall, the external friction angle is governed by the friction of the soil/steel interface. However, for a diaphragm wall the interface structure is more complex due to the presence of a 'filter cake' in between the soil and the concrete structure itself. Diaphragm wall construction involves the excavation of individual trenches in one or more cycles, in which a support fluid (most often a bentonite suspension) is applied to provide trench stability. Filtration of this support fluid into the surrounding soil leads to the formation of the filter cake on the excavation face. Figure 1.1 presents the global construction process of a diaphragm wall.

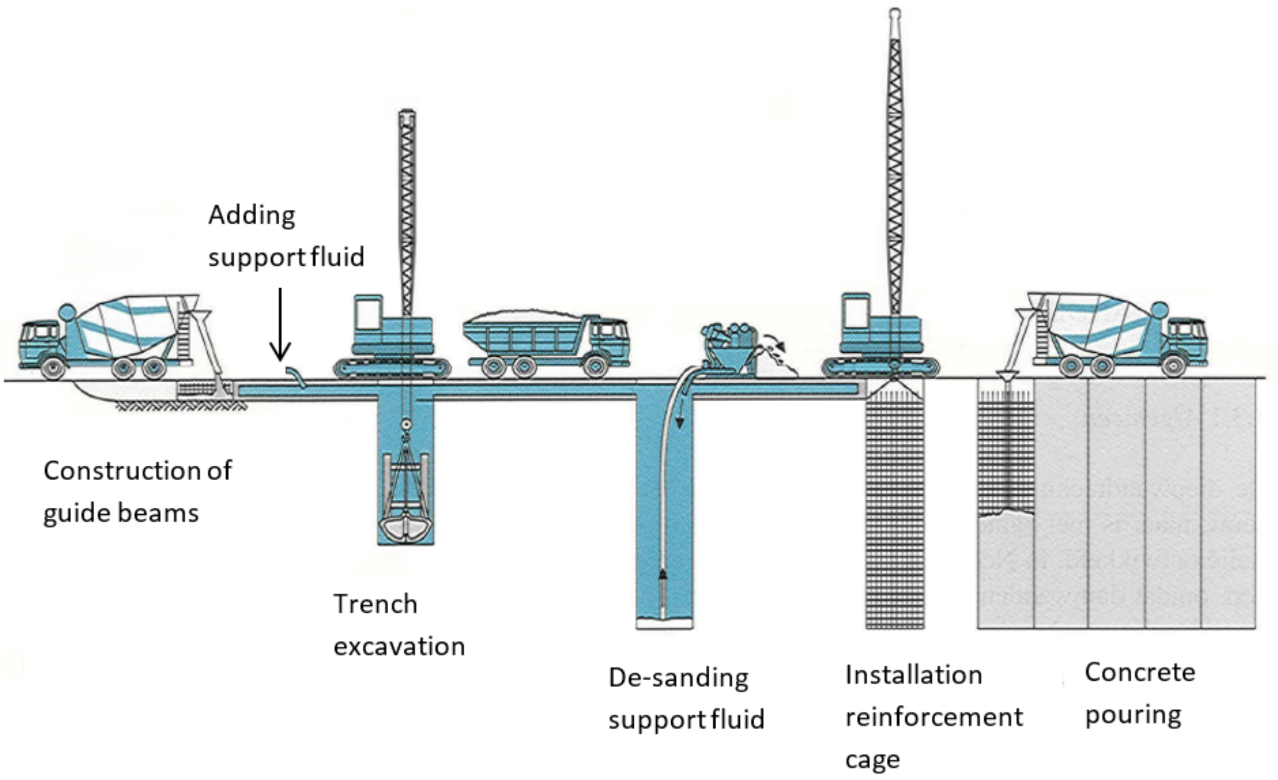

Figure 1.1: Global construction process diaphragm walls (Modified from: COB (1997))

For a conventional sheet pile wall, the CUR 166 presents recommendations for the external friction angle δ:

- For straight slip surfaces: $\delta = min\left[\frac{2}{3}\phi, 20°\right]$
- For curved slip surfaces: $\delta = min\left[\phi - 2.5°, 30°\right]$

In Dutch engineering practice, these values have also been applied in diaphragm wall design, but the suitability of these values is questionable, since the friction interface of a diaphragm wall is more complex compared to a steel sheet pile wall (CUR/COB, 2010). Therefore, the CUR 231 (Handboek Diepwanden) presents recommendations for the external friction angle δ of diaphragm walls, based on laboratory experiments which were performed in the context of the North-South metro line project in Amsterdam (Deltares, 2008):

- For straight slip surfaces: $\delta = min\left[\frac{2}{3}\phi, 13.3°\right]$
- For curved slip surfaces: $\delta = min\left[\phi, 20°\right]$

1.2. Problem description

The CUR 231 recommendations for the external friction angle δ should be interpreted as lower bound values (Deltares, 2008). The underlying experimental research has been performed by Deltares (2008), which has focussed primarily on the bentonite filter cake shear strength, omitting the influence of concrete roughness on the interface shear strength. The influence of the concrete roughness on the interface shear strength is a function of both the maximum concrete aggregate size and the filter cake thickness (Lam et al., 2014). Both parameters are not considered in the current CUR 231 recommendations. In addition, in their analysis of the filter cake shear strength, Deltares (2008) did not take into account the influence of the presence of excavated soil material in the filter cake. These aspects indicate that the current Dutch recommendations are conservative. With the upcoming revision of the CUR 231, further investigation of the external friction angle δ of diaphragm walls is therefore required.

1.3. Methodology

As the title of this thesis suggests, the primary focus of this research is on an experimental investigation on the shear strength of the soil/structure interface of diaphragm walls (most often quantified in the 'external friction angle δ '). The external friction angle describes the interface shear strength as a function of the applied normal stress. Based on the above presented problem description, the main research question of this thesis has been formulated as follows:

How conservative are the current Dutch recommendations on the external friction angle δ of diaphragm walls?

First a literature review is performed to analyse previously performed (experimental) research on the soil/structure interface of diaphragm walls. Based on the conclusions of the literature review the experimental methodology is established. For the literature review, the following research questions have been formulated:

1. What is the influence of the soil/structure interface shear strength on the performance of diaphragm walls?
2. Which factors influence the formation of the soil/structure interface of a diaphragm wall?
3. Which factors influence the shear strength of the soil/structure interface of a diaphragm wall?

The starting point of the experimental research of this thesis is the application of an experimental set-up developed by Van Dalen (2016). This set-up enables performing direct-shear tests on small-scale layered samples (Ø 67 mm), which replicate the soil/structure interface of a diaphragm wall. As part of this research also a large-scale direct-shear set-up (170 mm x 170 mm) is developed to enable the application of a realistic diaphragm wall concrete mixture into the interface samples. The experimental methodology, which is based on the conclusions of the literature review is explained in more detail in a later part.

1.4. Reading Guide

Chapter 2 *Literature Review* presents the investigation of the 3 literature research questions presented in the above, which form the starting point of this thesis. In Chapter 3 *Experimental Methodology*, based on the literature review, the experimental methodology is presented and experimental research questions are formulated. In addition, an overview of the performed tests and parameter configurations is presented. Chapter 4 *Experimental Phase 1: Filter cake shear strength* presents the results of the first experimental phase, which focusses on the filter cake. Chapter 5 *Experimental Phase 2: Development of a modified direct-shear set-up* describes the design process and sample preparation procedure of the newly developed direct-shear set-up. Chapter 6 *Experimental Phase 2: Interface shear strength as a function of filtration time* presents the results of a series of large-scale direct-shear tests performed with the newly developed direct-shear set-up to investigate the influence of the filtration time on the interface shear strength for clean and contaminated filter cakes. Finally, in Chapter 7 *Conclusions and Recommendations* the main research question is answered and recommendations for additional research are presented.

2

Literature Review

This chapter describes the results of a literature study. First the influence of skin friction on diaphragm wall performance is discussed. Next, the formation of the soil/structure interface of a diaphragm wall is discussed. Next, previous experimental research on skin friction of diaphragm walls is discussed. Finally, conclusions are presented, which form the basis for the experimental methodology.

2.1. Influence of skin friction on diaphragm wall performance

The soil retaining function of a structure is its ability to bridge a height difference in ground level (and often water level). This height difference generates active and passive lateral soil pressures. On the active side, the retaining structure deflects away from the soil due to the lateral pressure, while at the passive side, the retaining wall is pushed into the soil. The effective active and passive effective soil pressures, σ'_{hA} and σ'_{hP} are generally expressed as follows (Verruijt and Van Baars, 2009):

$$\sigma'_{hA} = K_a \cdot \sigma'_v - 2 \cdot c \cdot \sqrt{K_a} \tag{2.1}$$

$$\sigma'_{hP} = K_p \cdot \sigma'_v + 2 \cdot c \cdot \sqrt{K_p} \tag{2.2}$$

In equations 2.1 and 2.2, the coefficients K_a and K_p translate the vertical effective pressure σ'_v into an effective lateral soil pressure. Expressions for K_a and K_p are based on the stability of a soil wedge, which is on the point of sliding along a certain slip surface. Figure 2.1 presents the stability of a soil wedge with a straight slip surface for a non-cohesive soil.

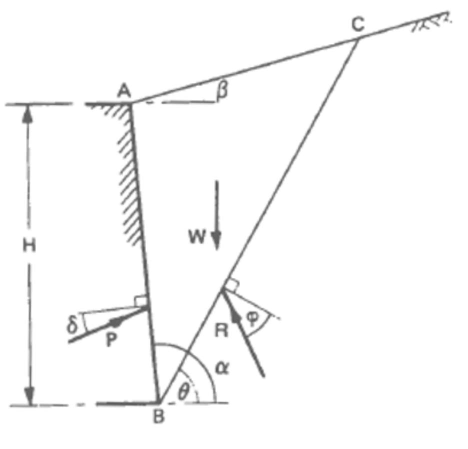

Figure 2.1: Wedge stability for a straight slip surface in non-cohesive soil (Craig, 1997)

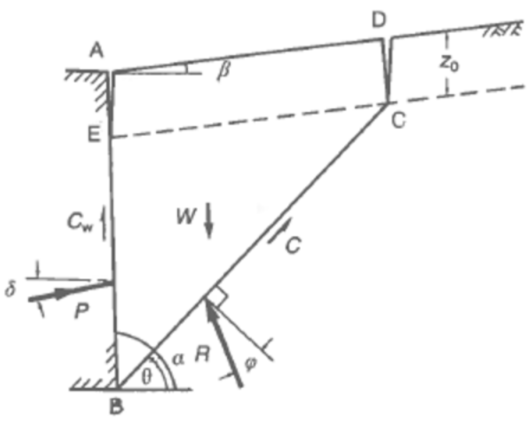

Figure 2.2: Wedge stability for a straight slip surface in cohesive soil (Craig, 1997)

For a cohesive soil, both cohesion c and adhesion c_w contribute to the wedge stability as shown in Figure 2.2. Expressions 2.1 and 2.2 include cohesion, but any influence of adhesion is neglected. The following expressions for σ'_{hA} and σ'_{hP} do take into account adhesion (Craig, 1997):

$$\sigma'_{hA} = K_a \cdot \sigma'_v - K_{ac} \cdot c \tag{2.3}$$

$$with: \; K_{ac} = 2 \cdot \sqrt{\left[K_a\left(1 + \frac{c_w}{c}\right)\right]} \tag{2.4}$$

$$\sigma'_{hP} = K_p \cdot \sigma'_v + K_{pc} \cdot c \tag{2.5}$$

$$with: \; K_{pc} = 2 \cdot \sqrt{\left[K_p\left(1 + \frac{c_w}{c}\right)\right]} \tag{2.6}$$

Various expressions for K_a and K_p exist. For the assumption of straight slip surfaces (Figure 2.1 and Figure 2.2) and a perfectly smooth wall, the following formula has been proposed by Rankine and Coulomb:

$$K_a = \frac{1 - sin(\phi)}{1 + sin(\phi)} \tag{2.7}$$

$$K_p = \frac{1 + sin(\phi)}{1 - sin(\phi)} \tag{2.8}$$

In equations 2.7 and 2.8 the influence of wall friction is not taken into account. In the active case, it is generally assumed that wall friction provides an upward force on the soil wedge, whilst for the passive case this friction force acts downwards. As shown in Figure 2.1 and Figure 2.2, this friction force can be described by both a frictional component (external friction angle δ) and an adhesive component c_w. For straight slip surfaces and $\delta \neq 0$, Coulomb proposed the following expressions for K_a and K_p, also including wall- and ground inclinations α and β:

$$K_a = \frac{\cos^2(\phi + \alpha)}{cos^2(\alpha) \cdot \left[1 + \sqrt{\frac{sin(\phi+\delta) \cdot sin(\phi-\beta)}{cos(\alpha-\delta) \cdot cos(\alpha+\beta)}}\right]^2} \tag{2.9}$$

$$K_p = \frac{\cos^2(\phi - \alpha)}{cos^2(\alpha) \cdot \left[1 - \sqrt{\frac{sin(\phi-\delta) \cdot sin(\phi+\beta)}{cos(\alpha-\delta) \cdot cos(\alpha+\beta)}}\right]^2} \tag{2.10}$$

For a vertical wall and horizontal ground surface ($\alpha = \beta = 0$), expressions 2.9 and 2.10 reduce to the following expressions (Müller-Breslau):

$$K_a = \frac{\cos^2(\phi + \alpha)}{\left(1 + \sqrt{\frac{sin(\phi) \cdot sin(\phi+\delta)}{cos(\delta)}}\right)^2} \tag{2.11}$$

$$K_p = \frac{\cos^2(\phi + \alpha)}{\left(1 - \sqrt{\frac{sin(\phi) \cdot sin(\phi+\delta)}{cos(\delta)}}\right)^2} \tag{2.12}$$

In expressions 2.7 to 2.12 straight slip surfaces are applied. However, with the assumption of straight slip surfaces, for high values of the internal friction angle ϕ, the resulting values of K_p tend to be strong overestimations (Verruijt and Van Baars, 2009). In reality, a straight slip surface might not be the governing slip surface along which failure takes place and a curved slip surface might by more realistic. Craig (1997) states that for both the active- and passive case, skin friction causes a curvature in the slip surface near the bottom of the retaining wall (Figure 2.3). This effect is strongest in the passive case.

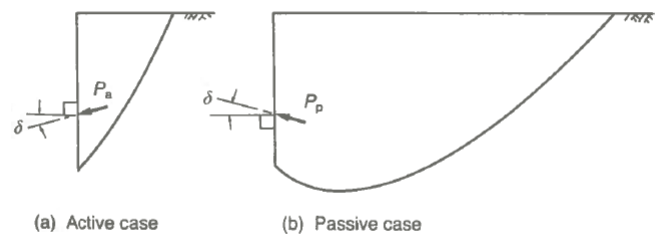

Figure 2.3: Slip surface curvature in the active- and passive case due to skin friction (Craig, 1997)

Various expressions for K_p have been derived for the case of curved slip surfaces. The method proposed by Kötter applies a slip surface consisting of a logarithmic spiral and a straight section. In the resulting expressions, skin friction is incorporated through the external friction angle δ:

$$K_a = \frac{1 - sin(\phi) \cdot sin(2\alpha + \phi)}{1 + sin(\phi)} \cdot exp\left[\left(-\frac{\pi}{2} + \phi + 2\alpha\right) \cdot tan(\phi)\right] \tag{2.13}$$

$$with\,\alpha : cos(2\alpha + \phi - \delta) = \frac{sin(\delta)}{sin(\phi)} \tag{2.14}$$

$$K_p = \frac{1 - sin(\phi) \cdot sin(2\alpha' + \phi)}{1 + sin(\phi)} \cdot exp\left[\left(\frac{\pi}{2} + \phi + 2\alpha'\right) \cdot tan(\phi)\right] \tag{2.15}$$

$$with\,\alpha : cos(2\alpha' - \phi + \delta) = \frac{sin(\delta)}{sin(\phi)} \tag{2.16}$$

Figure 2.4 presents a comparison of K_p expressions, in which the Müller-Breslau and Kötter expressions (2.12 and 2.16 are plotted for a range of ϕ values. As described before, for high ϕ values the application of straight slip surfaces leads to a rapid increase of K_p, which can be observed from Figure 2.4. For both straight- and curved slip surfaces, the influence of δ increases with increasing ϕ.

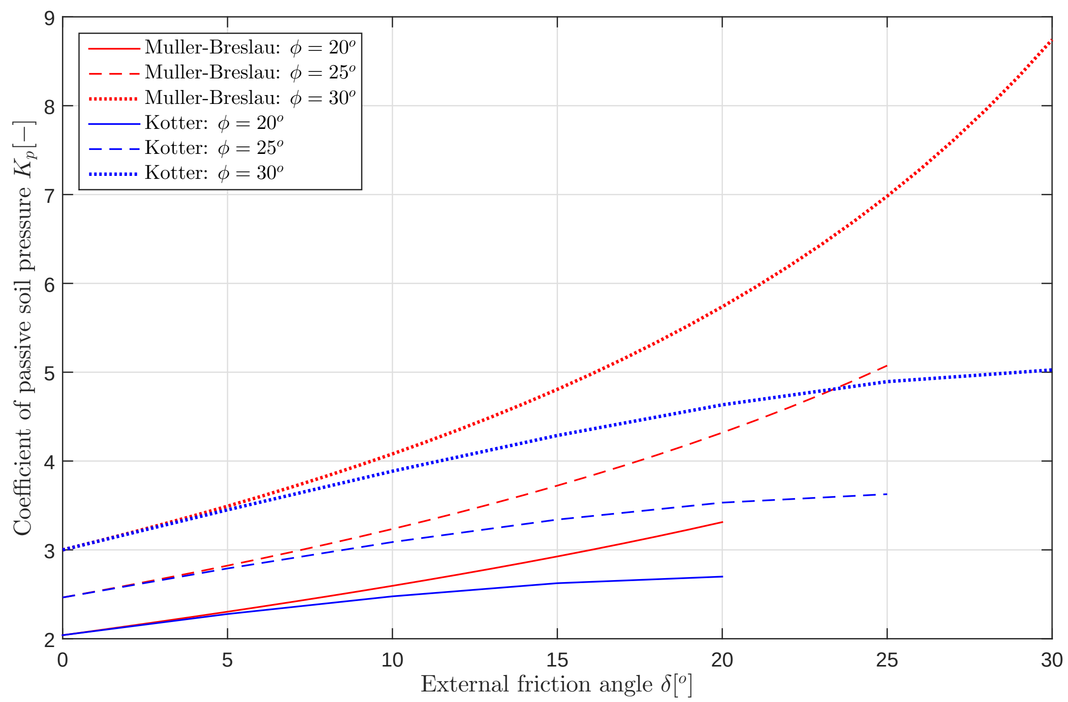

Figure 2.4: Comparison of K_p expressions and the influence of the external friction angle δ for different values of ϕ

As described in the above, the external friction angle δ influences the coefficients of horizontal soil pressure K_a and K_p. In a spring model (such as D-sheet piling), K_a and K_p transform vertical effective pressures into horizontal effective pressures. Therefore, δ influences the horizontal equilibrium situation, which determines the required wall embedment length and strut/anchor forces. However, for a diaphragm wall structure, horizontal equilibrium is not in all cases the governing mechanism for determining the required embedment length. Diaphragm walls are sometimes applied in very deep excavations, in which often an underwater concrete floor is applied, acting as a strut. In such a geometry, horizontal equilibrium is only partially dependent on the embedment length. In diaphragm wall design, the embedment length is often optimized with respect to the distribution of bending moments which governs the design of the wall cross-section. In addition, in some cases the required length of the wall is determined by the vertical bearing capacity. For a diaphragm wall acting as foundation element, skin friction can have a positive or negative contribution to the vertical bearing capacity, depending on the soil type. Buykx et al. (2009) evaluated the vertical equilibrium of a deep building pit of one of the stations of the North-South metro line project in Amsterdam. For the construction of this station, the wall-roof method is applied, in which compressed air is used to prevent an influx of ground water. The self-weight of the structure appeared not to be sufficient to counter the upward force from the compressed air. Including the downward friction resistance along the soil/diaphragm interface in the design did lead to vertical equilibrium. Numerical analyses by Diao and Zheng (2008) show the effect of the external friction angle δ on the deformation performance of a strutted diaphragm wall structure. Results show increased wall deflection (Figure 2.5) and ground surface settlement with decreasing δ (Figure 2.6). In addition, increased wall friction leads to a more uniform ground surface settlement (Diao and Zheng, 2008).

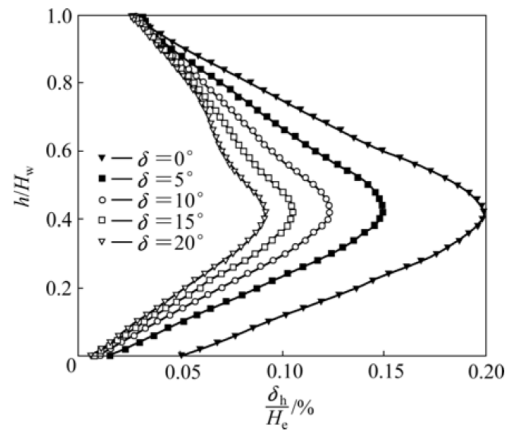

Figure 2.5: Wall deflection for different values of the external friction angle δ (Diao and Zheng, 2008)

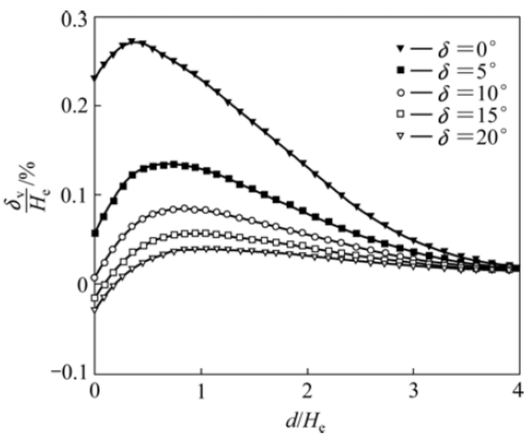

Figure 2.6: Ground surface settlement for different values of the external friction angle δ (Diao and Zheng, 2008)

2.2. Soil/diaphragm wall interface formation

The soil/structure interface of a diaphragm wall interface is a layered system, in which a filter cake is present in between the sand and concrete (Figure 2.7). During trench excavation, this filter cake acts as a membrane on the excavation face, upon which the support fluid exerts its hydrostatic pressure (micro stability) and thereby preventing a soil wedge from sliding into the trench (macro stability).

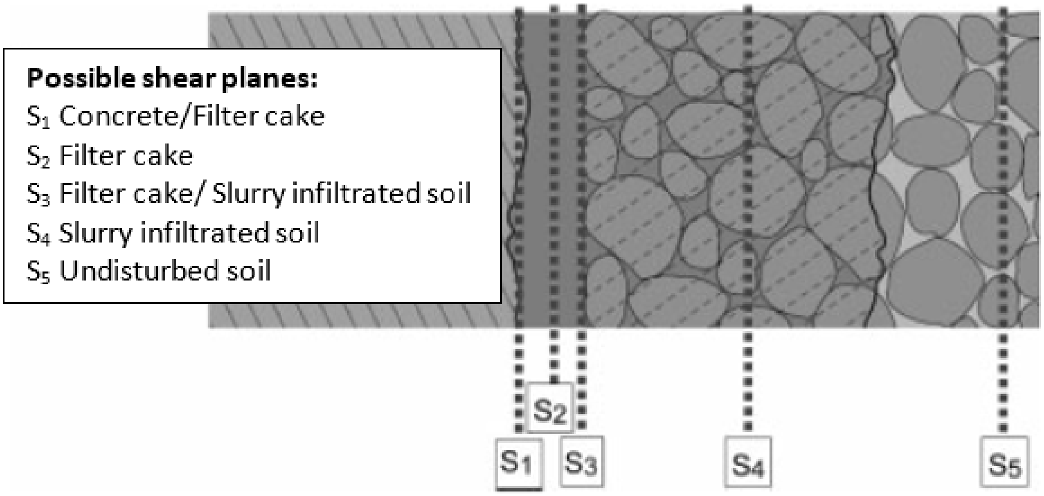

Figure 2.7: Soil/diaphragm wall interface: layered system (Modified from: Arwanitaki et al., 2007)

For cohesive soils, micro stability is not an issue (Van Tol and Everts, 2008) due to the low permeability, which also prevents the formation of a substantial filter cake. For non-cohesive soils, micro stability is an issue and bentonite suspensions can provide stability in different ways, depending on the soil conditions. For non-cohesive soils, the following mechanisms can be identified (Hutchinson et al., 1975):

- Surface filtration
- Deep filtration
- Rheological blocking

The first two mechanisms involve the formation of a filter cake. For surface filtration, this filter cake forms on the excavation face, while for deep filtration the filter cake forms inside the surrounding soil. For rheological blocking, micro stability is provided by the shear resistance generated by the soil skeleton on the support fluid during penetration of the soil. As stated before, the applicable mechanism depends on the soil conditions. For surface filtration, the following soil criteria have been found:

- Walz et al. (1983): $D10 \leq 0,20mm$
- Sherard et al. (1984): $D15 \leq 0,40mm$
- Henry et al. (1998): $D15 \leq 0,34 - 0,43mm$

Van Tol and Everts (2008) state that in Dutch soil conditions the criterion from Walz et al. (1983) is very often satisfied, even in Pleistocene formations ($D10 \leq 0,20mm$). Therefore, in The Netherlands the formation of a filter cake on the excavation face is the expected micro stability mechanism in sand layers. For cohesive soil, the presence of a filter cake is not expected. However, Deltares (2008) reported the presence of a thin filter cake in silty 'Eemclay' at the construction site of one of the stations of the North South metro line in Amsterdam.

2.2.1. Filter cake formation

For filter cake formation, filtration of the support fluid into the soil is required. This filtration process starts with trench excavation, during which the trench is filled with a bentonite suspension. To provide sufficient soil support, the bentonite level is often chosen around 2 meters above the ground water table (CUR/COB, 2010). This height difference is the driving force behind the filtration process.

Fluid filtration (also referred to as 'fluid loss') is highest at the start of filter cake formation. When an intial seal of the voids is achieved, fluid loss decreases and can be expressed by the following equation:

$$q = m \cdot \sqrt{t} \tag{2.17}$$

In which q is the flow rate of fluid loss, m is a constant and t represents time. This development of fluid loss over time is conceptually visualised in Figure 2.8.

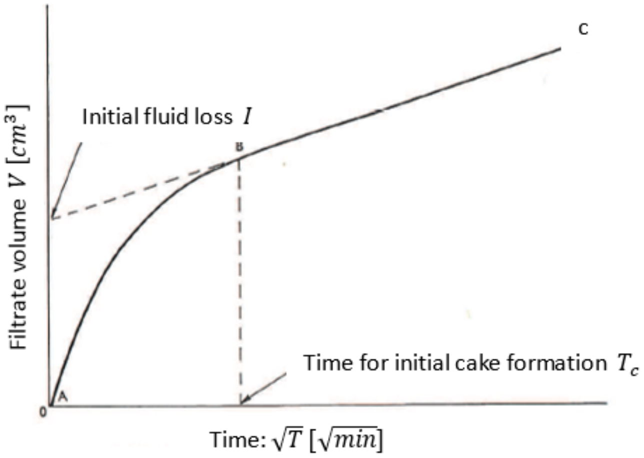

Figure 2.8: Development of fluid loss during filtration process (Modified from: Hutchinson et al., 1975)

The growth of the filter cake on the excavation face, as for the fluid loss, also develops as a function of the square root of time and can be described with the following expression (Nash, 1974):

$$u = \sqrt{\frac{2 \cdot k_c \cdot (1 - n_f) \cdot (\gamma_f \cdot z_1 - \gamma_w \cdot z_2}{(n_f - n_c) \cdot \gamma_w}} \cdot \sqrt{t} \tag{2.18}$$

In which:

- k_c = filter cake permeability [m/s]
- n_c = filter cake porosity [-]
- n_f = support fluid porosity [-]
- γ_f = support fluid unit weight [kN/m^3]
- z_1 = support fluid level [m]
- z_2 = ground water level [m]

The filter cake growth can also be expressed as an empirical factor times the square root of t, similar as expression 2.17:

$$u = n \cdot \sqrt{t} \tag{2.19}$$

Lubach (2010) found values for n ranging from 0,22 $mm/\sqrt{min}$ to 0,24 $mm/\sqrt{min}$ for a clean bentonite suspension with a filtration pressure of 20 kPa. This filtration pressure translates to a height difference of 2 meters between the slurry- and ground water level, which is a common value in Dutch practice (CUR/COB, 2010). Arwanitaki et al. (2007) observed that the filtration pressure does not have a large influence on the filter cake growth (Figure 2.9, bottom 2 lines). This is supported by Wates and Knight (1975), who state that an increase in filtration pressure in turn leads to additional filter cake compaction in the filtration phase. In addition, Tucker and Reese (1984) state that filtration pressure does not have much effect on filter cake formation for high-concentration bentonite slurries. For a filtration pressure of 100 kPa and clean bentonite suspension, test results of Arwanitaki et al. (2007) lead to a filter cake growth rate of $n \approx 0,25mm/\sqrt{min}$.

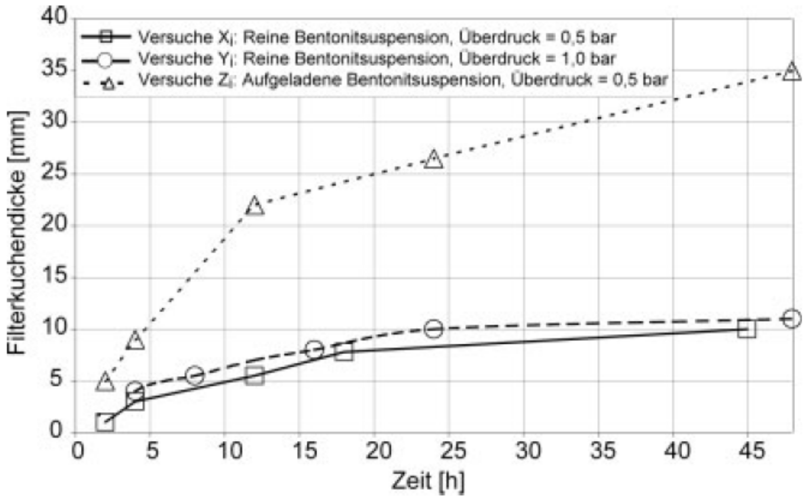

Figure 2.9: Development of filter cake thickness over time (Arwanitaki et al., 2007)

During trench excavation, the bentonite suspension becomes contaminated with excavated soil material. The CUR 231 states that the slurry density can increase to values of around 13,0 kN/m^3, compared to a clean slurry density of around 10,2 kN/m^3. As presented in Figure 1.1, prior to concrete pouring the bentonite suspension is 'de-sanded' to remove the soil material from the suspension. To prevent the formation of weak zones in the final concrete structure (bentonite inclusions), a complete replacement of the bentonite suspension by the concrete mix is desired. The increased viscosity and density of the slurry due to the suspended soil material increase the risk of bentonite inclusions (CUR 231). To reduce the risk of bentonite inclusions, the NEN-EN 1538 presents requirements concerning the slurry density and sand content prior to concrete pouring (11,3 kN/m^3, 4 %). To fulfil these requirements, the support fluid can either be de-sanded or completely replaced by a clean slurry. Slurry replacement requires the most bentonite, but leads the most favourable slurry properties (CUR/COB, 2010).

Undisturbed filter cake growth takes place in the period between excavation completion and the start of concrete pouring. Depending on the moment of de-sanding/replacement of the slurry, the undisturbed filter cake growth mainly involves filtration of the contaminated slurry. Therefore, the suspended soil material will be involved in the filtration process. Arwanitaki et al. (2007) analysed an in-situ sample of the filter cake present in the soil-/diaphragm wall interface at a construction project in Rotterdam. They showed that the filter cake holds a considerable amount of excavated soil material, which indicates that the suspended soil particles in the slurry take part in the filtration process. In addition, Arwanitaki et al. (2007) showed that these suspended soil particles cause a large increase of the filter cake growth rate (Figure 2.9, top line, $n > 0,6mm/\sqrt{min}$). In addition, Filz et al. (1997) state that slurry contamination enables filter cake formation in courser soils.

2.2.2. Filter cake/concrete interaction

Filter cake formation is stopped when the fluid bentonite is displaced by the rising concrete. In the past, there was doubt whether or not the filter cake 'survives' the concrete pouring phase. The rising concrete generates a scouring action on the filter cake and the filter cake might be chemically eliminated by the cement (Van Weele, 1981). However, the presence of a filter cake after concrete pouring has been observed and reported by Wates and Knight (1975) and Deltares (2008). In addition, Van Dalen (2016) numerically analysed the concrete pouring process in a diaphragm wall trench and found that a filter cake will stay in place for relatively low shear strengths. Although the filter cake is not removed by the rising concrete, the horizontal concrete pressure causes filter cake consolidation. In addition, some chemical interaction between the cement and the filter cake might take place.

Filter Cake Consolidation
When concrete is poured into the diaphragm wall trench, it exerts a horizontal load onto the excavation face, which acts as form work. As described in the above, the rising concrete does not remove the filter cake from the excavation face. Therefore, the horizontal load from the fluid concrete acts on the filter cake during concrete curing, causing filter cake consolidation. Wates and Knight (1975) observed a decreasing filter cake thickness with increasing depth (bored piles), which they attributed to this filter cake consolidation.

In general, the lateral pressure exerted by curing concrete (form work pressure) is less than the hydrostatic concrete pressure. During the curing process, the fresh concrete builds up shearing capacity, which reduces the lateral pressure to a value lower than hydrostatic. The lateral concrete pressure is therefore, amongst other factors, a function of the concrete pouring rate. In the CIRIA 108 calculation method, the maximum lateral concrete pressure P_{max} is expressed as follows :

$$P_{max} = \gamma_c \cdot \left[C_1\sqrt{v_c} + C_2 \cdot K\sqrt{H - C_1\sqrt{v_c}} \right] \ngtr \gamma_c \cdot h \tag{2.20}$$

$$with: \; K = \left(\frac{36}{T+16} \right)^2 \tag{2.21}$$

In which:

- γ = unit weight of concrete [kN/m^3]
- C_1 = shape coefficient [-] (for walls: $C_1 = 1.0$)
- C_2 = concrete material coefficient [-] (generally: $C_2 = 0.45$)
- v_c = concrete pouring rate [m/h]
- H = vertical form work height [m]
- h = height of fresh concrete above considered point [m]
- T = concrete temperature [°]

Lings et al. (1994) present a simplified bi-linear profile for the horizontal concrete pressure in a diaphragm wall trench. Down to a certain critical depth, the full hydrostatic concrete pressure is valid. However, from this critical depth downward, the pressure envelope follows the hydrostatic pressure from the support fluid. Based on in-situ measurements, Lings et al. (1994) recommend a critical depth h_{crit} of one third of the total panel depth. The bi-linear profile is described with the following expression:

$$P_{max} = \begin{cases} \gamma_c \cdot z, & z \leq h_{crit} \\ \gamma_b \cdot z + (\gamma_c - \gamma_b) \cdot h_{crit}, & z > h_{crit} \end{cases} \tag{2.22}$$

In which:

- γ_c = unit weight of concrete [kN/m^3]
- γ_b = unit weight of bentonite [kN/m^3]
- z = considered depth in panel [m]
- h_{crit} = critical depth [m] ($\frac{1}{3} \cdot H$)

- H = wall depth [m]

According to Van Weele (1981), for the design of diaphragm walls the average horizontal concrete pressure can be assumed to be 70 % of the hydrostatic concrete pressure. In addition, Van Weele (1981) states that in sand layers the horizontal concrete pressure (70 % of the hydrostatic concrete pressure) will remain after concrete curing and acts on the final structure. Figure 2.10 shows a comparison of the mentioned calculation methods of lateral concrete pressure as a function of depth for a wall depth of 30 meters after completion of pouring.

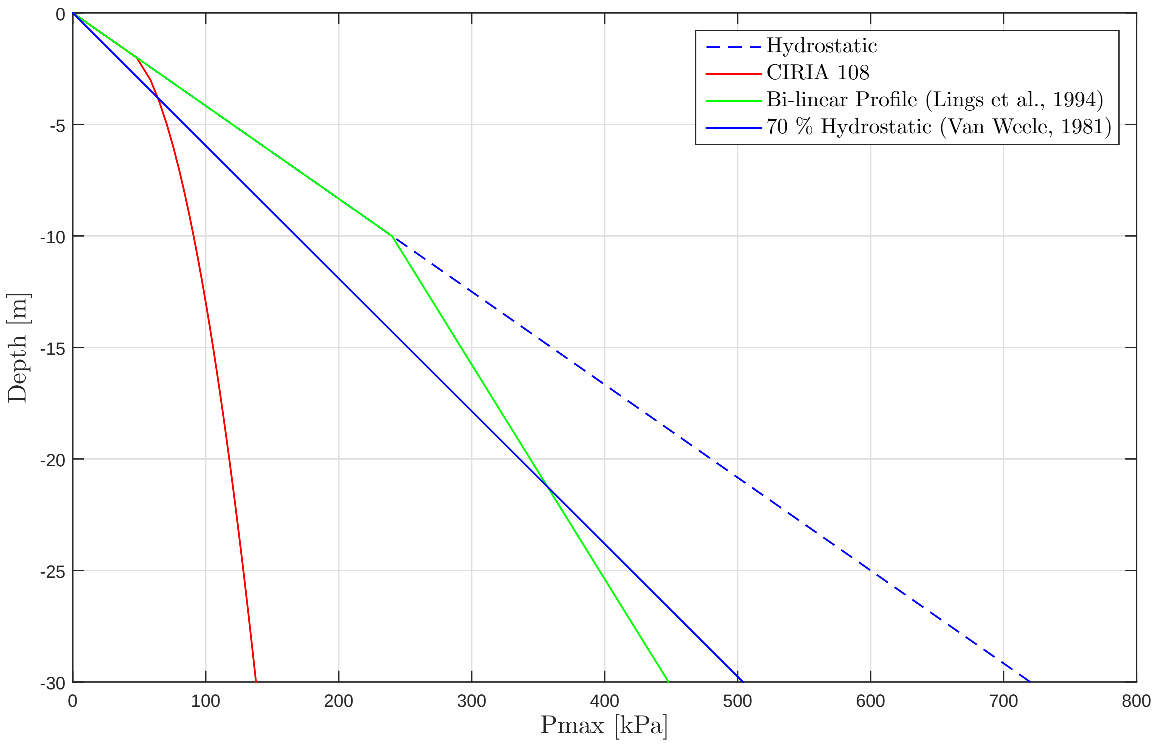

Figure 2.10: Comparison of calculation methods for lateral concrete pressures for a maximum wall depth of 30 m

Chemical interaction

In literature, different views exist on the chemical interaction between the bentonite filter cake and cement. Van Weele (1981) states that the calcium from the cement fully neutralizes the water-binding ability of the bentonite filter cake, which in time will therefore be eliminated. However, as described before, the presence of the filter cake in the final structure has been observed and reported by Wates and Knight (1975) and Deltares (2008). A full chemical elimination of the bentonite filter cake as reported by Van Weele (1981) therefore seems not realistic. The CUR 231 (CUR/COB, 2010) states that Ca^{+} ions from the cement affect the bentonite filter cake, which in addition mixes with hydration products from the concrete. However, Arwanitaki et al. (2007) did not observe any infiltration of cement particles into the bentonite filter cake. Influence on the shear strength of the bentonite filter cake was also not observed. This is supported by Cernak et al. (1973), who did not observe any chemical strengthening of the bentonite filter cake in the presence of hydrating cement.

2.3. Interface shear strength: previous research

Much research has been performed on the effect of bentonite filter cake on the shear strength of the soil-/structure interface. This research has been carried out in the context of both bored piles and diaphragm walls. Lam et al. (2014) present a comprehensive overview of experimental research on this subject. Different experimental approaches have been used in previous research, with different levels of scale. The general conclusion in previous research is that the presence of a filter cake in the soil-/structure interface reduces the interface shear strength (Lam et al., 2014). The effect of the bentonite filter cake has been quantified by different methods. For instance, load tests on (model) piles by Wates and Knight (1975), Thasnanipan et al. (1998) and Hamparuthi and Kumar (2011) show a decreased pile capacity due to the presence of bentonite filter cake. To quantify the effect of bentonite filter cake on the 'external friction angle' δ, different authors have performed (modified) direct-shear tests on interface samples. The direct-shear method is most suited for the determination of δ, since it allows for the modelling of the material around a prescribed interface (Lam et al., 2014).

As presented in Figure 2.7, the soil-/diaphragm wall interface is a layered system. Arwanitaki et al. (2007) showed that for a construction site in Rotterdam, the following 4 shear planes are relevant:

- Interface concrete/filter cake;
- Filter cake;
- Interface filter cake/sand (water saturated);
- Sand (water saturated).

The above mentioned layering is valid for cases with surface filtration as micro stability mechanism (negligible slurry infiltration of the soil), which is almost always the case for Dutch soil conditions (Van Tol and Everts, 2008). For coarser soil conditions, deep filtration or rheological blocking provide micro stability. Both mechanisms require slurry infiltration of the soil. In such cases, the slurry infiltrated zone is an additional layer in the interface system. Müller-Kirchbauer (1972) showed a friction angle decrease of 5° due to slurry infiltration in gravel.

In previous research, for the case of (modified) direct-shear tests, the above mentioned layering has been modelled in different sample configurations, using the direct-shear method. First of all, both in-situ and laboratory-made samples have been modelled. In literature, the following 4 sample configurations have been identified:

1. In-situ Filter Cake;
2. Laboratory: Isolated Clean Filter Cake: **IFC**;
3. Laboratory: Sand/Filter Cake/Cement Mortar (small/absent aggregates): **S/FC/MOR**;
4. Laboratory: Sand/Filter Cake/Concrete (aggregates present): **S/FC/CON**.

The shear strength of a layered interface system is governed by the shear strength of the weakest layer. For the case of the soil-/diaphragm wall interface, the filter cake shear strength is governing if a continuous shear plane through the filter cake is assumed. Most of the previous research has focussed on the filter cake shear strength, which is a lower boundary shear strength of the system. However, with the assumption of a continuous shear plane through the filter cake, the influence of the concrete roughness is ignored. Lam et al. (2014) identified the phenomenon of 'aggregate protrusion', in which individual concrete aggregates protrude through the filter cake, making direct contact with the sand. The degree of aggregate protrusion is a function of the maximum aggregate size in the concrete mix and the filter cake thickness (Lam et al., 2014). Of the above mentioned sample configurations, the in-situ, IFC and S/FC/MOR configurations model a continuous shear plane through the filter cake. In the next section, previous research on the filter cake shear strength is discussed first. Next, previous research on the influence of concrete roughness is analysed.

2.3.1. Direct-shear test principle

The direct-shear test involves the shearing of two shear boxes along a predefined shear plane under a certain normal load *N* (Figure 2.11). The shear force *T* is recorded during shearing. According to Coulomb, the shear strength can be expressed according to expression 2.26 for a direct-shear test (Verruijt and Van Baars, 2009):

$$\tau_f = c + \sigma_n \cdot tan(\delta) \tag{2.23}$$

$$with: \ \tau_f = \frac{T_f}{A} \tag{2.24}$$

$$and: \ \sigma_n = \frac{N}{A} \tag{2.25}$$

$$and: \ \delta = \phi \tag{2.26}$$

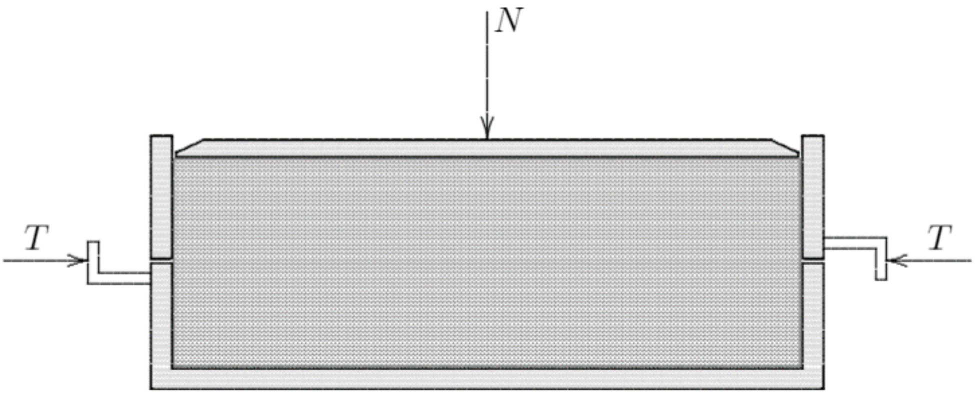

Figure 2.11: Principle of direct-shear (Verruijt, 2012)

As stated in the above, the direct-shear method is most suited to analyse the shear strength of the soil/structure interfaces, since it allows the modelling of the material adjacent to a certain plane. However, there are some objections to the direct-shear method in general. First of all, δ in Equation 2.26 is only based on the normal stress σ_n (vertical). In the direct-shear test, the horizontal stress σ_h is unknown. Since σ_h is unknown, it is not certain whether or not a horizontal plane is governing, as assumed in Equation 2.26. For the condition of $\sigma_n > \sigma_h$, it is likely that the critical stress state is reached first on a vertical plane (Verruijt, 2012), creating a 'bookrow' mechanism (Figure 2.12). Horizontal planes should be governing if $\sigma_h > \sigma_n$ (Figure 2.13). The uncertainty of σ_h leads to a general higher variability in direct-shear test results compared to triaxial tests (Verruijt, 2012).

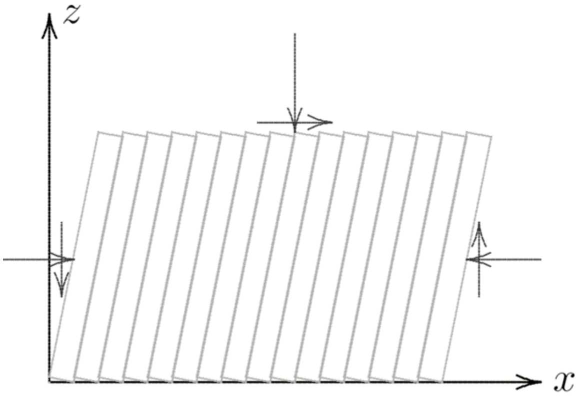

Figure 2.12: Direct-shear failure mechanism: vertical slices ($\sigma_n > \sigma_h$) (modified from: Verruijt (2012))

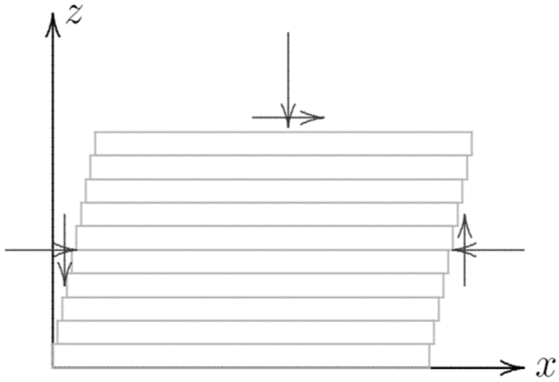

Figure 2.13: Direct-shear failure mechanism: horizontal slices ($\sigma_h > \sigma_n$) (modified from: Verruijt (2012))

2.3.2. Lower boundary shear strength: filter cake

In-situ filter cake samples

The shear strength of in-situ filter cake samples has been analysed by Arwanitaki et al. (2007) and Deltares (2008). The results of these analyses are summarized in Table 2.1. Arwanitaki et al. (2007) obtained filter cake samples from a construction project in Rotterdam and analysed the particle size distribution. The in-situ particle size distribution was replicated in laboratory filter cake samples. Triaxial tests and direct-shear tests on these remoulded filter cake samples showed friction angles around 29°. Deltares (2008) retrieved filter cake samples from the construction site of the North/South metro line project in Amsterdam. Both in the Pleistocene sand and Silty-'Eem' clay, filter cakes were observed and sampled. As described before, in general the formation of a filter cake in cohesive soils is not expected, due to low permeabilities. As expected, Deltares (2008) reported only a thin filter cake (less than 1 mm) in the Silty-'Eemclay'.

Table 2.1: Summary of friction angles of in-situ filter cake samples

Research	Description	Test method	Friction angle [°]
Deltares (2008)	Sand/filter cake	Direct-shear test*	22,5
	Silty-'Eemclay'/filter cake	Direct-shear test*	33,3
Arwanitaki et al. (2007)	Remoulded filter cake	Triaxial test (CU)	28,6
		Direct-shear test (CD)	30,7

**: Consolidation/drainage conditions not specified*

Deltares (2008) took vertical samples of the soil adjacent from the diaphragm wall, thereby including any present filter cake. For the purpose of performing direct-shear tests, horizontal samples were obtained from the vertical samples. The tested samples therefore consisted of 2 layers; filter cake and soil. Deltares (2008) report that multiple direct-shear tests have been performed on the sand/filter cake samples. The obtained shear strength was greatly influenced by the location of the shear plane. Samples with the shear plane (partially) located in the sand resulted in higher friction angles (Deltares, 2008). The lowest shear strength was observed in the sample with the shear plane completely located in the filter cake (22,5°). For the Silty-'Eemclay' samples, Deltares (2008) did not report the location of the shear plane with respect to the filter cake. It is likely that the filter cake thickness was not sufficient for the formation of a continuous shear plane through the filter cake. Therefore, it is concluded that from the Deltares (2008) results only the friction angle of the sand/filter cake sample represents the filter cake shear strength (Table 2.1). The shear strength observed by Arwanitaki et al. (2007) is significantly higher compared to Deltares (2008). This deviation might be caused by differences in consolidation/drainage conditions, which were not specified for the Deltares (2008) results. However, Deltares (2008) did report compaction during shearing, which indicates the dissipation of pore water pressures during shearing, indicating at least partially drained conditions. Both Arwanitaki et al. (2007) and Deltares (2008) performed tests on laboratory filter cake samples, which are discussed in later parts. Finally, Day et al. (1981) reported an in-situ filter cake friction angle of 34°, which they back-calculated from a full scale load test. As cited in Day et al. (1981), Scott (1978) observed in-situ filter cake friction angles ranging from 21° to 38°.

Isolated clean filter cake samples (IFC)

Literature results of shear strength of clean laboratory-made filter cake samples are presented in Table 2.2. A 'clean' filter cake refers to a filter cake only consisting of bentonite and water, unlike the previously discussed in-situ filter cakes which also hold a certain concentration of soil material. The filter cake shear strength values of isolated clean filter cakes found by Arwanitaki et al. (2007) and Cernak et al. (1973) show good comparison, showing friction angles around 14°. However, Lam et al. (2014) found considerably lower filter cake shear strength. It should be noted that the consolidation and drainage conditions of the test results presented in Table 2.2 have not all been specified. Possibly, the relatively low friction angle found by Lam et al. (2014) is explained by undrained conditions. Lam et al. (2014) performed direct-shear tests on S/FC/MOR and S/FC/CON samples with a shear-rate of 2mm/min. These test results are mentioned in later parts. If the same, high shear-rate has also been applied on the isolated filter cake material, the found friction angle relates to undrained conditions. In addition, Lam et al. (2014) applied a modified direct-shear apparatus for the S/FC/MOR and S/FC/CON tests. In between the shear boxes, a 2cm spacing was present. The presence of this spacing leads to a reduction of confining pressure at the shear plane, which might also cause the apparent reduction in shear strength. When comparing the shear strength results by Arwanitaki et al. (2007) for the remoulded filter cake (Table 2.1) and the clean filter cake (Table 2.2), the presence of soil particles in the filter cake seems to cause a significant increase of shear strength (from around 14° to around 29°).

Table 2.2: IFC test results (clean, isolated filter cakes)

Research	**Test method**	**Friction angle** [°]
Lam et al. (2014)	Direct-shear test*	6
Arwanitaki et al. (2007)	Direct-shear test* / Triaxial test*	11 - 15
Cernak et al. (1973)	Direct-shear test (CD)	14
**: Consolidation/drainage conditions not specified*		

Sand/Filter Cake/Mortar samples (S/FC/MOR)
The previously discussed sample configurations have been tested both in direct-shear and triaxial tests. However, for the analysis of layered interface samples the direct-shear test is the preferred method, since it allows the modelling of the material along a certain interface (Lam et al., 2014). In the Sand/Filter Cake/Mortar configuration the concrete from the diaphragm wall panel is modelled by a cement mortar. Contrary to actual concrete, a cement-mortar does not hold large aggregates. Table 2.3 presents an overview of shear strength results of (modified) direct-shear tests on S/FC/MOR samples by different authors.

Table 2.3: S/FC/MOR test results

Research	**Filter cake composition**	**Filter cake thickness** [mm]	**Friction angle** [°]
Lam et al. (2014)	Clean filter cake	3,4 (After consolidation)	7,9
Deltares (2008)	Clean filter cake	25 (Before consolidation)	19,5
Arwanitaki et al. (2007)	Clean filter cake	1 – 8 (After consolidation)	22,9
Henry et al. (1998)	Clean filter cake Contaminated filter cake	4 (Before consolidation) 4 (Before consolidation)	14 – 20 31 – 33
Wates and Knight (1975)	Not specified	Not specified	7 (c' = 50 kPa)
**:Henry et al. (1998) applied soil-bentonite instead of cement mortar*			

Compared to the isolated filter cake tests, with a S/FC/MOR sample configuration some layer-interaction is modelled. For a S/FC/MOR configuration, the following interaction processes are identified:

- Filter cake consolidation by cement curing pressure;
- Chemical strengthening of the filter cake due to hydration process of the cement;
- Discontinuity in filter cake due to varying filter cake thickness and uneven cement mortar surface.

As described in a previous part, the lateral concrete pressure in a diaphragm wall trench acts on the filter cake, causing filter cake consolidation. This consolidation pressure increases with depth. However, filter cake consolidation can also be taken into account in regular direct-shear or triaxial tests by including a consolidation stage prior to shearing. Concerning the chemical interaction between filter cake and hydrating cement, different views exist in literature. Cernak et al. (1973) and Arwanitaki et al. (2007) state that a bentonite filter cake does not experience chemical strengthening in the presence of hydrating cement. The CUR231 states that on the contact interface of bentonite slurry and concrete a bentonite cake is formed, which is the result of a reaction between the bentonite slurry and Ca+ ions. In addition, this cake is mixed with hydration products of the concrete (CUR/COB, 2010).

For the presented S/FC/MOR tests (Table 2.3) all authors, with exception of Wates and Knight (1975), report the applied filter cake thickness. Depending on the cement-mortar surface roughness and the filter cake thickness, the possibility of discontinuities in the filter cake layer increases. Lam et al. (2014) refer to this process as 'aggregate protrusion', in which individual concrete aggregates penetrate the filter cake, making direct contact with the sand layer. However, it is assumed that in the S/FC/MOR sample configuration a continuous filter cake layer is modelled. In fact, the S/FC/MOR test performed by Lam et al. (2014) served as a reference test for their S/FC/CON tests to quantify the effect of aggregate protrusion. These results will be discussed in a later part. Lam et al. (2014) state that the phenomenon of aggregate protrusion is a function of filter cake thickness and maximum aggregate size in the concrete. However, the method of mortar/concrete placement will also influence the 'integrity' of the filter cake layer. Lam et al. (2014) very gently placed their mortar (S/FC/MOR test) and concrete (S/FC/CON tests) to minimize the disturbance of the filter cake. Deltares (2008) and Henry et al. (1998) also report their efforts not to cause disturbance of the filter cake due to placement of their cement-mortar. It should be noted that Henry et al. (1998) applied soil-bentonite instead of cement-mortar. Wates and Knight (1975) did not specify the method of cement-mortar placement. As described before, in diaphragm wall construction the concrete is poured in the trench starting at the bottom, thereby vertically displacing the bentonite slurry. As described before, observations by Wates and Knight (1975) and Deltares (2008) showed that the filter cake is not displaced (at least not completely) in this process. These observations are supported by numerical analyses by Van Dalen (2016). Arwanitaki et al. (2007) included the concrete pouring process in their sample preparation, in which cement-mortar was injected at the bottom of their vertically placed shear boxes, thereby displacing the fluid bentonite slurry. This placement method lead to an uneven filter cake surface, leading to a filter cake thickness of 1 mm near the injection point, upto 8 mm around the slurry outlet (Table 2.3). Although the cement-mortar placement lead to an uneven filter cake surface, Arwanitaki et al. (2007) did not report discontinuities in the filter cake layer. In fact, Arwanitaki et al. (2007) analysed the location of the shear plane and observed a continuous shear plane through the filter cake.

The shear strength results presented in Table 2.3 are assumed to be the result of continuous shear planes through the filter cake, thereby representing filter cake shear strength. As for the shear strength of isolated filter cakes (Table 2.2), Lam et al. (2014) show a low friction angle compared to the other authors. As stated before, it is assumed that the shear box geometry (spacing of 20 mm in between shear boxes) is the main cause of this relatively low shear strength due to the absence of confinement at the shear plane. Wates and Knight (1975) also show a relatively low friction angle, together with an effective cohesion of 50 kPa. However, in general the friction angle of S/FC/MOR samples with clean filter cake (around 20°) seem to be higher than the isolated clean filter cake samples (around 14°). It is concluded that this shear strength increase is mainly caused by the reduced filter cake thickness, since Cernak et al. (1973) and Arwanitaki et al. (2007) showed no chemical strengthening of the filter cake occurs in the presence of hydrating cement. A lower filter cake thickness causes an increase in shear strength in 2 ways for a continuous shear plane through the filter cake:

- The drainage path of the filter cake layer is shorter, thereby allowing a faster dissipation of excess pore water pressures during shearing;
- The shear stress along the sand/filter cake and filter cake/cement-mortar interfaces (bottom and top boundaries of the filter cake) cause zones of increased horizontal stress in the filter cake. A lower filter cake thickness causes increased overlapping of these zones.

Henry et al. (1998) performed S/FC/MOR tests on both clean and contaminated filter cakes. The presence of soil particles in the filter cake leads to a friction angle increase from 14°-20° upto 31°-33°. This 'contaminated shear strength' is in accordance with the shear strength for an in-situ filter cake observed by Arwanitaki et al. (2007) and Day et al. (1981).

2.3.3. Influence of concrete roughness

When considering the layered interface system as presented in Figure 2.7, the filter cake is a continuous layer, which has been modelled in S/FC/MOR sample configurations (see previous part). Arwanitaki et al. (2007) measured the concrete roughness of a diaphragm wall panel at a construction site in Rotterdam. The shear strength of a rough surface with a granular material is a function of the surface roughness and particle size of the granular material. This is expressed in the normalized roughness R_n, which is a function of the maximum concrete roughness R_{max} and the mean grain size D_{50} (Kishida and Uesugi, 1986):

$$R_n = R_{max}/D_{50} \tag{2.27}$$

Arwanitaki et al. (2007) found a normalized roughness $R_n > 1$ for the analysed concrete surface and adjacent filter cake. Paikowsky et al. (1995) showed that for $R_n > 0,5$, the transfer of shear forces takes place through the granular material, independent on the roughness of the surface. Therefore, Arwanitaki et al. (2007) state that the concrete/filter cake interface is not governing, since the interface shear strength is equal to the filter cake itself. This conclusion is only valid for a continuous filter cake layer. Lam et al. (2014) studied the phenomenon of 'aggregate protrusion'. With aggregate protrusion, individual concrete aggregates penetrate the filter cake, making direct contact with the sand layer. The degree of aggregate protrusion is a function of both the maximum aggregate size in the concrete mix and the filter cake thickness (Lam et al., 2014). Cernak et al. (1973) and Lam et al. (2014) showed a decreasing interface shear strength with increasing filter cake thickness. On the other hand, Shakir and Zhu (2010) showed an increase of the shear strength of sand/concrete interface samples in the presence of bentonite slurry (applied with a spatula, 1-2 mm thickness) for different concrete surface textures. However, since bentonite slurry is applied in stead of a filter cake and the slurry layer thickness has not been varied, the results by Shakir and Zhu (2010) are less suitable to assess the phenomenon of aggregate protrusion. An overview of experimental results by Cernak et al. (1973) and Lam et al. (2014) is presented in Table 2.4. Lam et al. (2014) only reported shear strength values (kPa). To be able to compare results, these values have been translated into friction angles based on the applied normal pressure (360 kPa), omitting cohesion.

Table 2.4: S/FC/CON test results

Research	**Filtration pressure** [kPa]	**Filtration time** [hours]	**Normal pressure** [kPa]	**Friction angle** [°]
Lam et al. (2014)	230	0 0,5 3 7,5 12 24	360	30,3 27,8 17,7 16,3 12,5 6,3
Cernak et al. (1973)	25	0 18 168	100	33 33 14

Lam et al. (2014) and Cernak et al. (1973) found that a decrease of the interface shear strength in the presence of a bentonite filter only takes place from some value of filter cake thickness. Cernak et al. (1973) found that after 18 hours of filtration time the interface shear strength did not yet show a decrease, whilst Lam et al. (2014) found that the shear strength reduction starts after a filtration time of 0,5 hours. It should be noted that Lam et al. (2014) applied a filtration pressure of 230 kPa, which is expected to result in a high filter cake growth rate compared to Cernak et al. (1973), who applied a filtration pressure of 25 kPa. Lam et al. (2014) found that the decrease of interface shear strength only starts when less than half of the interface surface shows direct contact between concrete and sand ($r \leq 0,5$). In other words, the shear strength of the sand is still mobilized, even when in half of the considered surface area the filter cake separates the sand and concrete. Cernak et al. (1973) also suggest that the 'delayed' decrease of interface shear strength is caused by the concrete roughness, but they did not study this phenomenon in more detail.

Both Lam et al. (2014) and Lam et al. (2014) found that with increasing filter cake thickness, eventually the shear strength of the filter cake is reached, which forms the lower boundary of the interface shear strength. Cernak et al. (1973) found that the interface shear strength is reduced to the filter cake shear strength after 168 hours of filtration time. It should be noted that no tests were performed for filtration times in between 18 hours and 168 hours. Therefore, the filter cake shear strength could have been reached earlier than 168 hours. Lam et al. (2014) found that the filter cake shear strength is reached after 24 hours. As stated before, Lam et al. (2014) applied a much higher filtration pressure which probably caused a higher filter cake growth rate. As stated before, the filter cake shear strength found by Lam et al. (2014) is considerably lower compared to other authors, which is most probably caused by the application of a large spacing between the shear boxes (20 mm). As stated before, the Dutch CUR 231 does not include the filtration time in the recommendations on δ. However, the German DIN 4126 does include this time effect, stating that for sand- and gravel soils, δ should be reduced to 0 for filtration times exceeding 30 hours.

Figure 2.14 provides a conceptual presentation of the experimental results by Cernak et al. (1973) and Lam et al. (2014). On the vertical axis the interface reduction factor δ/ϕ is plotted. On the horizontal axis filtration time is plotted (most authors report the applied filtration time rather than the subsequent filter cake thickness). Filter cake shear strength results from previous research, which can be interpreted as lower boundary shear strength of the interface system, are added on the right hand side of Figure 2.14. The dotted boxes show that for contaminated filter cakes higher shear strengths have been found in previous research compared to clean filter cakes. For both categories the range of friction angles is quite large, however the increased filter cake shear strength by contamination of soil particles is evident. It should be noted that the vertical positioning of the different filter cake shear strength results is not scaled.

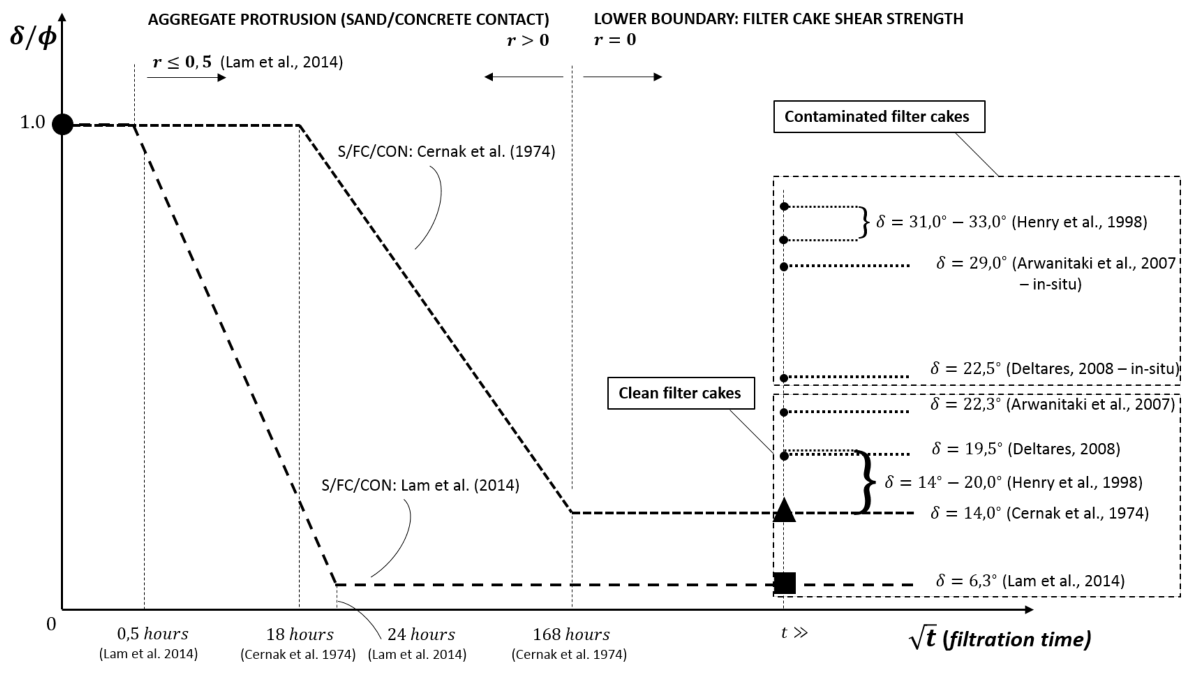

Figure 2.14: Overview of Literature results: δ/ϕ as a function of filtration time (not on scale)

2.4. Conceptual model of interface shear strength development

The development of interface shear strength with increasing filtration time has only been investigated for the case of clean filter cakes. For the case of contaminated filter cakes, only the lower boundary shear strength has been investigated. Contamination of the filter cake by excavated soil particles leads to an increase of filter cake shear strength, as indicated by Henry et al. (1998) and Arwanitaki et al. (2007). In addition, Arwanitaki et al. (2007) showed that the filter cake growth rate is strongly dependant on the presence of excavated soil particles in the support fluid (Figure 2.9).

Based on this existing knowledge, the conceptual model presented in Figure 2.15 predicts the development of interface shear strength (δ/ϕ) as a function of filtration time for the case of a contaminated filter cake compared to a clean filter cake. For the conditions of equal concrete roughness and filtration pressure, the decrease of δ/ϕ commences earlier for a contaminated filter cake (t_{a1}) compared to a clean filter cake (t_{b1}). For increased filtration time, the lower boundary shear strength is reached earlier for a contaminated filter cake (t_{a2}) compared to a clean filter cake (t_{b2}). However, the lower boundary value of δ/ϕ for a contaminated filter cake (r_a) is higher compared to a clean filter cake (r_b).

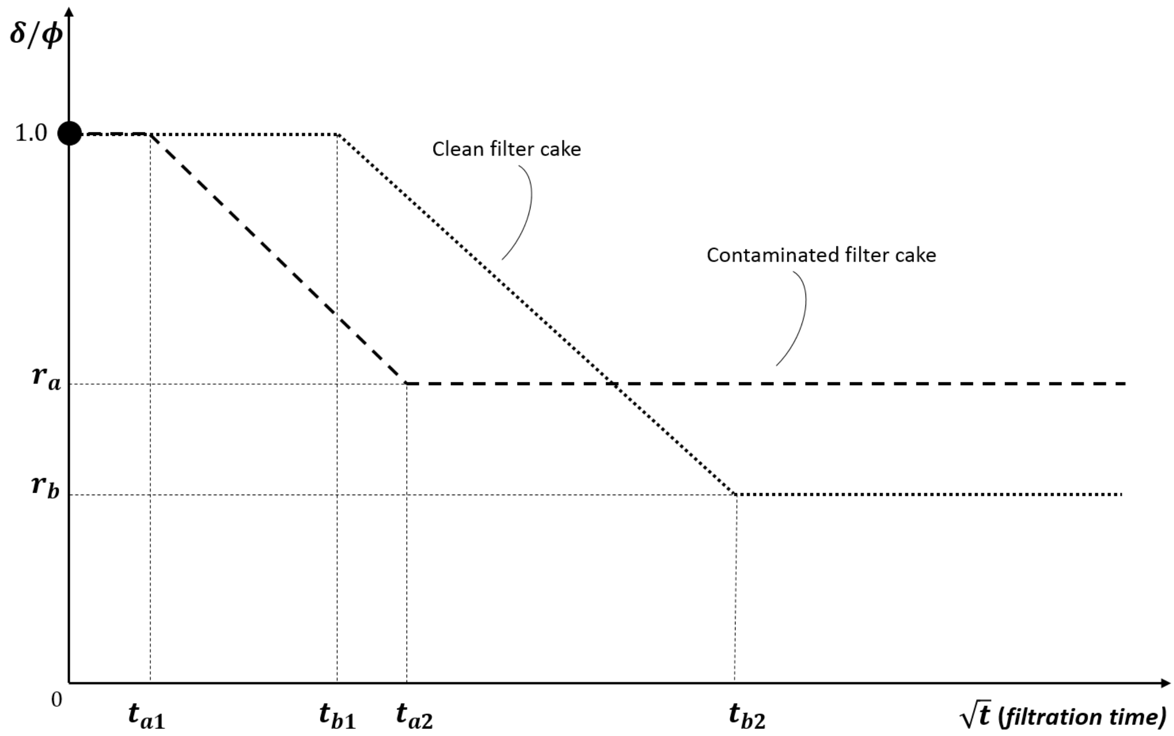

Figure 2.15: Conceptual model of development of friction reduction factor for clean and contaminated filter cakes

2.5. Conclusion

In the design of retaining structures, wall friction is generally expressed in the external friction angle δ. For both straight and curved slip surfaces the influence of δ on the coefficient of passive soil pressure K_p is considerable, as shown in Figure 2.4. For the assumption of straight slip surfaces, the influence of δ is largest. However, the suitability of straight slip surfaces is questionable, since the resulting values for K_a and K_p seem to be under- and overestimations respectively (Verruijt and Van Baars, 2009). Curved slip surfaces therefore seem to be more appropriate approximations. Craig (1997) states that the slip surface curvature near the wall toe can be attributed to wall friction. Numerical analyses of a strutted diaphragm wall (multiple strut layers) by Diao and Zheng (2008) show an increase of wall deflection and surface settlement with decreasing external friction angle δ.

The soil-/structure interface of a diaphragm wall is characterised by the presence of a bentonite filter cake in between the concrete panel and the surrounding soil. This bentonite filter cake acts as a membrane upon which the support fluid (bentonite suspension) can exert its hydrostatic pressure (micro stability), preventing a soil wedge from sliding into the trench (macro stability). For Dutch soil conditions, 'surface filtration' is the expected micro stability mechanism, since the filter criterion of Walz et al. (1983) ($D10 \leq 0,20mm$) is almost always met (Van Tol and Everts, 2008). Filter cake formation starts during panel excavation. However, because of the disturbance caused by excavation equipment, undisturbed filter cake growth starts when panel excavation is completed and ends when the support fluid is replaced by the rising concrete. Results by Arwanitaki et al. (2007) show that the filter cake growth rate is strongly influenced by the presence of soil particles in the support fluid.

Observations by Wates and Knight (1975) and Deltares (2008) showed the presence of filter cake after concrete pouring, which means that the filter cake has sufficient shear strength to sustain the scouring action of the rising concrete. This is supported by numerical simulations by Van Dalen (2016). Wates and Knight (1975) reported a decreasing filter cake thickness with depth, caused by consolidation under the horizontal concrete pressure. Different expressions exist for the horizontal concrete pressure envelop in a diaphragm wall trench, which are all less than hydrostatic (Figure 2.10). Different views exist on the chemical interaction between hydrating cement and the bentonite filter cake. Van Weele (1981) and the CUR 231 mention a chemical alteration of the bentonite filter cake. However, Arwanitaki et al. (2007) states no chemical interaction takes place between bentonite filter cake and hydrating cement based on visual inspection. In addition, Cernak et al. (1973) observed no increase of bentonite filter cake increase in the presence of hydrating cement.

In the considered direct-shear research on the interface shear strength of diaphragm walls, different test configurations have been applied. Both in-situ samples and laboratory-made filter cakes have been analysed. For the laboratory-made filter cakes, 3 different sample configurations have been applied in previous research:

1. In-situ samples
2. Laboratory: Isolated Filter Cake: **IFC**;
3. Laboratory: Sand/Filter Cake/Mortar (small/absent aggregates): **S/FC/MOR**;
4. Laboratory: Sand/Filter Cake/Concrete (aggregates present): **S/FC/CON**.

IFC (isolated filter cake) tests on clean filter cakes by Cernak et al. (1973), Arwanitaki et al. (2007) and Lam et al. (2014) show friction angles around 14°. S/FC/MOR (sand/filter cake/mortar) tests on clean filter cakes by Lam et al. (2014), Deltares (2008), Arwanitaki et al. (2007) and Henry et al. (1998) show friction angles around 20°. For both the IFC and S/FC/MOR tests, Lam et al. (2014) show significantly lower friction angles. It could be that the presence of a large interface gap (20 mm) in their direct-shear geometry is the cause of this strong reduction in interface shear strength, since the confining pressure around the shear plane is reduced. A large range of increased friction angles for contaminated filter cakes has been found in previous research. Results by Day et al. (1981), Henry et al. (1998) and Arwanitaki et al. (2007) show contaminated filter cake friction angles around 30°. However, Scott (1978) and Deltares (2008) show a wide range, with lower bounds of 21° and 22,5° respectively. For the S/FC/CON tests, both Lam et al. (2014) and Cernak et al. (1973) show a reduction in interface shear strength with increasing filtration time. Furthermore, Lam et al. (2014) showed that the interface shear strength increases from the isolated filter cake strength upto the shear strength of the sand with decreasing filter cake thickness. The authors attribute this strength increase to the protrusion of aggregates through the filter cake, reaching the sand layer. This aggregate protrusion is a function of both the filter cake thickness and concrete aggregate size (Lam et al., 2014). Finally, a large variation is observed in the modelling of the lateral concrete pressure, which causes filter cake consolidation.

A conceptual model has been presented, which shows the development of interface shear strength (δ/ϕ) as a function of filtration time for clean and contaminated filter cakes. Results by Arwanitaki et al. (2007) have shown that the filter cake growth rate for contaminated filter cakes is considerably higher compared to clean filter cakes. Cernak et al. (1973) and Lam et al. (2014) have shown that the interface shear strength decreases with increasing filter cake thickness with the filter cake shear strength as lower boundary. In the conceptual model, the lower boundary shear strength is reached at smaller filtration time for contaminated filter cakes due to the higher filter cake growth rate. On the other hand, as results by Henry et al. (1998) and Arwanitaki et al. (2007) have shown, the shear strength of contaminated filter cakes is higher due to the presence of excavated soil particles.

3 Experimental Methodology

Previous research has mainly focussed on the filter cake shear strength, which is the lower boundary shear strength of the layered interface system of a diaphragm wall. A large range of filter cake friction angle values has been found in literature. First of all, the presence of excavated soil particles in the filter cake causes a strong increase of filter cake shear strength according to Henry et al. (1998) and Arwanitaki et al. (2007). In addition, the applied test/sample configuration also influences the measured filter cake shear strength. Direct-shear tests on sand/filter cake/mortar samples (S/FC/MOR) generally lead to higher shear strength values compared to tests on isolated filter cake material. The underlying experimental research for the current CUR 231 recommendations (Deltares, 2008) applied an S/FC/MOR sample configuration to analyse the filter cake shear strength, modelling a continuous shear plane through the filter cake, which is a conservative approach. In addition, Deltares (2008) did not take into account the influence of filter cake contamination by excavated soil particles, indicating additional conservatism.

Cernak et al. (1973) and Lam et al. (2014) investigated the development of interface shear strength for increasing filter cake thickness and found that the interface shear strength increases from the filter cake shear strength towards the shear strength of the sand for decreasing filter cake thickness. Given a certain concrete roughness, decreasing filter cake thickness allows for an increase of direct contact between concrete and sand. Lam et al. (2014) refer to this phenomenon as 'aggregate protrusion'. In addition, Lam et al. (2014) found that upto a certain filter cake thickness, no decrease of the interface shear strength occurs due to a 'ploughing' action of the concrete through the sand. However, the influence of filter cake thickness on the interface shear strength has only been investigated for clean filter cakes. The conceptual model proposed in the literature review predicts the development of interface shear strength for a contaminated filter cake compared to a clean filter cake.

3.1. Research scope

In this research an experimental investigation is performed to further analyse the conservatism in the current CUR 231 recommendations on the shear strength of the soil/structure interface of diaphragm walls. As described in the above, the literature review has revealed 2 sources of conservatism:

- Filter cake contamination by excavated soil particles is not taken into account;
- Continuous shear plane through filter cake is assumed (influence of concrete roughness and filter cake thickness is ignored).

Both sources of conservatism are captured in the proposed conceptual model in Section 2.4. As guidance for the experimental investigation in this thesis, the conceptual model serves as hypothesis. The experimental investigation is divided into 2 phases, both involving the direct-shear method. As stated by Lam et al. (2014), the direct-shear method is most suited for the analysis of interface shear strength, since in the direct-shear method shearing occurs along a more or less predefined shear plane.

The first experimental phase focusses on the filter cake shear strength, which is the lower boundary interface shear strength in the conceptual model. The lower boundary interface shear strength assumes a continuous shear plane through the filter cake as conceptually presented in Figure 3.1.

The second experimental phase investigates the development of the interface shear strength as a function of filtration time (and subsequent filter cake thickness) towards the lower boundary shear strength, thereby considering discontinuities in the filter cake shear plane, as conceptually presented in Figure 3.2. As described in the literature review, the filtration time and support fluid composition are the main factors governing the development of filter cake thickness. Both experimental phases only consider sand as the modelled soil material, since the presence of a filter cake is not expected in cohesive soils (Tucker and Reese, 1984; Van Tol and Everts, 2008). In addition, only bentonite filter cakes are considered. The influence of polymers on the interface shear strength is not investigated.

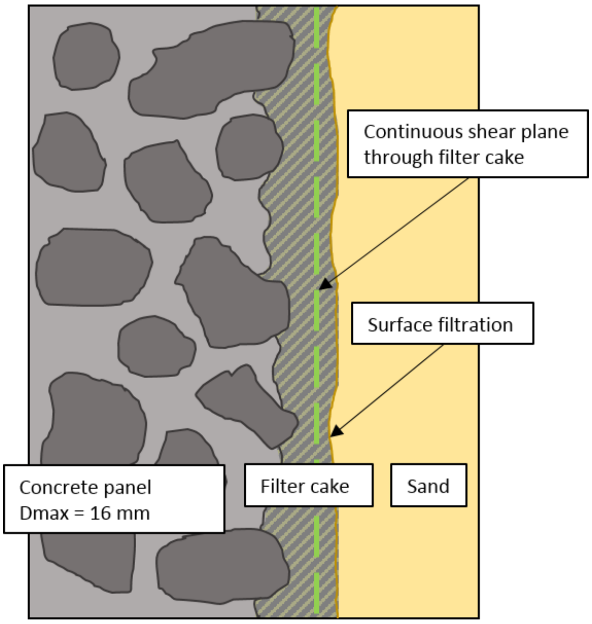

Figure 3.1: Experimental phase 1: no aggregate protrusion, continuous shear plane through filter cake

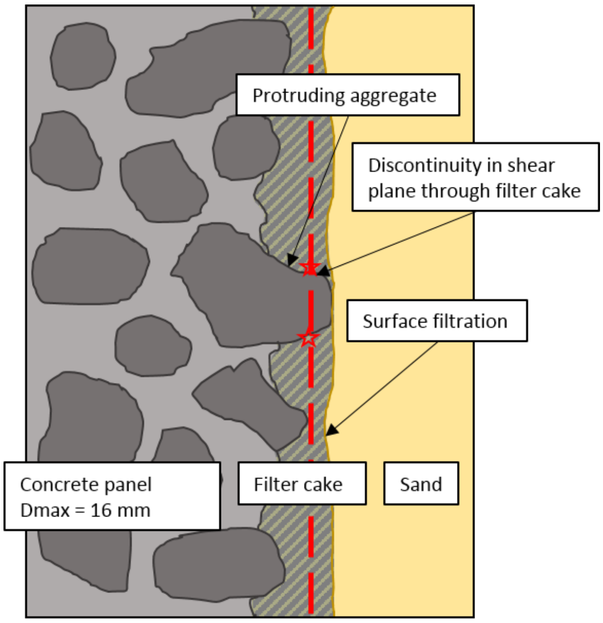

Figure 3.2: Experimental phase 2: aggregate protrusion, discontinuities in shear plane through filter cake

3.2. Research questions

To further guide the experimental investigation, for both experimental phases research questions have been formulated.

3.2.1. Experimental Phase 1

In experimental phase 1, an experimental procedure developed by Van Dalen (2016) is applied, which enables direct-shear tests on circular sand/filter cake/cement-mortar (Ø 67 mm). This type of layered samples is suited to model the filter cake shear strength (Figure 3.1). Concerning the filter cake shear strength, the following research questions have been formulated for Experimental Phase 1:

1. What is the influence of filter cake consolidation on the filter cake shear strength?
2. What is the influence of the filter cake composition on the filter cake shear strength?

3.2.2. Experimental Phase 2

The existing small-scale set-up (Ø 67 mm) applied in experimental phase 1 is not suited for the investigation of the development of the interface shear strength as a function of filtration time (and subsequent filter cake thickness), since discontinuities in the filter cake shear plane (Figure 3.2) can not be modelled in a realistic way due to the small sample scale relative to the maximum aggregate size in diaphragm wall concrete of 16 mm, which is commonly applied in Dutch construction practice (CUR/COB, 2010). Therefore, the following research questions have been formulated for Experimental Phase 2:

3. How can a direct-shear set-up be developed which enables the modelling of sand/filter cake/concrete samples?

4. What is the influence of filter cake thickness on the interface shear strength for clean and contaminated filter cakes?

3.3. Overview of experiments

Table 3.1 presents an overview of the performed tests for both experimental phase 1 and phase 2. More detailed explanations on the applied parameter configurations are provided in the next chapters. It should be noted that slight deviations of the presented parameter values have occurred, which are discussed in later chapters.

Table 3.1: Overview of experiments for Experimental phase 1 and phase 2: parameter configuration and goal of tests

Test ID	**Sample size**	**Max agg. size**	$t_{filt.}$	γ_{slurry}	$t_{cons.}$	σ_N*	**OCR**	**Shear rate**	**Goal of test**
	[mm]	[mm]	[hours]	[g/cm^3]	[days]	[kPa]	[-]	[mm/min]	
Experimental Phase 1: Filter cake shear strength (lower boundary interface shear strength)									
C1.1 - C1.4	∅ 67	4	+/-168	1,03	6	200	1	1,2	A
C2.1 - C2.4	∅ 67	4	+/-168	1,03	6	300	1	1,2	A
C3.1 - C3.4	∅ 67	4	+/-168	1,03	6	400	1	1,2	A
C4.1 - C4.4	∅ 67	4	+/-168	1,03	6	200	4	1,2	B
C5.1 - C5.4	∅ 67	4	+/-168	1,03	6	400	4	1,2	B
C6.1 - C6.2	∅ 67	4	+/-168	1,03	6	200	1	0,0072	C
C6.3	∅ 67	4	+/-168	1,03	35	200	1	1,2	D
S1.1 - S1.4	∅ 67	4	+/-168	1,06	6	200	1	1,2	E
S2.1 - S2.4	∅ 67	4	+/-168	1,26	6	200	1	1,2	E
S3.1 - S3.4	∅ 67	4	+/-168	1,26	6	400	1	1,2	E
S4.1 - S4.2	∅ 67	4	+/-72	1,26	6	200	1	1,2	F
S4.3 - S4.4	∅ 67	4	+/-72	1,26	6	200	1	0,0072	C
Experimental Phase 2: Development of interface shear strength as a function of filtration time									
P2.1	170 x 170	16	0	-	2-3	200	1	1,2	G
P2.2	170 x 170	16	48	1,03	2-3	200	1	1,2	H
P2.3	170 x 170	16	24	1,03	2-3	200	1	1,2	H
P2.4	170 x 170	16	12	1,03	2-3	200	1	1,2	H
P2.5	170 x 170	16	12	1,26	2-3	200	1	1,2	I
P2.6	170 x 170	16	3	1,26	2-3	200	1	1,2	I
P2.7	170 x 170	16	1	1,26	2-3	200	1	1,2	I

A: Shear strength of normally-consolidated, clean filter cakes
B: Shear strength of over-consolidated, clean filter cakes
C: Influence of shear rate on filter cake shear strength (clean/contaminated)
D: Influence of cement-curing time on clean filter cake shear strength
E: Shear strength of normally-consolidated, contaminated filter cakes
F: Influence of filter cake thickness on contaminated filter cake shear strength
G: Reference test: shear strength of sand/concrete interface (no filter cake)
H: Development of interface shear strength as a function of filtration time for clean filter cakes
I: Development of interface shear strength as a function of filtration time for contaminated filter cakes
**: Normal pressure in direct-shear test*

4

Experimental Phase 1: Filter cake shear strength

This chapter describes the experimental investigation of the bentonite filter cake shear strength. The shear strength of the filter cake is governing as interface shear strength if a continuous shear plane through the filter cake is assumed. This conservative assumption is the basis for the first experimental phase of this research. In the second experimental phase the interaction between filter cake thickness and concrete roughness is analysed. In this chapter, first the methodology is discussed (experimental procedure and parameter configurations). Next, experimental results are presented and discussed. The discussion of experimental results is divided into 'clean filter cakes' and 'contaminated filter cakes'. Finally, conclusions are drawn based on the experimental results and recommendations are presented.

4.1. Methodology

For evaluation of the filter cake shear strength, direct-shear tests are performed on sand/filter cake/cement-mortar samples with a diameter of 67 mm. The applied experimental set-up and procedure is developed by Van Dalen (2016) in the context of his PhD research. As described before, the direct-shear test method is commonly applied for the investigation of the shear strength of an interface. To ensure a continuous shear plane through the filter cake, the following 3 main measures are adopted:

1. Exaggerated filtration time to ensure a thick filter cake prior to consolidation;
2. Small maximum aggregate size in the applied concrete mix (cement-mortar);
3. Gentle placement of cement-mortar (no drop height) to ensure filter cake integrity.

In this section, first the different stages in the experimental procedure are explained. Next, the used materials in the sample preparation are discussed. Finally, the applied parameter configurations for the different stages are discussed.

4.1.1. Experimental procedure

The preparation of the layered interface sample (sand/filter cake/cement-mortar) and subsequent shearing involves a number of stages:

1. Filter cake formation (filtration);
2. Cement-mortar curing / filter cake consolidation;
3. Direct-shear test.

The layered sample is contained in a sample tube, consisting of 2 sections. When placed in the direct-shear apparatus, the interface of the sample tube sections aligns with the shear box interface. Sample preparation starts with placing the bottom sample tube section on a permeable element and applying a filter paper on its surface. The bottom section is subsequently filled with sand (Figure 4.1, left) and densified in layers by tamping. More details on the applied sand are provided in the 'materials' section. The sand is saturated by placing the bottom section in a water container (Figure 4.1, left). After saturation, the top sample tube section is placed on the bottom section, connected with a watertight sleeve joint (Figure 4.1, right). The top section is gently filled with the bentonite suspension, whilst avoiding disturbance of the sand surface. More details on the applied bentonite are provided in the 'materials' section. The top section is then connected to a manifold by a second sleeve joint. Through this manifold, 4 sample tubes are connected to a single standpipe with a height of 2 meters. When completely filled, the bentonite suspension column in the standpipe generates a filtration pressure of around 20 kPa, depending on the volumetric weight of the suspension inside.

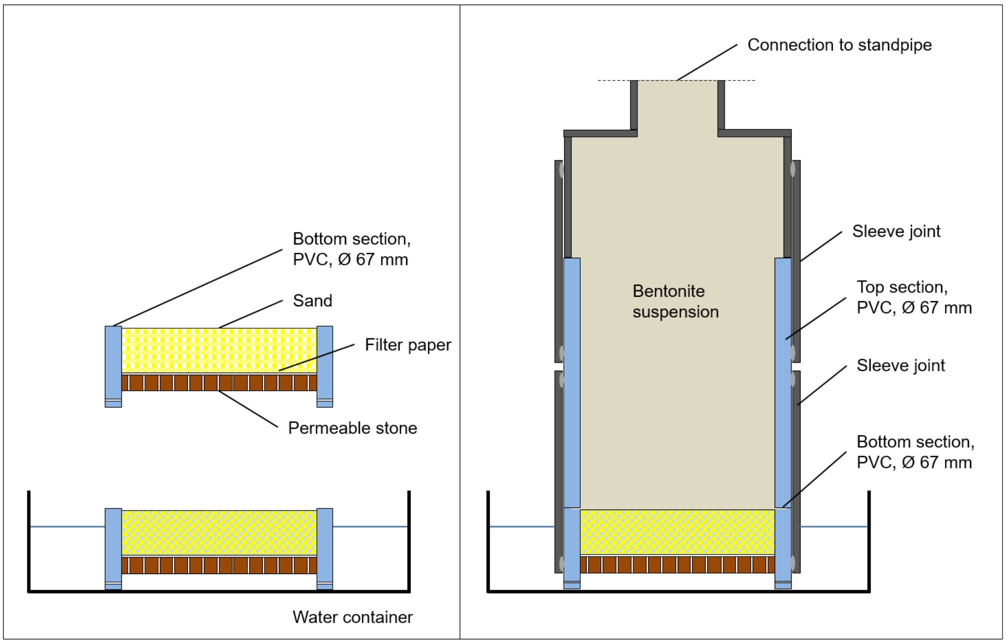

Figure 4.1: Bottom sample container, sand saturation and bentonite filtration

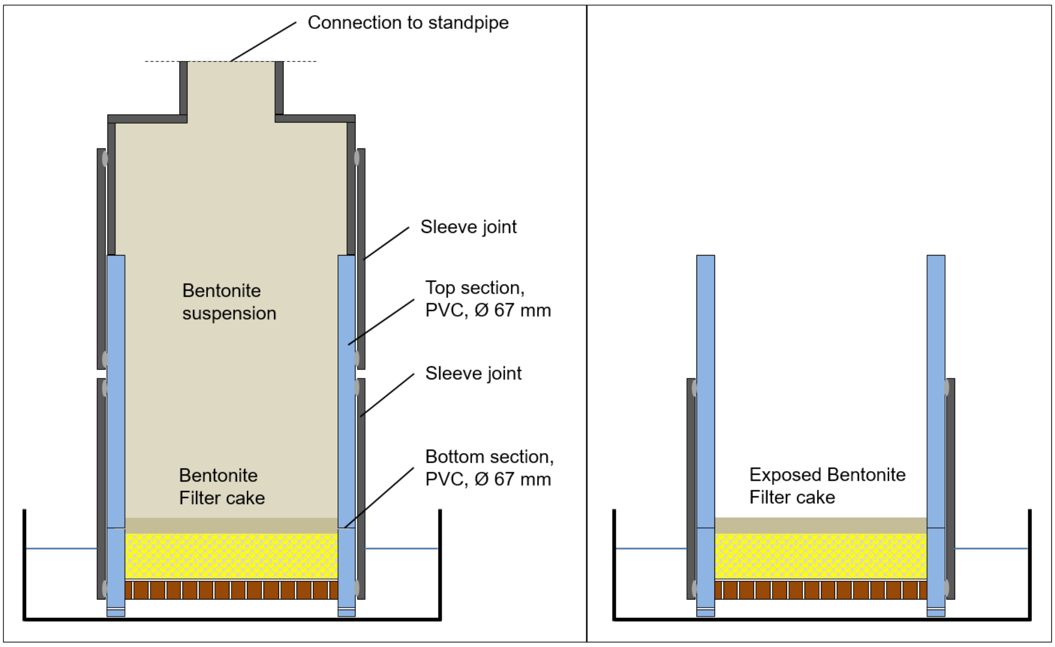

Figure 4.2: Filter cake formation and set-up disassembly

Due to filtration of the bentonite suspension through the sand a filter cake is formed on the sand surface (Figure 4.2, left). During the filtration phase, the fluid level in the standpipe is frequently refilled to maintain the filtration pressure. After filtration, the fluid bentonite is removed using a syringe, hereby exposing the solid bentonite filter cake (Figure 4.2, right). A latex membrane is placed along the inner perimeter of the top section to reduce friction between the cement and sample container (Figure 4.3, left). In addition, vaseline is applied in between the membrane and sample container. The cement is very gently placed on top of the filter cake to prevent disturbance of the filter cake surface. When the top section is filled until the top of the latex membrane, a pressure plate is placed on top of the cement. The sample is then placed in an oedometer to let the cement harden under pressure, causing filter cake consolidation (Figure 4.3, right). The normal load in the oedometer is applied in increments to prevent squeezing of the bentonite filter cake. After the consolidation stage, the sample tubes are placed inside the shear boxes of the direct-shear apparatus (Figure 4.4, left). The interfaces of the shear boxes and sample tube sections are aligned in such a way that the shear plane runs through the filter cake (Figure 4.4, right).

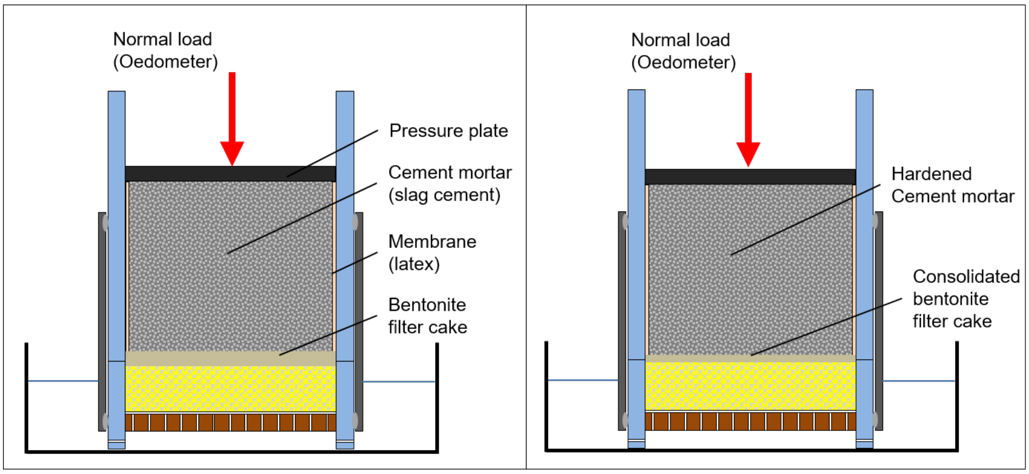

Figure 4.3: Filter cake consolidation in oedometer

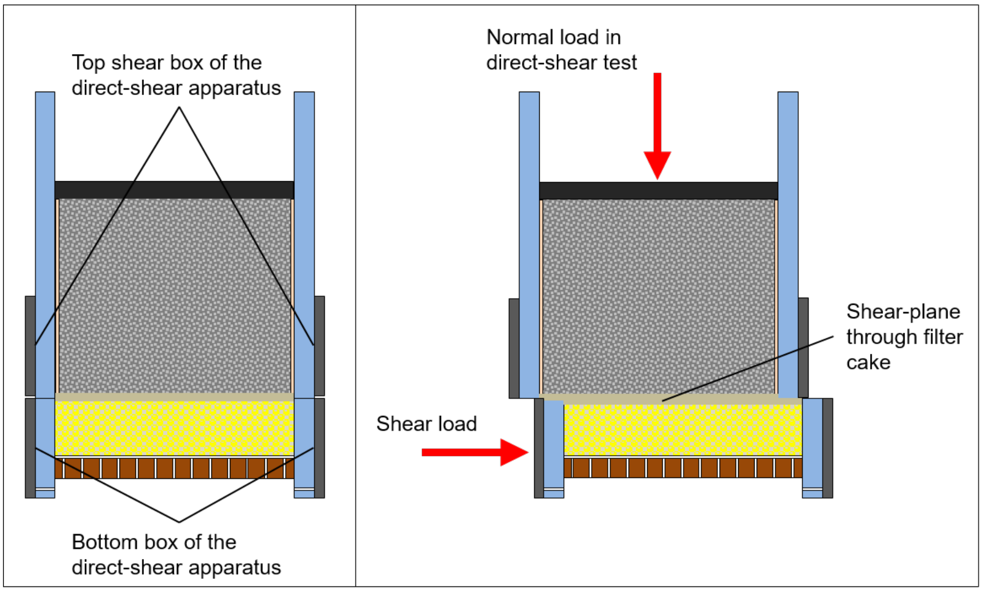

Figure 4.4: Set-up disassembly and direct-shear test

Due to the horizontal displacement during shearing the tested sample surface decreases (Figure 4.5). With progressing horizontal displacement, the normal pressure will therefore increase. The surface area is corrected by a factor F (Equation 4.1 and 4.2), which is a function of the sample diameter and horizontal displacement (Equation 4.3). Another factor which requires correction is the fact that at the start of shearing some horizontal displacement is required before the shearing force is fully acting on the sample. In the sample configuration and the direct-shear apparatus several tolerances need to covered before all components are in tension. The spacing between the inner perimeter of the shear boxes and the outside of the sample tubes is the main tolerance in the system (Figure A.6).

$$A = A_0 F \tag{4.1}$$

$$A_0 = \frac{\pi}{4} D^2 \tag{4.2}$$

$$F = \frac{2}{\pi}\left\{\cos^{-1}\left(\frac{\Delta h}{D}\right) - \left(\frac{\Delta h}{D}\right)\sqrt{1-\left(\frac{\Delta h}{D}\right)^2}\right\} \tag{4.3}$$

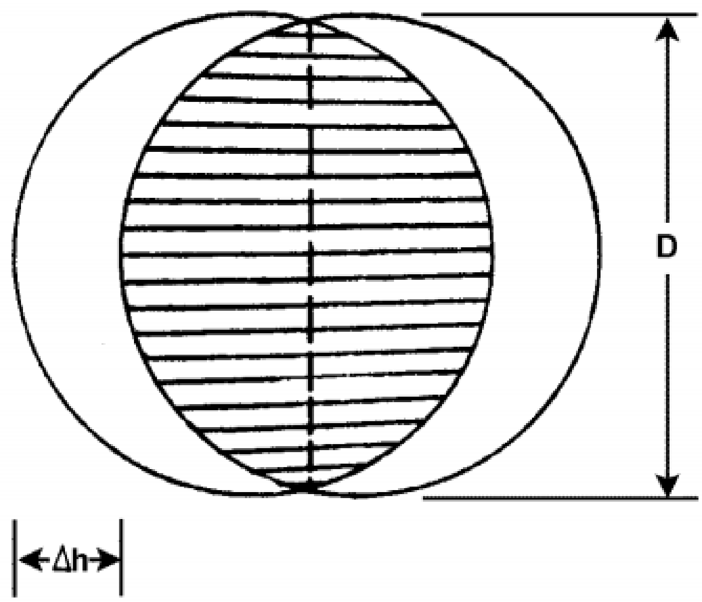

Figure 4.5: Decreased surface area during shearing (Olson and Lai, 2004)

4.1.2. Applied materials

Below an overview is provided of the applied materials in the preparation of the layered sand/bentonite filter cake/cement mortar samples.

Sand

The sand in the bottom sample tube section acts as a filter during filter cake formation. For Dutch soil conditions, surface filtration is the expected formation mechanism, since the criterion $D10 \leq 0,20mm$ is almost always met, even in Pleistocene formations (Van Tol and Everts, 2008). To apply a representative sand for Dutch conditions, Strukton has provided sieve analyses of Pleistocene sand at a construction site in Benthuizen (Zuid-Holland), which have been replicated. Figure 4.6 shows that the replicated sieve curve meets the filtration criteria by Walz et al. (1983) and Henry et al. (1998):

- Walz et al. (1983): $D10 = 0,16mm \leq 0,20mm$
- Henry et al. (1998): $D15 = 0,22mm \leq 0,34 - 0,43mm$

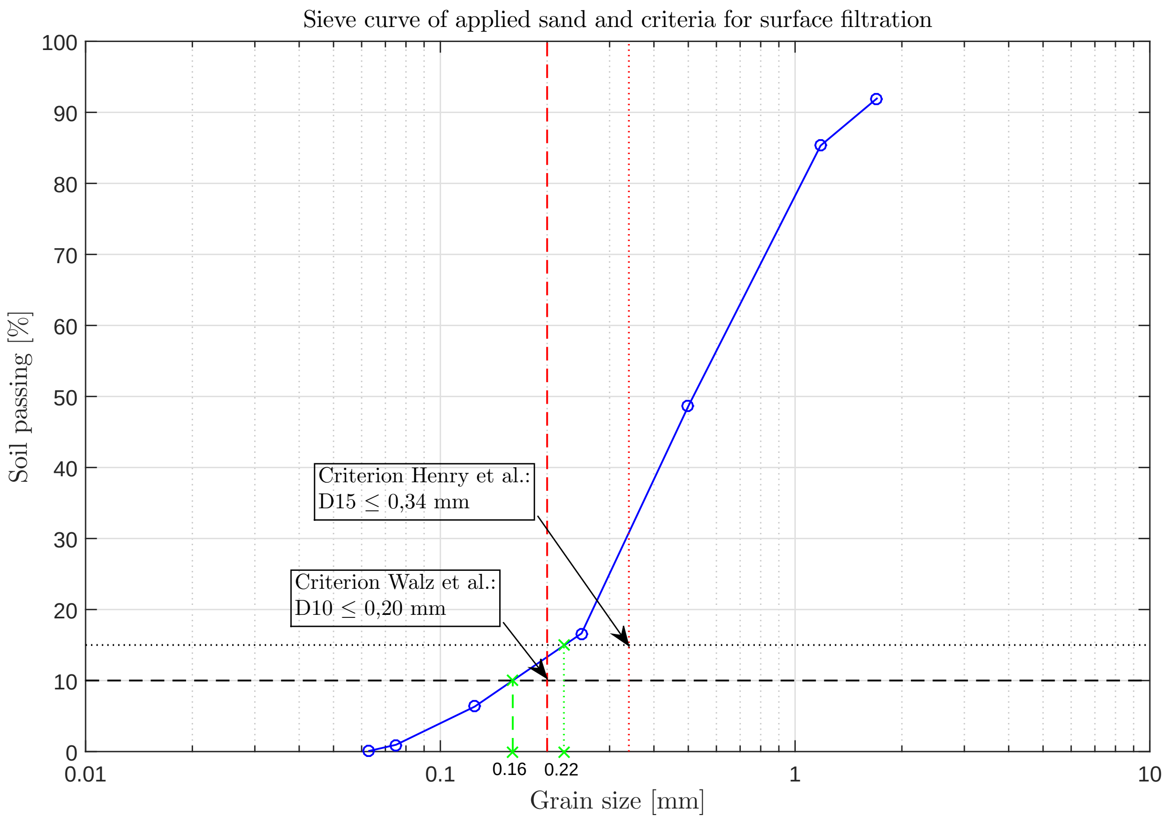

Figure 4.6: Sieve curve of applied sand, based on Benthuizen sieve analysis (Boskalis, 2015), with added criteria for surface filtration.

The sieve curve is 'constructed' by combining different grain fractions. Figure 4.6 shows the results of dry sieving of the constructed sand mixture. Further properties of the applied sand are presented in Table 4.1. The minimum and maximum void ratios have been determined according to the standard of the Japanese Geotechnical Society, as described in Anaraki (2008). The effective friction angle of the sand has been determined by direct-shear tests (Appendix B, Figure B.7, B.8).

Table 4.1: Characteristics of applied sand

Parameter	Value
D10	0,16 mm
D15	0,22 mm
Minimum void ratio	0,45
Maximum void ratio	0,66
ϕ' (dense)	40,7°

Bentonite

The applied bentonite suspension is based on the sodium-actived Cebogel Trenchcontrol AT, kindly provided by Cebo Holland. Cebogel Trenchcontrol AT is commonly applied in support fluids in Dutch construction practice. In this research, the bentonite concentration is fixed to 4 %, which is a commonly applied value in Dutch construction practice (CUR/COB, 2010). For each series of 4 samples, a volume of 10 L of bentonite suspension is prepared. This volume is sufficient for filling of the standpipe and subsequent refilling during the filtration stage. The dry Cebogel Trenchcontrol AT powder is mixed with regular tap water using an industrial mixer and is left to 'rest' overnight to allow for the bentonite plates to fully swell. Further product specifications are provided in Appendix C.

Cement mortar
For the cement mortar, the maximum aggregate size is 4 mm. CEM III/B 42,5 (blast furnace slag cement) is applied as binder. To be sure that the aggregate size equals 4 mm, the aggregate mixture is sieved through a 4 mm sieve prior to mixing. Table 4.2 presents the mix recipe, in which a water/cement ratio of 0.5 is applied. Since only a small volume of the cement-mortar is required for each series of 4 samples, the constituents are mixed by hand.

Table 4.2: Cement-mortar mix design

Constituent	**Quantity** [kg/m^3]
CEM III/B 42,5	350
Aggregate 0-4 mm	1813
Water	175

4.1.3. Parameter configurations

Table 4.3 presents an overview of the general test parameters. As described in the above, in experimental phase 1 a continuous shear plane through the filter cake is modelled. For this purpose, an exaggerated filtration time is applied to achieve a thick filter cake. In addition, a cement-mortar is applied in stead of concrete. The applied filtration time is based on Cernak et al. (1973), who found that for a filtration time of 7 days (at 20 kPa filtration pressure), the interface shear strength is reduced to the filter cake shear strength. Therefore, a filtration pressure of 7 days (at 20 kPa) is assumed to be sufficient.

Table 4.3: Overview of general test parameters for experimental phase 1

Parameter	**Value**
Bentonite concentration in slurry	4 %
Sand/silt concentration in contaminated slurry	**Variable**
Filtration time	7 days
Filtration pressure	20 kPa
Maximum aggregate size	4 mm
Consolidation time	6 days
Consolidation pressure	**Variable**
Normal pressure in direct-shear test	**Variable**
Shear rate	1,2 mm/min

The general consolidation (cement-curing) time is set to 6 days. Within this time frame, the cement-mortar is able to reach a strength which is much higher than the sand and filter cake. In addition, the consolidation process of the filter cake is allowed to reach the creep phase (this will be discussed in more detail in the result section). Lam et al. (2014) applied a consolidation time of 7 days. However, for this research, a consolidation time of 6 days allowed for more efficient planning. During cement curing, some chemical interaction might take place between the filter cake and the cement-mortar. Although Cernak et al. (1973) and Arwanitaki et al. (2007) have shown that no chemical strengthening of the filter cake takes place, the influence of the consolidation/cement-curing time on the filter cake shear strength will be analysed in a reference test, which will be discussed later on.

The high shear rate (1,2 mm/min, maximum speed of direct-shear apparatus) is based on recommendations by Lam et al. (2014), who applied a shear rate of 2 mm/min. In addition, a high shear rate allows to perform multiple direct-shear tests within a short time-span. As described before, during the filtration- and consolidation stage 4 samples are produced simultaneously, whilst only 1 sample can be sheared at a time. A longer shearing duration would result in a spreading in consolidation time (during which cement-curing takes place). Lam et al. (2014) applied a shear rate of 2,0 mm/min. They applied such a high shear rate to prevent the filter cake from drying out during shearing. In addition, Lam et al. (2014) state that such a shear rate resembles the rate of an in-situ load test. Lam et al. (2014) also state that for a shear rate of 2,0 mm/min the sand is sheared drained, whilst the filter cake is sheared in undrained conditions. The influence of the shear rate on the filter cake shear strength is analysed by means of reference tests at lower shear rate, which will be discussed later on.

The first test series of this experimental phase focus on the influence of the consolidation pressure on the shear strength of the filter cake. In these tests the slurry composition (and hence the filter cake composition) is constant. The consolidation- and normal pressure during shearing are the main variables. Additional test series focus on the influence of filter cake composition, in which the slurry composition is the main variable. For the tests on clean filter cakes, consolidation pressures of 200 kPa, 300 kPa and 400 kPa are applied, which model the lateral concrete pressures at different depths in a diaphragm wall trench. For the test series on contaminated filter cakes, the applied slurry composition is the main variable. The slurry compositions are based on an analysis of an in-situ slurry sample from the Spoorzone Delft project. This analysis is described in a later part. Table 4.4 presents the applied general parameter configurations for the tests on clean filter cakes (left section of the table, indicated with C'serie'x.'sample'y) and on the contaminated filter cakes (right section of the table, indicated with S'serie'x.'serie'y). As described before, in the filtration stage 4 samples are produced simultaneously. To assess the quality and variability of test results, the 4 samples are tested under equal conditions. In this way, each data point is based on 4 measurements. As described before, the influence of shear rate and cement-curing time is analysed in additional tests, as indicated in Table 4.4. Details of these tests are provided in a later part.

Table 4.4: Parameter configurations for tests on clean filter cakes and filter cakes with added sand/silt

Test ID (clean)	**P-cons** [kPa]	**P-normal** [kPa]	**Test ID (contaminated)**	**Concentration sand/silt** [kg/kg·100%]*	**P-cons** [kPa]	**P-normal** [kPa]
C1.1 - C1.4	200	200	S1.1 - S1.4	9,8**	200	200
C2.1 - C2.4	300	300	S2.1 - S2.4	45***	200	200
C3.1 - C3.4	400	400	S3.1 - S3.4	45	400	400
C4.1 - C4.4	200	50	S4.1 - S4.4****	45	200	200
C5.1 - C5.4	400	100				
C6.1 - C6.3****	200	200				

**: mass of sand/silt compared to mass of water*
***: Based on in-situ sample analysis, only sand curve*
****: Based on in-situ sample analysis, complete curve*
*****: Reference tests*

The different consolidation pressures correspond to different lateral concrete pressures at certain depths in a diaphragm wall trench. As described before, different methods exist to determine lateral concrete pressures. Table 4.5 presents the corresponding depths for the calculation methods of Lings et al. (1994) and Van Weele (1981). Lings et al. (1994) assumes a bi-linear pressure profile (Equation 2.22), while Van Weele (1981) assumes a lateral pressure of 70 % of the hydrostatic concrete pressure.

Table 4.5: Considered consolidation pressures and corresponding depths in trench for different calculation methods

Pressure [kPa]	**Depth in diaphragm wall trench according to:** Lings et al. (1994) [m]	Van Weele (1981) [m]
200	8,3	11,9
300	15,8	17,9
400	25,4	23,8

4.2. Shear strength of clean filter cakes

This section presents the experimental results of the test series performed on clean filter cake samples (C1 to C6). First, the results of the sample preparation stages are discussed, mainly focussing on the filter cake formation and consolidation. Next, the analysis of filter cake shear strength is divided into 3 parts. First, the influence of the filter cake consolidation pressure on the filter cake shear strength is discussed, followed by an analysis of the influence of shear rate and cement-curing time.

4.2.1. Sample preparation results

Filtration stage

As described in the methodology section of this chapter, the first step of sample preparation is the formation of a filter cake on top of a sand bed. For this purpose, a filtration pressure is applied by means of a standpipe. The refilled volume of slurry of the standpipe over time has been recorded and shows a development with $\sqrt{t}$, as shown in Appendix B, Figures B.1 and B.2. The development of filtration volume is consistent except for test series C3, which shows a vertical offset. This large initial 'fluid loss' at the start of the filtration process is explained by the fact that for test series C3, the sand was not saturated prior to slurry filtration (C3 was the first test series performed). However, the slope of C3 shows good comparison with the other test series, despite of the higher fluid loss. This indicates that after the initial seal formation the filtrate volume is governed by the filter cake (also see Figure 2.8).

The resulting filter cakes formed on the sand bed during the 7 days filtration time have a thickness of around 20 mm (Table 4.6). Figures A.1 and A.2 (Appendix A) show the process of filter cake exposure when filtration is complete. The development of filter cake thickness over time has not been recorded, since the filter cake is not visible during the filtration stage. Based on equation 2.19 and the observed development of filtrated slurry volume, the development of filter cake thickness is expected to develop with $\sqrt{t}$. The measured filter cake thickness of 20 mm after 7 days translates to growth rate values around 0,2 $mm/\sqrt{min}$. This value corresponds with observations by Lubach (2010), who a filter cake growth rate ranging from 0,22 to 0,24 $mm/\sqrt{min}$ for a filtration pressure of 20 kPa. The slightly lower filter cake growth rate in this research might be caused by the fact that the filtration pressure is achieved by means of a standpipe in stead of a constant air pressure. Although the standpipe is refilled frequently, the filtration pressure is not constant due to the dropping slurry level, which might cause this slightly lower filter cake growth rate. Another factor could be the development of slurry shear strength, because of its thixotropic behaviour. Since the manifold connecting the sample tubes to the standpipe contains a horizontal section above the sample tubes, the development of shear strength in the slurry might cause a reduction of the filtration pressure to a value lower than hydrostatic.

Consolidation stage

The first step of the consolidation stage is applying cement-mortar on top of the exposed filter cake. As described before, the cement-mortar is gently placed with a spatula to avoid disturbance of the filter cake surface (Appendix A, Figure A.3). A latex membrane is placed in between the cement-mortar and the sample tube to reduce friction between the hardening cement and the sample tube. The cement-mortar is placed as dense as possible, without damaging the filter cake underneath. This is done by placing the cement-mortar in thin layers and gently compacting the fresh layer with the spatula. On top of the cement-mortar a pressure plate is placed. Finally, each sample tube is placed in an oedometer set-up (Appendix A, Figure A.4).

The main purpose of the consolidation phase is the (mechanical) application of a stress level in the filter cake, which represents a certain lateral concrete pressure (Table 4.5). The increased stress levels result in filter cake compression. Table 4.6 provides an overview of filter cake compression results. The total measured compression is presented, as well as the relative compression compared to the filter cake thickness prior to compression. The measured values of final compression almost all lie above 70%. The measured compression is mainly the result of the filter cake compression. However, part of the measured compression will be the result of slight compression of the cement-mortar. In addition, the sand layer underneath the filter cake might cause some additional compression as well. To reduce the contribution of the cement-mortar to the total compression, the cement-mortar is applied and compacted in layers with a spatula (Appendix A, Figure A.3).

Table 4.6: Results of sample preparation stage for test series on clean filter cakes (C1 to C6)

Test ID	**Slurry density** [g/cm^3]	**Filtration time** [hours]	**Filter cake thickness** [mm]	**Filter cake growth rate** [$mm/\sqrt{min}$]	**Consolidation pressure** [kPa]	**Filter cake Compression** [mm]	[%]
C1.1	1,03	168	20	0,199	200	14,3	72
C1.2						14,1	71
C1.3						14,7	74
C1.4						13,7	68
C2.1	1,03	161	20	0,204	300	17,9	90
C2.2						17,3	86
C2.3						19,0	95
C2.4*						5,9	30
C3.1	1,03	166	20	0,201	400	18,0	90
C3.2						15,1	76
C3.3						16,8	84
C3.4						16,0	80
C4.1	1,03	192**	23	0,215	200	17,6	77
C4.2						17,9	78
C4.3						19,7	86
C4.4						18,4	80
C5.1	1,04	164	20	0,202	400	15,0	75
C5.2						18,3	91
C5.3*						19,9	100
C5.4						16,8	84
C6.1	1,03	166	20	0,202	200	16,8	84
C6.2						17,4	87
C6.3						19,2	96

**: Sample failed in consolidation phase (squeezing)*
***: Longer filtration time due to planning difficulties*

The measured compression is also influenced by friction between the cement-mortar and the sample container, which increases in time due to cement curing, despite the presence of a latex membrane (coated with vaseline). Therefore, with a quicker application of the consolidation load steps, less consolidation load is 'lost' through skin friction. However, for the early test series the speed of applying successive load steps was low to prevent squeezing of the filter cake. In later test series successive load steps were applied quicker. For instance, test series C6 shows more compression compared to test series C1 and C4 for equal consolidation pressure. Figure B.3 (Appendix B) presents filter cake consolidation results of test series C1 to C6. Teries C2 was one of the later test series in with a less conservative rate of successive load steps and which shows more filter cake compression despite the lower consolidation pressure.

Figure B.3 (Appendix B) shows that within the 6 days of cement-curing time the filter cakes are able to fully consolidate and reach the creep phase. Based on the consolidation data of test series C2 (Figure B.3, Appendix B), the consolidation coefficient C_v is estimated with the 'log-t' method (Equation 4.4). As described before, the total consolidation load is applied in increments. Considering the number of available data points (Figure B.3, Appendix B), it is not possible to estimate C_v for each load step. Therefore, the series of load steps towards the total consolidation pressure is assumed to be 1 load step, which is a crude assumption. The filter cake is assumed to be drained at both the bottom (sand layer) and top (cement-mortar). Therefore, h in Equation 4.4 is half of the filter cake thickness (20 mm). Based on these assumptions, the consolidation coefficient is roughly estimated on $2,0 \cdot 10^{-9} m^2/s$.

$$c_v = 0,197 \frac{h^2}{t_{50\%}} \tag{4.4}$$

Wates and Knight (1975) reported a decreasing filter cake thickness with increasing depth and they attribute this to filter cake consolidation. The fact that the measured values of filter cake compression do not show a strong increase with consolidation pressure is mainly the cause of the increasing skin friction with time. Therefore, for future tests, it is recommended to apply the consolidation load as quick as possible to reduce the influence of skin friction on the final filter cake compression.

The final stage in the experimental procedure is a direct-shear test on the consolidated samples (Figure 4.4). For this purpose, the samples are transferred from the oedometer to the direct-shear apparatus. This transfer causes unloading/reloading of the sample. To allow the bottom and top sample tubes to be sheared, the sleeve joint is removed by use of a pulley tool (Appendix A, Figure A.5). The sample container is then placed inside the shear boxes and sheared (Appendix A, Figure A.6).

4.2.2. Influence of filter cake consolidation

In this section, the influence of filter cake consolidation on the shear strength of clean filter cakes is analysed based on the results of test series C1 to C5 (Table 4.4). In these tests, the consolidation- and normal pressures are the main variables. The influence of shear rate and cement-curing time on the filter cake shear strength is discussed in later sections.

In test series C1, C2 and C3 the consolidation pressures are equal to the normal pressure during shearing, leading to 'normally consolidated' direct-shear tests (OCR = 1). Test series C4 and C5 are over-consolidated, since the consolidation pressure is higher than the normal pressure during shearing by a factor 4 (OCR = 4). As described in the above, due to the transfer between the oedometer and direct-shear apparatus, the samples are temporarily unloaded. For all samples (normally- and over-consolidated) the unloading and reloading times are set to 10 minutes. This means that the transfer from the oedometer to the direct-shear apparatus takes place within the first 10 minutes (unloading). After these 10 minutes, with the sample placed in the direct-shear apparatus, the normal pressure is applied. After 10 minutes, the direct-shear test is performed.

Figure 4.7 presents the strain-stress results of the direct-shear tests of test series C1 to C5. Figure 4.8 presents the horizontal versus vertical displacement of tests series C1 to C5. Table 4.7 presents an overview of the peak shear stresses and corresponding strain values. To analyse the variability and reproducibility of test results, each series of 4 samples is tested under the same conditions. The variability of the test results is expressed in the mean, standard variation and margin. When observing the strain-stress results (Figure 4.7), distinct peaks can be observed (peak values are summarized in Table 4.7), followed by shear softening. However, the post-peak behaviour shows irregularities, which are most probably caused by roughness or interlocking of the shear boxes interface. In addition, for some tests smaller peaks or irregularities occur prior to the main peak as well. As shown in Appendix A, Figure A.6, the sample tubes are placed within the existing shear boxes. Therefore, friction between both the shear boxes and the sample tubes influence the results. The interface of the sample tubes (PVC) has been smoothed. In addition, prior to each test, irregularities of the interface are sanded down as good as possible. Although the post-peak behaviour shows irregularities, in general the peak shear stresses show good comparison. For test series C4, the relatively large spread in results is mainly caused by one outlying result (C4.4), which shows a very sharp peak (Figure 4.7). For test series C3 the spreading of results is not caused by a single outlying result, but it is felt that the differences in peak strength are caused by differences in friction between the sample and the sample container. There seems to be a correlation between the final achieved filter cake compression (Table 4.6). Within test series C3, samples C3.1 and C3.3 show the largest compression, which indicates that for these samples, the friction between the container and sample is lowest. During the direct-shear test, as for the oedometer, the amount of friction between the sample and sample container influences the load which is effectively acting on the sample. When observing the horizontal versus vertical displacement (Figure 4.8), sample C3.1 shows the largest contractant behaviour, which also indicates relatively low friction between the sample and the sample container.

Table 4.7: Direct-shear test results for clean filter cakes (C1 to C5)

Test ID	P-cons [kPa]	N-shear [kPa]	Peak shear stress [kPa]	Strain at peak [%]	μ_{peak} [kPa]	σ_{peak} [kPa]	Margin [%]
C1.1 C1.2 C1.3 C1.4	200	200	59,5 66,6 65,6 63,5	1,04 1,03 0,99 0,71	63,8	2,7	10,7
C2.1 C2.2 C2.3	300	300	97,7 97,0 96,1	0,99 0,70 0,87	96,9	0,6	1,6
C3.1 C3.2 C3.3 C3.4	400	400	142,0 111,1 138,1 119,6	1,08 0,90 0,93 2,58	127,7	12,8	21,8
C4.1 C4.2 C4.3 C4.4*	200	50	45,8 36,6 39,4 58,5	1,15 1,82 1,17 0,81	45,1	8,4	37,4
C5.1 C5.2 C5.4	400	100	90,9 86,0 86,6	1,66 2,84 2,54	87,8	2,2	5,4

**: Relatively sharp peak, probably caused by interlocking of sample tube*

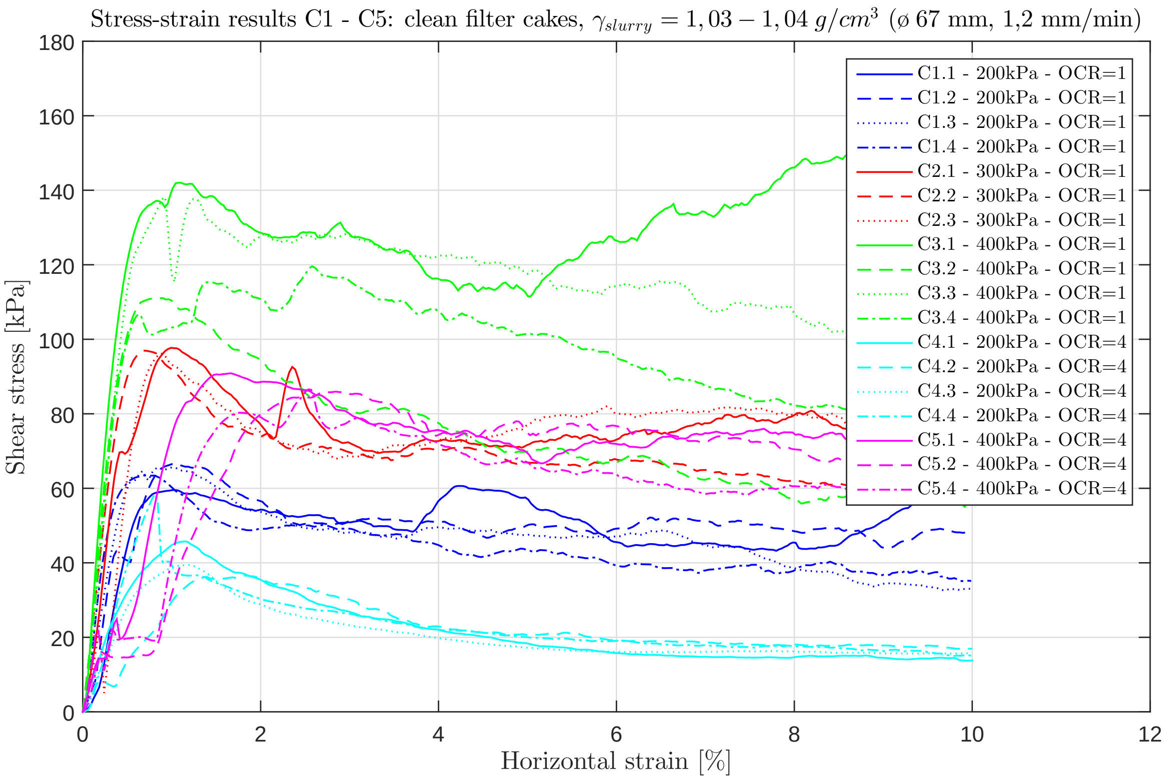

Figure 4.7: Stress-strain results direct-shear tests C1 to C5

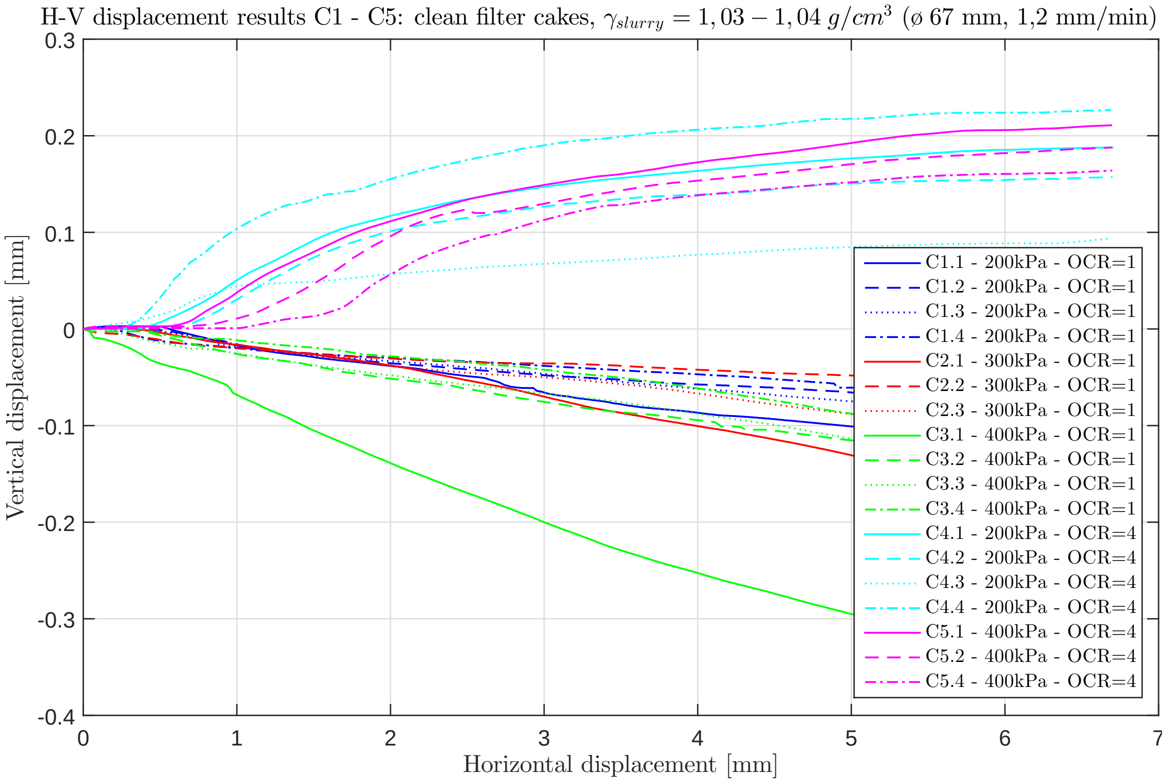

Figure 4.8: Horizontal-vertical displacement results direct-shear tests C1 to C5

The contractant behaviour during shearing of the samples in test series C1, C2 and C3 (normally consolidated filter cakes) indicates that shearing has taken place through the filter cake. However, The over-consolidated samples of test series C4 and C6 (consolidation pressure greater than normal pressure during shearing) show dilatant behaviour. This dilatant behaviour is an indication that shearing has taken place through the sand in stead of the filter cake, which means that the shear strength of the sand is lower than the filter cake. This is explained by the fact that pore water pressures generated by the consolidation pressure are not fully recovered by the lower normal stress during shearing, which causes pore water under pressure. The pore water under pressure causes an increase of effective stress, which in turn causes an increase of the filter cake shear strength. For the sand layer, these under pressures are dissipated quickly due to the high permeability of the sand. For the filter cake, the pore water under pressures can not be dissipated during shearing, due to the high shear rate (1,2 mm/min).

For the shear tests on the normally consolidated samples, pore water pressures can only be generated during shearing. The fact that contractant behaviour can be observed (Figure 4.8) indicates that some pore water dissipates from the filter cake during shearing, which allows for the volumetric strain to develop. To further analyse the drainage conditions during shearing, a comparison can be made between the hydrodynamic period of the filter cake and the time it takes to reach the peak shear strength. Equation 4.5 shows that the hydrodynamic period is a function of the consolidation coefficient and the layer thickness. As described before, it is assumed that drainage can take place on both the sand/filter cake and filter cake/cement-mortar interfaces.

$$T_{100\%} = 2,0\frac{h^2}{c_v} \tag{4.5}$$

Based on the previously estimated filter cake c_v of $2,0 \cdot 10^{-9} m^2/s$, the hydrodynamic period ranges from 16,4 minutes to 102,8 minutes, for a filter cake thickness of 2 mm to 5 mm respectively. Considering the shear rate of 1,2 mm/min and the fact that the peak shear strength occurs around 1% shear strain (less than 1 mm shear displacement), it leads to the conclusion that not all pore water pressures are allowed to dissipate within the time frame towards peak shear strength, which means that shear tests are (partially) undrained. However, at least some pore water is allowed to dissipate, since contractant behaviour is observed.

The peak shear strength values summarized in Table 4.7 are plotted in Figure 4.9. In addition, the shear strength envelop of the sand layer is provided as reference. This envelop has also been established by means of direct-shear testing. The normally consolidated samples (test series C1, C2 and C3) show a linear trend through the origin with an angle of 18,3°, which shows good comparison with results of Deltares (2008), who found a filter cake friction angle of 19,5° for a sand/filter cake/cement-mortar sample configuration. As described before, the dilatant behaviour of the over-consolidated samples (C4 and C5) indicates that a shear plane has developed through the sand layer. This is confirmed by Figure 4.9, which shows that the C4 and C5 data points are located on the shear strength envelop of the sand.

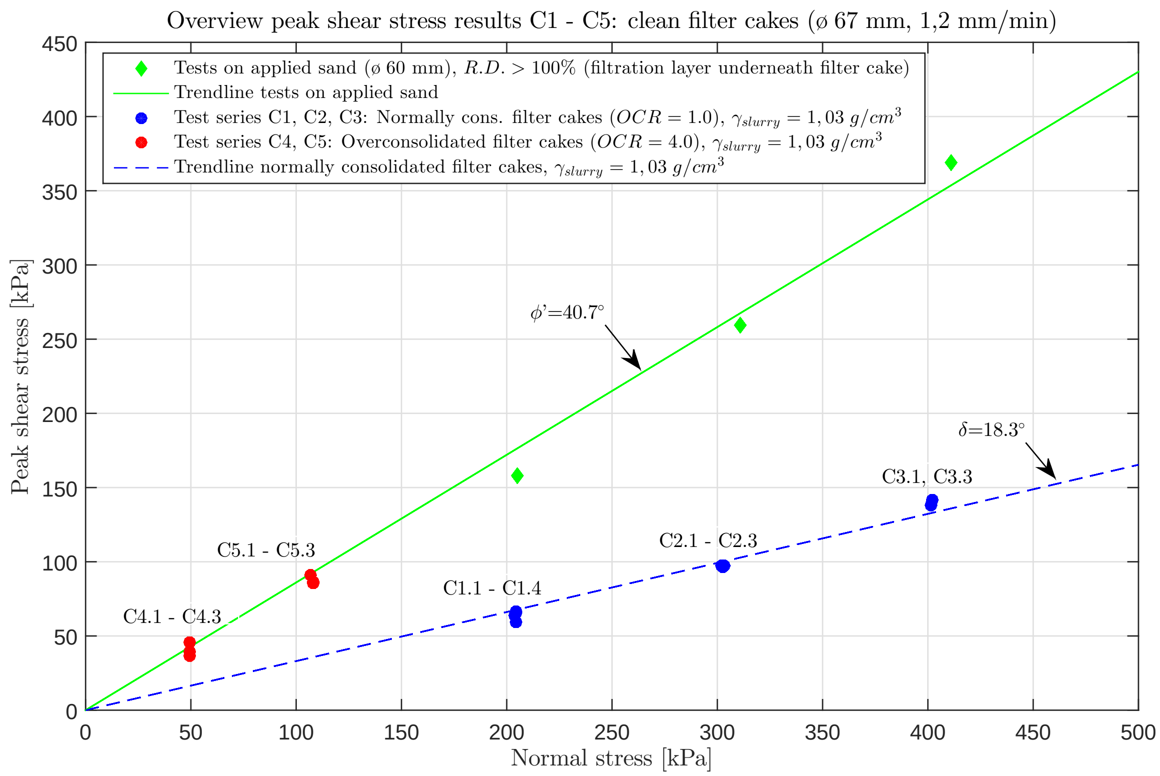

Figure 4.9: Overview of direct-shear results on clean filter cakes (C1 to C5) and added sand shear strength envelop

4.2.3. Influence of shear rate

For test series C1 to C3 (normally consolidated filter cakes), a comparison of the hydrodynamic period and shear rate led to the conclusion that a shear rate of 1,2 mm/min leads to partially undrained conditions, which causes a reduction of filter cake shear strength (although test series C1 to C3 showed contractant behaviour, indicating the dissipation of pore water pressures).

In this section, the results of tests C6.1 and C6.2 are analysed, which have been performed at a shear rate of 0,0072 mm/min. This shear rate has been chosen such that, based on the previously estimated consolidation coefficient c_v of $2,0 \cdot 10^{-9} m^2/s$, theoretically for a filter cake thickess of 5 mm the hydrodynamic period is less than the time required to reach the peak shear strength (occurring around 1 % shear strain, see Table 4.7 and Figure 4.7). The applied normal pressure for C6.1 and C6.2 is chosen at 200 kPa to be able to compare results with test series C1. Table 4.8 presents the parameter configuration and direct-shear results of tests C6.1 and C6.2.

Table 4.8: Parameter configuration and results of test series C6 (200 kPa, OCR = 1)

Test ID	**Consolidation time** [days]	**Shear rate** [mm/min]	**Peak shear stress** [kPa]	**Strain at peak** [%]	**Friction angle** [°]
C6.1	6	0,0072	88,0	1,28	23,2
C6.2	7*	0,0072	91,2	3,10	23,5
C6.3	35	1,2	66,1	0,67	18,2

**: Extra consolidation time because the long test duration of C6.1 (around 24 h)*

Figure 4.10 presents the stress-strain results of samples C6.1, C6.2 and C6.3. In addition, the results of test series C1 (200 kPa consolidation pressure and normal pressure during shearing) to serve as reference. Tests C6.1 and C6.2 (shear rate 0,0072 mm/min) clearly show a higher peak shear strength compared to test series C1 (shear rate 0,0072 mm/min) at equal normal stress during shearing (200 kPa). This causes an increase of the peak friction angle to 23,2° and 23,5° compared to the linear trend of 18,3° found for the test series C1, C2 and C3 as shown in Figure 4.9. It should be noted that the strain at peak strength of sample C6.2 is considerably larger compared to the other tests. In addition, for both sample C6.1 and C6.2 the stress-strain curve towards the peak shows some uneven behaviour, which is most probably caused by roughness of the sample tube interface. As described before, this issue is generally applicable with the applied experimental set-up. The mitigation of this issue in the new shear box design is described in a later chapter.

Figure 4.11 presents the horizontal displacement versus vertical displacement of the same tests as Figure 4.10. The larger vertical displacement observed with samples C6.1 and C6.2 shows that additional outflow of pore water has taken place during shearing compared to test series C1. The additional dissipation of pore water pressure results in an increase of effective stress, which in turn causes the higher peak shear strength observed in Figure 4.10.

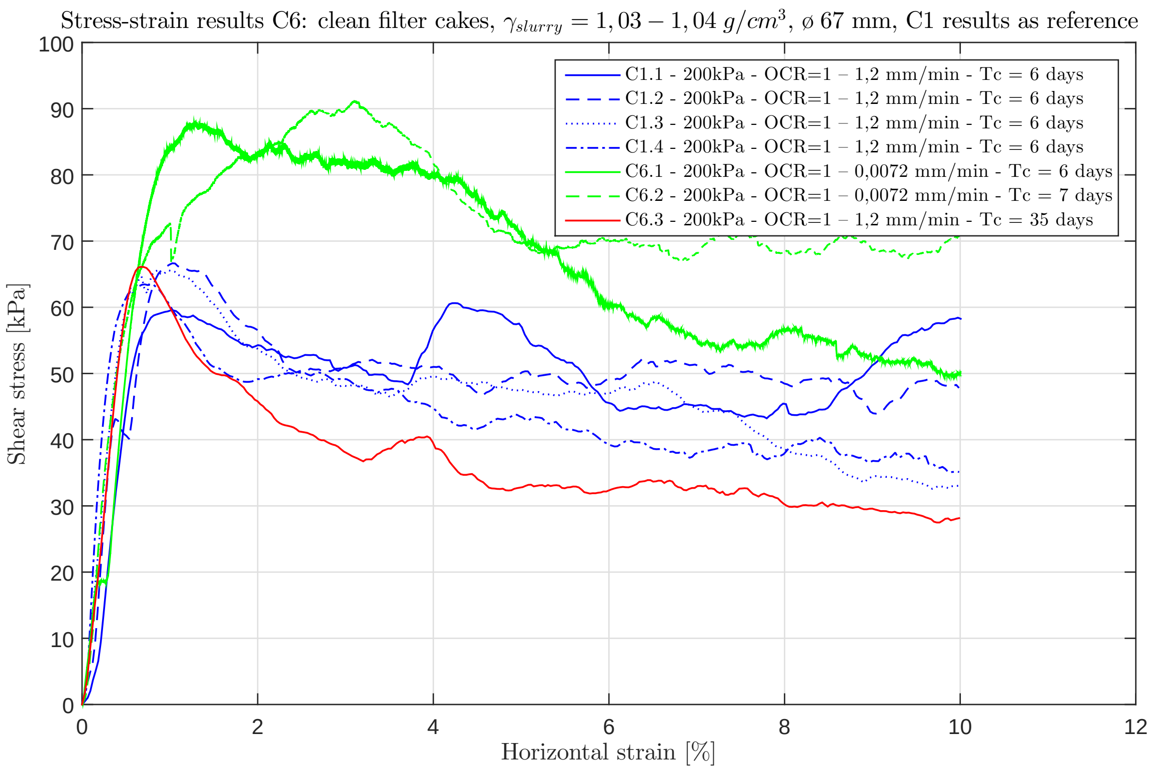

Figure 4.10: Stress-strain results direct-shear tests C1 and C6: influence of shear rate and cement-curing time T_c

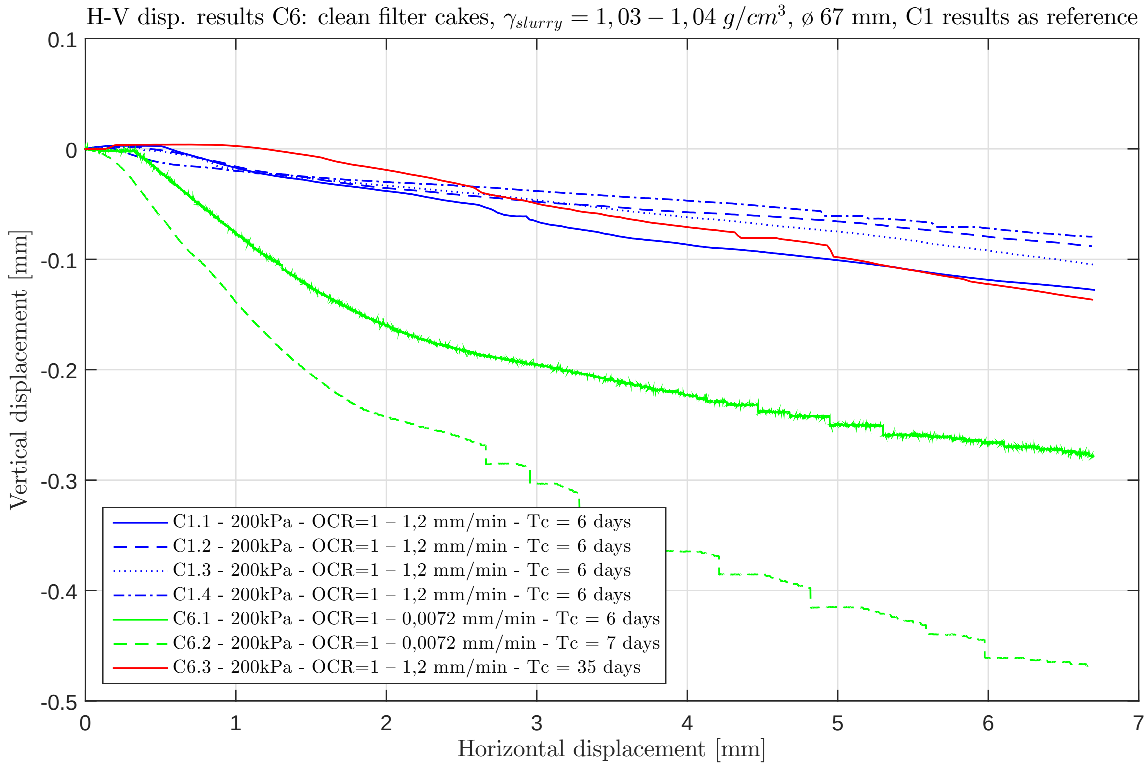

Figure 4.11: Horizontal-vertical displacement results direct-shear tests C1 and C6: influence of shear rate and cement-curing time T_c

The difference in vertical displacement between samples C6.1 and C6.2 is most probably caused by differences in friction between the sample and curing cement. However, the additional vertical displacement compared to the other tests is evident.

4.2.4. Influence of cement-curing time

To analyse the influence of the cement-curing time on the filter cake shear strength, test C6.3 has been performed with 35 days cement-curing time (Table 4.8). Comparing the peak shear strength of sample C6.3 with peak shear strength results from test series C1 (6 days cement curing time) indicates that an increase in cement-curing time does not lead to an increase in filter cake shear strength. The friction angle of 18,2° corresponds with the linear trend of 18,3° for clean filter cakes with a cement-curing time of 6 days (Figure 4.9). Thus, there seems to be no chemical strengthening effect of the filter cake due to the presence of hydrating cement after 35 days. The absence of this chemical strengthening has also been observed by Cernak et al. (1973) and Arwanitaki et al. (2007). However, it should be noted that an increase cement curing time is also expected to cause an increase of friction between the sample tube and the cement-mortar, thereby reducing the effective normal load exerted on the sample. This effect is visible in Figure 4.11, where the vertical displacement of sample C6.3 seems to be delayed compared to the other samples. In addition, only 1 test has been performed at 35 days cement-curing time.

4.3. Shear strength of contaminated filter cakes

This section presents the experimental results of the test series performed on contaminated filter cake samples (S1 to S4). First, an analysis is presented of an in-situ slurry sample from the Spoorzone Delft project. This in-situ sample analysis forms the basis for the applied slurry mixture in sample preparation. Next, the results from the sample preparation stages are discussed. This is followed by an analysis of the influence of filter cake composition on the filter cake shear strength, based on the direct-shear results from test series S1 to S3. Finally, the influence of shear rate and filter cake thickness on the filter cake shear strength are discussed (test series S4).

4.3.1. In-situ bentonite slurry sample analysis

In the context of the PhD research projects of Spruit (2015) and Van Dalen (2016) 2 'test diaphragm wall panels' were constructed at the 'Spoorzone Delft' construction project. Van Dalen (2016) obtained in-situ slurry samples from the trench during concrete pouring at different moments in time. The slurry sample analysed in this research comes from a test trench which was not de-sanded prior to concrete pouring. Therefore, the soil particles which became suspended during trench excavation were still present in the slurry. Table 4.9 presents an overview of the in-situ slurry analysed characteristics and the applied testing methods. The density of the in-situ slurry sample (1,27 g/cm^3) is considerably higher compared to the 'clean' slurry applied in the previously discussed experiments (1,03-1,04 g/cm^3). The in-situ slurry density in this research is also higher compared to the average slurry density (prior to de-sanding) found at the Houtwal project in Harderwijk (1,22 g/cm^3) (Van Dalen, 2016).

Table 4.9: Overview of properties in-situ sample Spoorzone Delft

Property	**Value**	**Test method**
Slurry density	1,27 g/cm^3	Mudbalance
Water content	203 %	Oven drying
Organic content (LOI)	6,8 %	Oven ignition (According to NEN-EN 15935)
Sand content ($\geq 63\mu m$, relative to total mass of solids)	34,4 %	Dry sieving / Hydrometer (According to BS 1377-2:1990)

The slurry composition is mainly determined by the soil profile in which trench excavation takes place. Trench excavation causes soil particles to 'fall' from the excavation face or equipment and become suspended in the support fluid. During excavation, the vertical movement of the excavation equipment causes mixing of the support fluid over the complete trench depth. Due to this mixing, it is expected that the composition of the support fluid is more or less constant over the height of the trench. The organic content of the examined slurry sample is most probably the result of trench excavation through a peat layer. Figure 4.12 presents the sieve curve of the in-situ slurry sample.

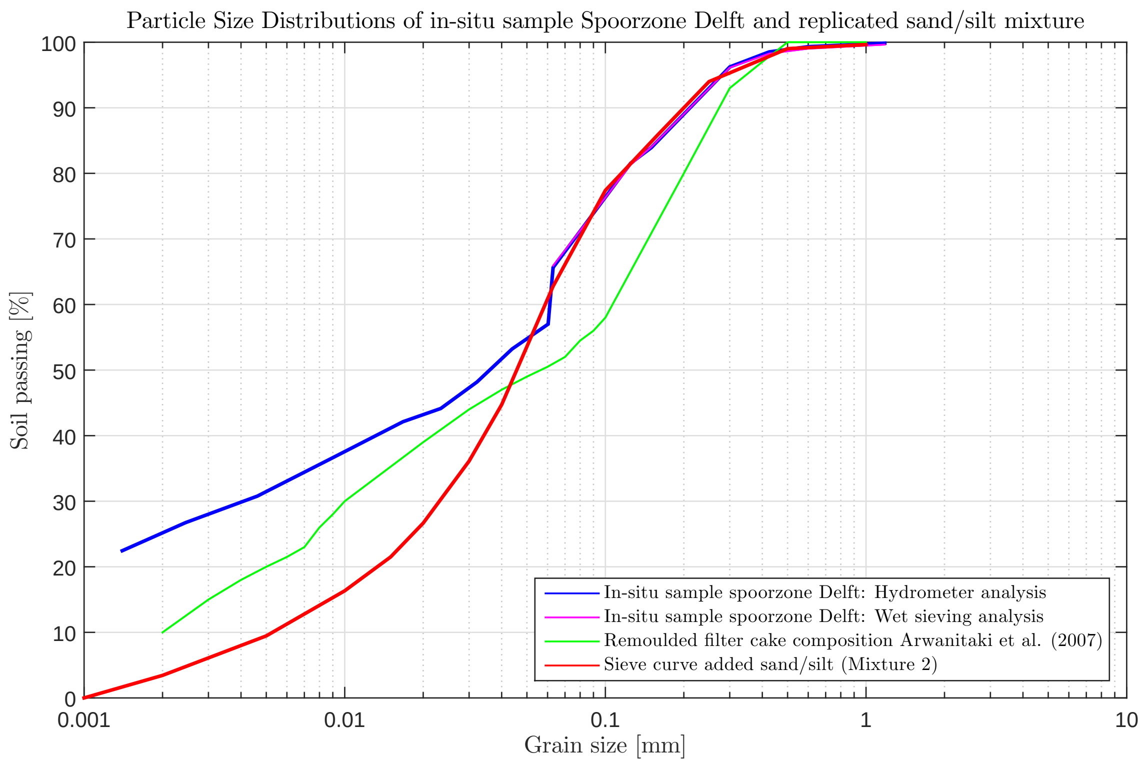

Figure 4.12: Spoorzone Delft in-situ sample analysis and sand/silt mixture applied in sample preparation. Sieve curve by Arwanitaki et al. (2007) added as reference

The filter cake sieve curve found by Arwanitaki et al. (2007) at the 'Conradstraat' project in Rotterdam is added to Figure 4.12 as a reference. Compared to the 'Conradstraat Rotterdam' sieve curve by Arwanitaki et al. (2007), the 'Delft Station' sieve curve shows a finer distribution. Arwanitaki et al. (2007) found a clay content of around 10 %, whilst the clay content found in the 'Delft Station' sample is above 20 %, based on the particle size distribution (Figure 4.12). In addition, Arwanitaki et al. (2007) did not report an organic content.

Arwanitaki et al. (2007) replicated the 'Conradstraat Rotterdam' filter cake composition by mixing bentonite powder and quartz (fine sand and silt), according to the in-situ particle distribution. Their water content was chosen such to replicate the in-situ consistency and tests were performed directly on the replicated filter cake (also see Literature Review). In this research, the filter cake is formed by a filtration process. Therefore, the filter cake composition is governed by the slurry composition. Based on the in-situ sample analysis, 2 experimental slurry compositions are established. The recipes of the 2 slurry compositions are presented in Table 4.10. Based on the approach by Arwanitaki et al. (2007), the in-situ particle distribution is replicated by a combination of quartz powder (silt) and different sand fractions. The first recipe replicates the material $\geq 0,125mm$, by means of adding 3 different sand fractions. The second recipe aims to replicate the complete sieve curve. The proportion of these different constituents is based on the in-situ sieve curve. The bentonite concentration is kept at 4%, equal to the bentonite concentration applied for the 'clean' filter cakes. The total amount of added solids is based on the measured water content of the in-situ slurry. Table 4.10 presents the mixture recipe. The particle size distribution is presented in Figure 4.12. It should be noted that the replicated sieve curve is based on the particle size distribution as stated on the product specification of the Microsil M6 (D).

Table 4.10: Recipes of contaminated slurry, based on in-situ slurry analysis

Mixture 1		**Mixture 2**	
Constituent	**Quantity** [kg]	**Constituent**	**Quantity** [kg]
Water	10,0	Water	10,0
Bentonite (Trench Control AT)	0,40	Bentonite (Trench Control AT)	0,40
Sand fraction: 0,125 mm - 0,25 mm	0,68	Microsil M6	4,21
Sand fraction: 0,25 mm - 0,5 mm	0,22	Sand fraction: 0,25 mm - 0,5 mm	0,25
Sand fraction: 0,5 mm - 1,0 mm	0,074	Sand fraction: 0,5 mm - 1,0 mm	0,048

Figure 4.12 shows that the replicated mixture is finer compared to the in-situ sieve curve. This is caused by the particle size distribution of the available Microsil M6. In addition, no organic or clay content is taken into account. It is thought that the increased filter cake shear strength for contaminated filter cakes found by Henry et al. (1998) and Arwanitaki et al. (2007) is mainly caused by the presence of granular material. The organic and clay content will have an effect on the compressibility of the filter cake. The friction angle of the added soil mixture (Microsil and sand fractions) was found to be around 40° for a loose packing (around 1,40 kg/dm^3) and around 50° for a dense packing (around 1,60 kg/dm^3) based on triaxial tests on the dry material (Appendix E).

4.3.2. Sample preparation results

Filtration stage

Contaminated filter cakes are produced by filtration of a contaminated slurry (Table 4.10). As described in the parameter configurations section (Table 4.4), 2 different contaminated slurry compositions are applied. In test series S1 slurry mixture 1 is applied, which leads to a slurry density of 1,06 g/cm^3, only slightly heavier compared to the 'clean' slurries applied in the previous experiments on clean filter cakes (1,03 - 1,04 g/cm^3). In test series S2, S3 and S4 slurry mixture 2 is applied, which leads to slurry densities in the range of 1,26 - 1,27 g/cm^3, which corresponds to the measured in-situ density (Table 2.1). Appendix B, Figure B.4 shows that the refilled slurry volume during filtration develops with $\sqrt{t}$. This has also been observed for the 'clean' slurry in the previous section (Appendix B, Figures B.1 and B.2). Figure B.4 shows that the development of refilled slurry volume for clean slurry (samples

C1.1 - C1.4), contaminated slurry, mixture 1 (samples S1.1 - S1.4) and contaminated slurry, mixture 2 (test series S2.1 to S4.4) is almost identical. However, Table 4.11 shows that the measured filter cake growth rate increases for a contaminated slurry compared to the clean bentonite suspension (Table 4.6). For test series S1 (contaminated slurry mixture 1) the filter cake growth rate is increased from around 0,2 $mm/\sqrt{min}$ for a clean slurry to just under 0,24 $mm/\sqrt{min}$ due to the presence of the added sand fractions (slurry density increased from 1,03 g/cm^3 to 1,06 g/cm^3). For test series S2 to S4 (contaminated slurry mixture 2), the addition of the silt caused a further increase of the filter cake growth rate to over 0,31 $mm/\sqrt{min}$. This increase is less severe than the filter cake growth rate of over 0,6 $mm/\sqrt{min}$ found by Arwanitaki et al. (2007) for a contaminated slurry at a filtration pressure of 50 kPa.

Consolidation stage

The observed filter cake compression in test series S1 (Table 4.11) is of the same order as for the clean filter cakes (Table 4.6). For test series S2, S3 and S4 the observed filter cake compression is considerably lower compared to the clean filter cakes. Apparently the presence of the large silt content causes a strong reduction in the filter cake compressibility. As stated before, the organic and clay content of the in-situ slurry have not been taken into account, which may influence the filter cake compressibility considerably. Based on Equation 4.4, the consolidation coefficient is estimated to be around $9,0 \cdot 10^{-9} m^2/s$. When comparing the consolidation data of the clean filter cakes with the contaminated filter cakes (Appendix B, Figures B.3 and B.6) the consistency of results has improved. The combination of increased filter growth rate and decreased compressibility causes a much thicker filter cake after the consolidation stage for test series S2 and S3 compared to the tests on clean filter cakes (around 20 mm versus 2 to 5 mm).

Table 4.11: Results of sample preparation stage for test series on contaminated filter cakes (S1 to S4)

Test ID	**Slurry density** [g/cm^3]	**Filtration time** [hours]	**Filter cake thickness** [mm]	**Filter cake growth rate** [$mm/\sqrt{min}$]	**Consolidation pressure** [kPa]	**Filter cake Compression** [mm]	[%]
S1.1	1,06	184*	25	0,238	200	21,5	86
S1.2						20,5	82
S1.3						19,7	79
S1.4						21,1	84
S2.2**	1,26	164	34	0,342	200	12,4	36
S2.3						11,9	35
S2.4						12,7	37
S3.3***	1,26	161	31	0,315	400	13,8	44
S3.4						15,0	48
S4.1	1,27	72****	22	0,336	200	9,8	45
S4.2						11,7	53
S4.3						10,7	49
S4.4						10,9	50

**: Longer filtration time due to planning difficulties*
***: Sample S2.1 failed when removing top sample tube to expose filter cake*
****: Samples S3.1 and S3.2 failed in consolidation phase (squeezing)*
*****: Shorter filtration time to analyse the influence of filter cake thickness (reference tests)*

4.3.3. Influence of filter cake composition

In this section the influence of filter cake composition on the filter cake shear strength is analysed based on the results of test series S1 to S3 (Tabel 4.4). Contaminated filter cakes are produced by filtration of a bentonite slurry contaminated with soil material, of which the composition is based on the previously discussed in-situ sample analysis. Table 4.12 presents the direct-shear results of test series S1 to S3.

The stress-strain curves of test series S1 to S3 are presented in Figure 4.13, Figure 4.14 presents the horizontal versus vertical displacement.

Table 4.12: Direct-shear test results for contaminated filter cakes (S1 to S3)

Test ID	**P-cons** [kPa]	**N-shear** [kPa]	**Peak shear stress** [kPa]	**Strain at peak** [%]	μ_{peak} [kPa]	σ_{peak} [kPa]	**Margin** [%]
S1.1 S1.2 S1.3 S1.4	200	200	66,6 66,7 114,8* 72,2	1,03 1,15 1,85 0,89	68,5	2,6	7,7
S2.2** S2.3 S2.4**	200	200	86,3 94,8 87,3	0,7 0,94 0,52	89,5	3,8	9,0
S3.3 S3.4	400	400	212,6 205,2	3,95 5,39	208,9	3,7	3,5

**: Relatively sharp peak, probably caused by interlocking of sample tube*
***: Second, higher peaks ignored*

The peak shear strength results of test series S1 (based on slurry mixture 1, Table 4.10) show good comparison with the peak shear strength results from test series C1 (Table 4.7), which involved clean filter cakes at equal normal stress (200 kPa) and shear rate (1,2 mm/min). This indicates that the addition of part of the sand curve into the slurry (increasing γ_{slurry} from 1,03 g/cm^3 to 1,06 g/cm^3), does not lead to an increase of filter cake shear strength. It should be noted that sample S1.3 shows a sharp peak, which is most probably caused by interlocking of the sample tubes. This peak is interpreted as an outlying result and has therefore not been taken into account for further analyses.

Test series S2 shows an increased peak shear strength compared to test series C1 and S1 at equal normal stress (200 kPa) and shear rate (1,2 mm/min). It should be noted that for test series S2, samples S2.2 and S2.4 reach a peak in 2 steps (Figure 4.13). Since it is thought that the second peak is caused by interface roughness or interlocking of shear boxes, the first peaks are considered as peak shear strength. Test series S3 also shows 2 peaks towards the final peak shear strength. However, for these tests the second peaks are interpreted as peak shear strengths, because it is thought that the first peak is caused by shear box interlocking or slipping of the tension rod. It should be noted that the peak stress for samples S3.3 and S3.4 occurs at higher strain values compared to the other tests.

When analysing the development of vertical displacement of test series S2 and S3 (Figure 4.14), it shows that a higher normal pressure during shearing causes an increase in contractant behaviour. In addition, when comparing the vertical displacement of test series S1 and S2 (both 200 kPa normal pressure), test series S1 shows more contractant behaviour, which is most probably caused the lower filter cake thickness (Table 4.11), allowing more dissipation of pore water pressures during shearing. For test series S1 to S3, as for the consolidation results (Appendix B, Figure B.6), the vertical displacement during shearing of test series S1 to S4 also shows better consistency (Figure 4.14) compared to test series C1 to C6 (Appendix B, Figures B.3 and 4.8). It is felt that this improved consistency is mainly caused by gained experience with the experimental procedure. The influence of friction between the curing cement mortar and the sample tube, which increases with continuing cement curing, seems to decrease or at least stay more constant. This can be both caused by more consistent application of the cement-mortar and quicker application of the consolidation load. However, the interface roughness of the shear boxes and sample tubes seems to influence the direct-shear results. Although the post-peak behaviour appears to be more consistent than is the case for the clean filter cakes (Figures 4.7, 4.10 and 4.13), especially test series S2 and S3 showed multiple peaks at small horizontal strains.

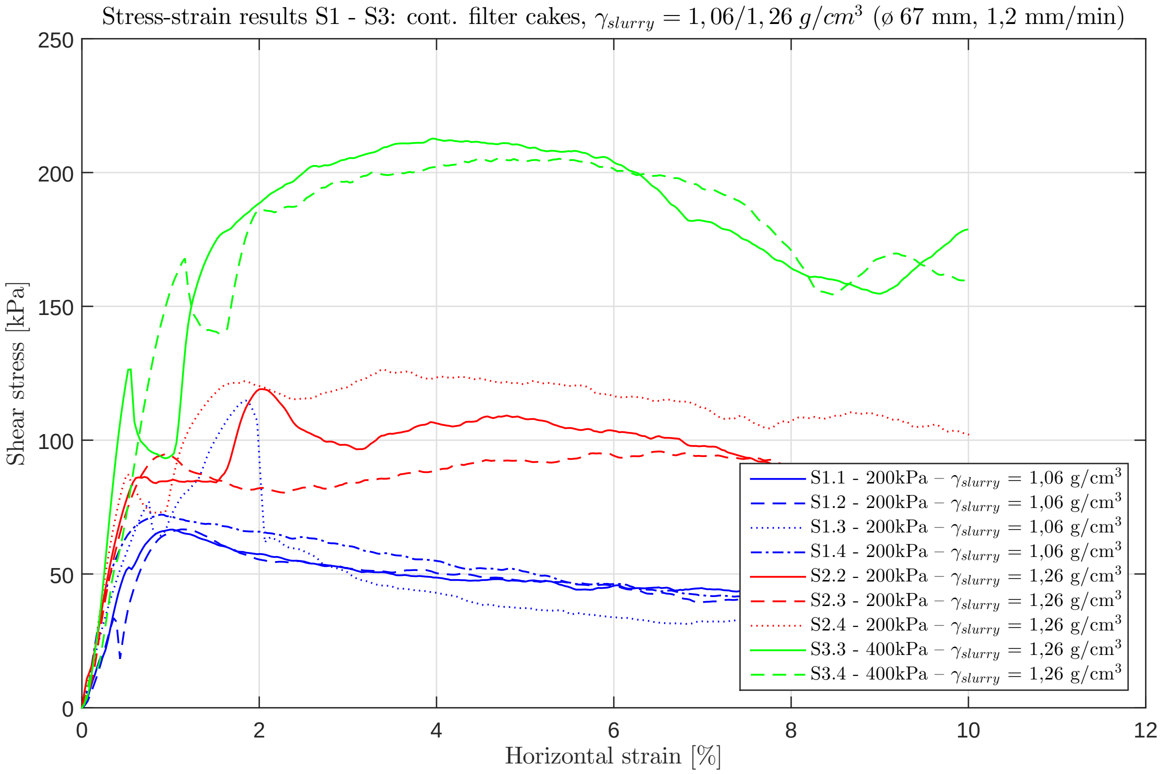

Figure 4.13: Stress-strain results direct-shear tests S1 to S3

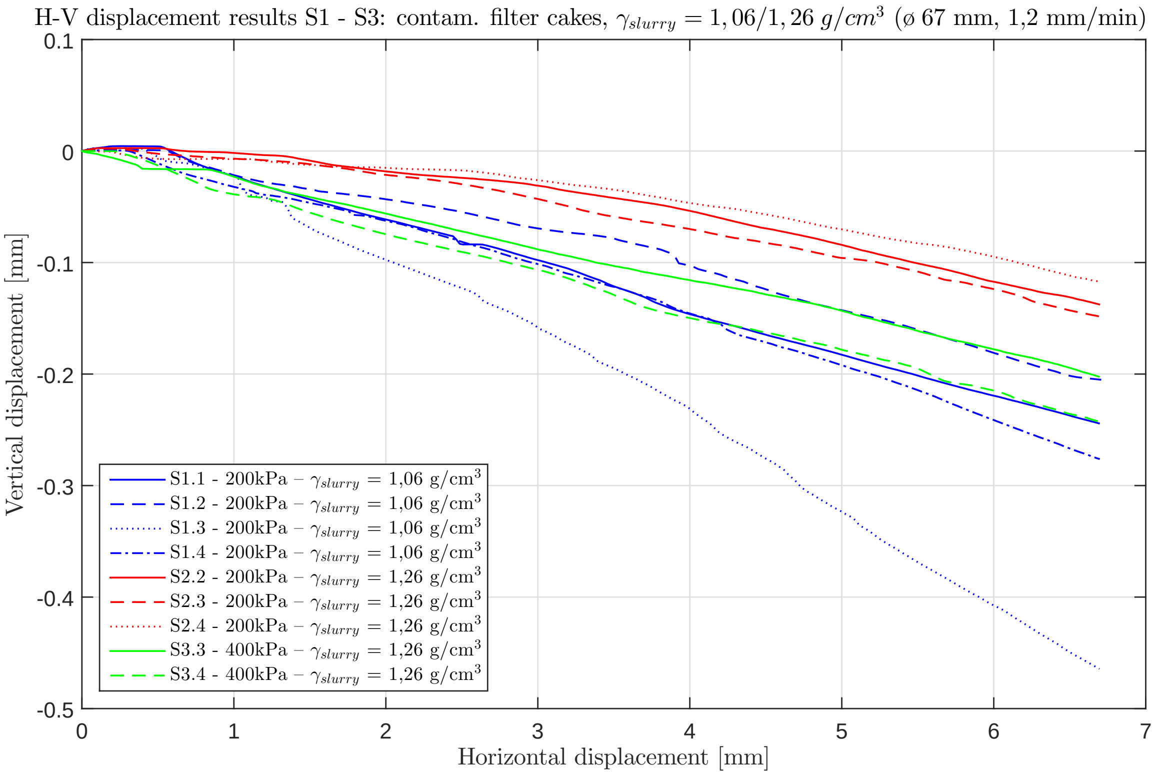

Figure 4.14: Horizontal-vertical displacement results direct-shear tests S1 to S3

The peak shear stress results presented in Table 4.12 are plotted in Figure 4.15. As already mentioned, the peak shear strength of test series S1 (contaminated slurry mixture 1, 1,06 g/cm^3) show only a slight increase compared to the clean filter cakes (clean slurry, 1,03 g/cm^3) at equal normal pressure (200 kPa) and shear rate (1,2 mm/min), but still corresponding to the linear trend of 18,3° based on test series C1, C2 and C3. The peak shear strength results of test series S2 and S3 (contaminated slurry mixture 2, 1,26 g/cm^3) show a linear trend of 25,6°. This increased friction angle is mainly caused by the presence of the silt material in the filter cake. Triaxial on the sand/silt mixture (dry) showed a friction angle of around 40° (Appendix E). As already mentioned in the literature review, Henry et al. (1998) found friction angles between 31° and 33° for filter cakes with added sand and silt. Arwanitaki et al. (2007) found friction angles of 28,6° (Triaxial test, CU) and 30,7° (Direct-shear, CD) for a remoulded filter cake, also based on the addition of sand and silt to replicate an in-situ filter cake composition (Figure 4.12).

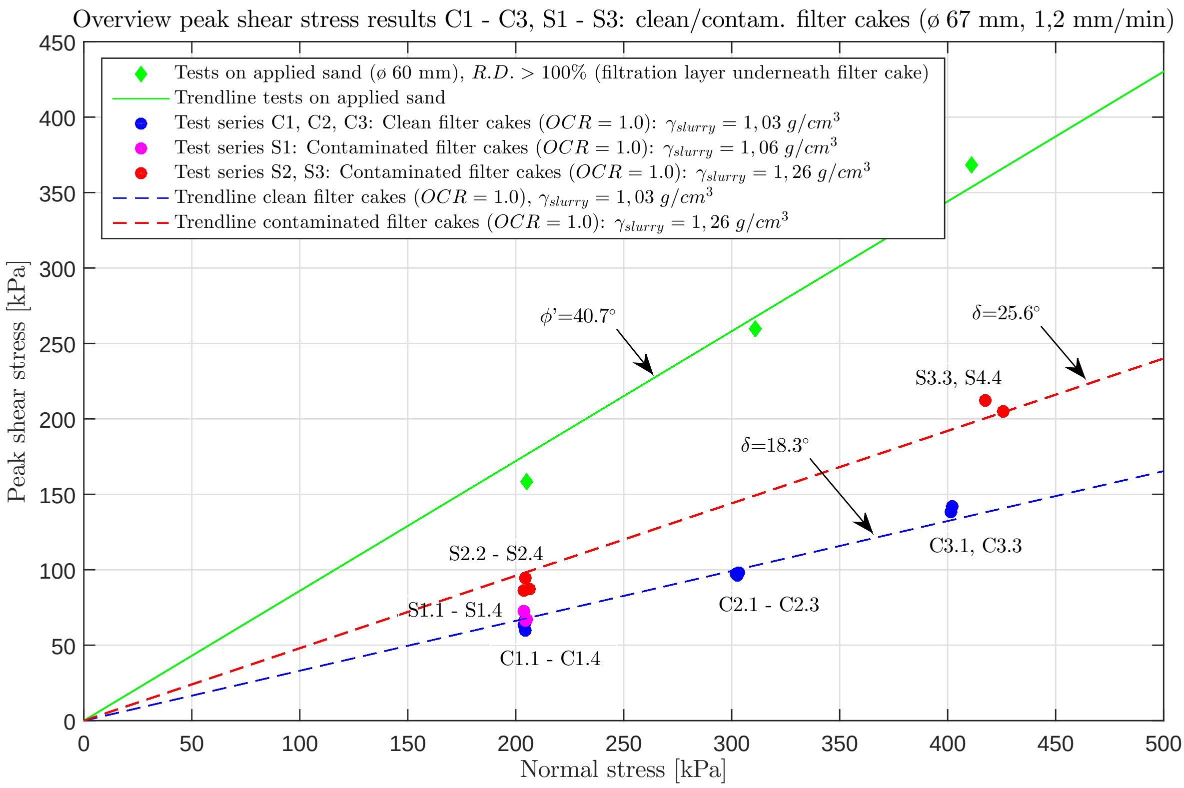

Figure 4.15: Overview of direct-shear results on clean and contaminated filter cakes, with added sand shear strength envelop

4.3.4. Influence of filter cake thickness and shear rate

As for test series C1 to C3, test series S1 to S3 showed contractant behaviour, indicating the dissipation of pore water pressures during shearing. Based on a comparison of the shear rate and hydrodynamic period, in test series C1 to C3 shearing has taken place (partially) undrained. Due to the higher filter cake growth rate for the contaminated filter cake tests (Table 4.11) compared to clean filter cake tests (Table 4.6), the filter cake thickness during shearing is higher, leading to an increase of the hydrodynamic period as indicated by Equation 4.5. This indicates that for test series S1 to S3, shearing was (partially) undrained. As shown in Table 4.11, test series S4 involves a reduced filtration time, leading to filter cake thickness values of 22 mm, which is of the same order as for the clean filter cake test series (around 20 mm). Tests S4.1 and S4.2 investigate the influence of filter cake thickness on the filter cake shear strength. The influence of the shear rate (0,0072 mm/min, equal for test series C6) is analysed in tests S4.3 and S4.

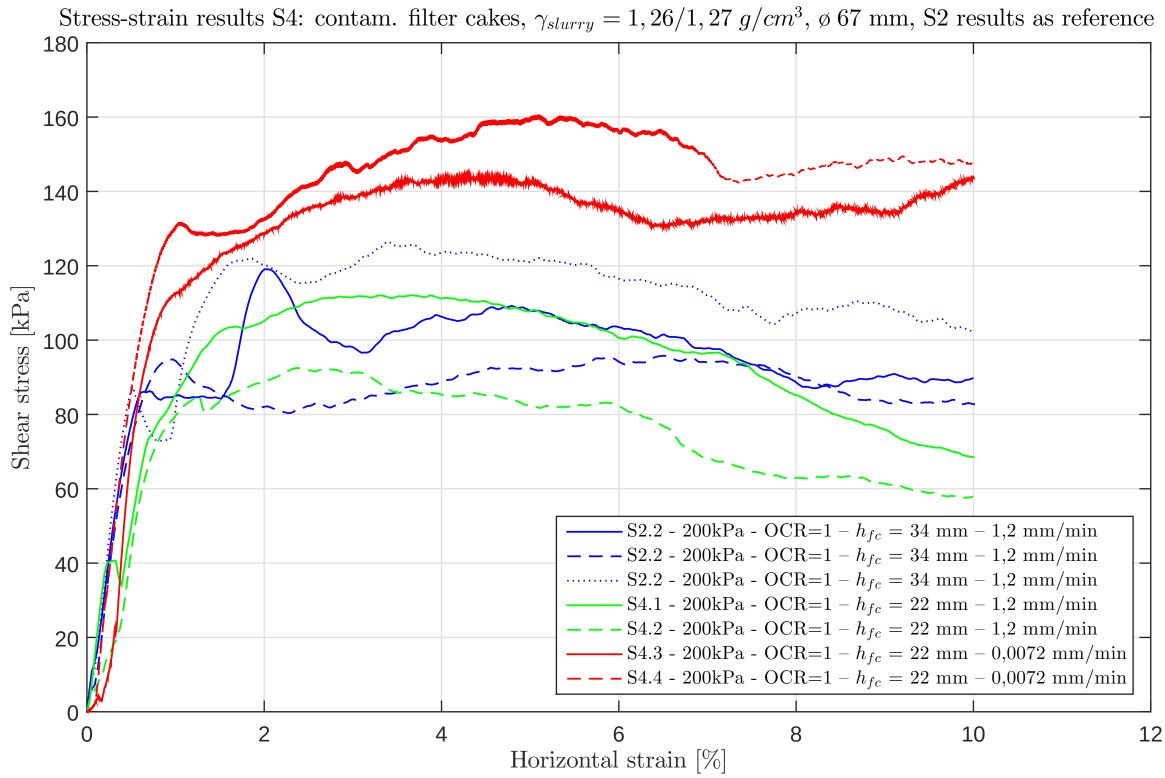

Figure 4.16: Stress-strain results direct-shear tests S2 and S4

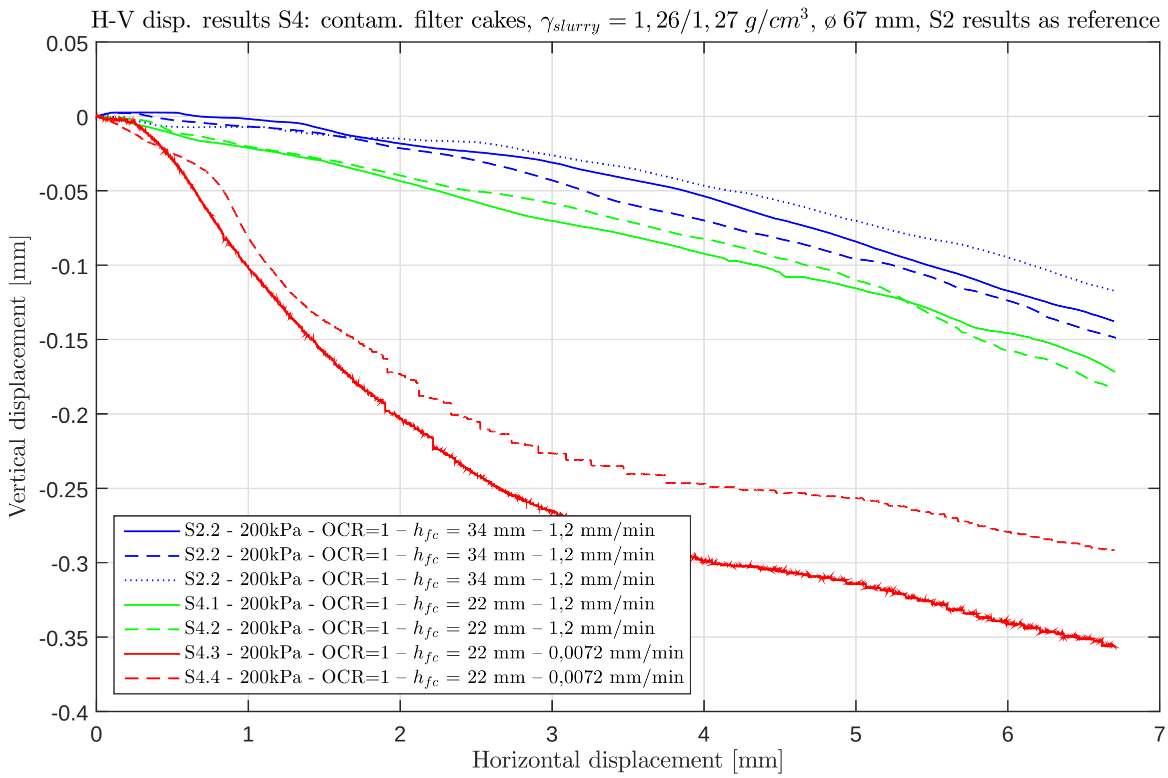

Figure 4.17: Horizontal-vertical displacement results direct-shear tests S2 and S4

Table 4.13: Parameter configuration and results of reference tests on contaminated filter cakes (200 kPa, OCR = 1)

Test ID	**Filter cake thickness*** [mm]	**Consolidation time** [days]	**Shear rate** [mm/min]	**Peak shear stress** [kPa]	**Strain at peak** [%]	**Friction angle** [°]
S4.1	22	6	1,2	111,0	3,31	28,01
S4.2	22	6	1,2	92,5	2,38	23,97
S4.3	22	6	0,0072	110,7	0,92	28,48
S4.4	22	7**	0,0072	131,5	1,07	32,75

**: Filter cake thickness prior to consolidation*
***: Extra consolidation time due to the long test duration of S4.3 (around 24 h)*

Figure 4.16 shows that the shear rate of 0,0072 mm/min results in an increased peak shear strength compared to a shear rate of 1,2 mm/min. The same was observed for the clean filter cakes. The reduced filter cake thickness does not lead to a clear increase of peak shear strength. The reduced shear rate allows for additional dissipation of pore water pressures during shearing, which is indicated by the increased vertical deformation during shearing (Figure 4.17). The reduced filter cake thickness at equal shear rate also shows an increase of vertical deformation during shearing. However, as stated before, this is not accompanied by a clear increase of peak shear strength (Figure 4.16).

4.4. Conclusion

The first experimental phase of this thesis has focussed on the shear strength of the filter cake, which is the lower boundary shear strength of the soil/diaphragm wall interface. Direct-shear tests have been performed on sand/filter cake/cement-mortar samples, applying a large filter cake thickness to avoid discontinuities in the filter cake shear plane. Both clean and contaminated filter cakes have been analysed to investigate the influence of filter cake composition on the filter cake shear strength.

For sample preparation of the clean filter cake samples, a bentonite suspension based 4% Cebogel Trenchcontrol AT (relative to mass of water) has been applied (1,03 g/cm^3). A filter cake growth rate has been observed around 0,20 $mm/\sqrt{min}$ (20 kPa filtration pressure), which corresponds to the range of 0,22 - 0,24 $mm/\sqrt{min}$ found by Lubach (2010) for equal filtration pressure. The difference might be explained by the fact that the filtration pressure was not constant during filtration, due to the lowering of the slurry level in the standpipe, despite of regular refilling. Normally consolidated (OCR = 1) direct-shear tests have been performed at normal pressures of 200 kPa, 300 kPa and 400 kPa at a shear rate of 1,2 mm/min. An analysis of peak shear strength results shows a linear trend with a friction angle of 18,3°. This value corresponds to the Deltares (2008) result of 19,5°, which forms the basis of the current recommendations on δ in the CUR 231 . Based on these test results, the current recommendations are not conservative. However, although contractant behaviour was observed for all normally consolidated direct-shear tests (1,2 mm/min), a comparison of shear rate and hydrodynamic period (based on oedometer results) leads to the conclusion that shearing has at least taken place partially undrained. Reference tests with a shear rate of 0,0072 mm/min showed additional contractant behaviour, with peak friction angles around 23°. It should be noted that only 2 tests have been performed with this shear rate. In addition, test results indicate that shear box friction has generally influenced the direct-shear tests, causing irregular development of shear stress both towards the peak as in post-peak behaviour. An additional reference test on clean filter cake (1,2 mm/min) indicates that no shear strength increase takes place for increased exposure time of filter cake with hydrating cement, which indicates the absence of chemical strengthening of the filter cake by cement hydration, as already stated by Cernak et al. (1973) and (Arwanitaki et al., 2007).

For the direct-shear tests on over-consolidated filter cake samples (OCR = 4), the filter cake shear strength exceeded the shear strength of the sand layer. This indicates that for conditions where the lateral concrete pressure exceeds the normal soil pressure, an increased filter cake shear strength can be taken into account. However, part of the observed increased filter cake shear strength is caused by the presence of pore water under pressure prior to shearing due to the short reloading time. For further research it is therefore recommended to apply a longer reloading time to ensure complete pore water dissipation prior to shearing, which better models in-situ conditions, since building pit excavation is a slow process.

An analysis of an in-situ slurry sample from the Spoorzone Delft project shows a strong increase of the volumetric weight (1,27 g/cm^3) due to contamination by excavated soil material. Based on the obtained sieve curve (combination of dry sieving and hydrometer analysis), a replicated contaminated slurry has been applied in sample preparation to create contaminated filter cakes. The in-situ sieve curve has been replicated by adding a sand/silt mixture to a clean suspension (4 % bentonite) according to the measured in-situ water content. An important limitation of this method is that the organic- and clay content has not been taken into account. As already shown by (Arwanitaki et al., 2007), a higher filter cake growth rate has been observed for the contaminated slurry (> 0,30 $mm/\sqrt{min}$) for equal filtration pressure (20 kPa). The addition of the sand/silt material causes lower filter cake compression in the consolidation stage. However, since the organic- and clay content are not taken into account, it is concluded that the observed compressibility is not representative for in-situ filter cakes. The addition of only the sand curve (mixture 1, volumetric weight increased to 1,06 g/cm^3) shows negligible increase of filter cake shear strength compared to the clean filter cake tests (shear rate 1,2 mm/min). However, direct-shear tests on samples based on slurry mixture 2 (volumetric weight increased to 1,26 g/cm^3) show a linear trend of 25,6° (no cohesion) for a shear rate of 1,2 mm/min. As for the clean filter cakes, a comparison of the shear rate and hydrodynamic period leads to the conclusion that shearing has taken place (partially) undrained, although contractant behaviour has been observed. Reference tests for a lower filter cake thickness at equal shear rate showed additional contractant behaviour during shearing, which is explained by the decreased drainage length. The lower filter cake thickness combined with a decreased shear rate (0,0072 mm/min) showed additional contractant behaviour and a considerable increase of peak shear strength, resulting in friction angles of 28,5° and 32,8°. This range corresponds to Henry et al. (1998) and Arwanitaki et al. (2007), who showed contaminated filter cake friction angles of 31° - 33° and 29° respectively.

Finally, the applied experimental set-up and procedure showed some issues, which have influenced the test results. First of all, the influence of shear box friction on the direct-shear test results has already been mentioned. For most of the tests, the shear stress development shows irregularities. The mitigation of this issue is an important recommendation for the development of the 'phase-2' direct-shear set-up. In addition, in future tests the consolidation pressure should be applied as fast as possible to decrease the influence of sample tube friction by the curing cement-mortar or concrete, whilst avoiding squeezing of the sample. In addition, the applied filtration method with the standpipe does not provide a constant filtration pressure.

5

Experimental Phase 2: Development of a modified direct-shear set-up

In this chapter the design of a new modified direct-shear set-up is presented. The internal plan dimensions of the new shear boxes are 170 mm x 170 mm. The bottom and top shear boxes have a height of 52 mm and 100 mm respectively. First the different design considerations are discussed and an overview of the direct-shear set-up is presented. Next, the process of sample preparation and the corresponding design features are presented. Finally, some conclusions are drawn.

5.1. Design considerations and equipment overview

The main purpose of the development of a larger modified direct-shear set-up is to enable the analysis of the effect of aggregate protrusion on the interface shear strength. In The Netherlands a maximum aggregate size of 16 mm is commonly applied in diaphragm wall concrete mix designs (CUR/COB, 2010). The smaller 'phase-1' direct-shear set-up (Ø 67 mm) is not suited for this purpose due to its small scale relative to the maximum aggregate size. Table 5.1 presents an overview of the shear box characteristics in previous research. Only Lam et al. (2014) reported their maximum aggregate size (20 mm). They state that their shear box dimensions do not have a theoretical basis, but are chosen to provide 'reasonable' scale with respect to the maximum aggregate size. Both Lam et al. (2014) and Cernak et al. (1973) chose rectangular plan dimensions for their S/FC/CON tests.

Table 5.1: Test characteristics previous research

Research	**Sample Configuration**	**Shear box dimensions** [mm]	**Max aggregate size** [mm]	**Interface spacing** [mm]	**Max normal pressure** [kPa]
Lam et al. (2014)	S/FC/CON	175 x 275	20	20	360
Deltares (2008)	S/FC/MOR	Ø 65	n.s.*	n.s.	250
Arwanitaki et al. (2007)	S/FC/MOR	300 x 300	n.s.	n.s.	160
Henry et al. (1998)	S/FC/MOR	100 x 100	n.s.	n.s.**	100
Cernak et al. (1973)	S/FC/CON	150 x 400	n.s.	n.s.	100

**: Not specified*
***: Henry et al. (1998) applied an interface spacing, size not specified*

Considering the shear box dimensions of Lam et al. (2014) relative to their maximum aggregate size, a shear box width and length of at least 10 times the maximum aggregate size (16 mm in this research) is desired. This would lead to minimum dimensions of 160 mm x 160 mm. The main design philosophy of the new set-up is the development of special shear boxes which can be placed in an existing direct-shear machine. Figure 5.1 presents an overview of the modified direct-shear set-up, showing the existing direct-shear frame including the special shear boxes. The dimensions of the available direct-shear machine limited the shear box size. The main limitation is the location and capacity of the lever arm which provides a normal load during shearing, whilst allowing vertical deformation. By increasing the sample area, the required normal load for a certain normal stress increases. In addition, the normal load must act in the center of the sample. An increase in shear box length shifts the sample center towards the weight arm, reducing the effective lever arm. Eventually, internal shear box dimensions of 170 mm x 170 mm provide sufficient scale with respect to the maximum aggregate size. In addition, the dimensions allow for the application of 200 kPa normal pressure by using the existing lever arm (Figure 5.1).

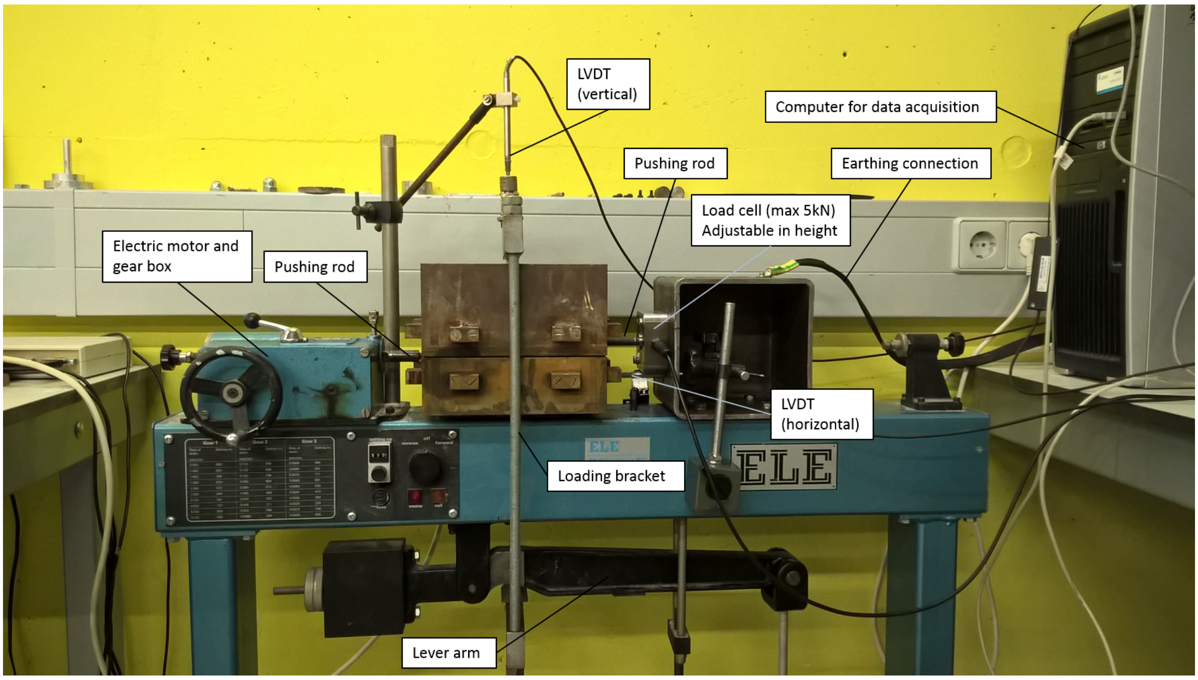

Figure 5.1: Overview of the modified direct-shear machine

The following components of the original direct-shear set-up are applied in the new configuration:

- General steel frame (accommodates all other components);
- Electric motor and gearbox;
- Frame for vertical displacement measuring device;
- Lever arm to apply normal load (using weights) and to allow for vertical deformation.

The following components have been modified or added to the existing frame:

- Modified loading frame to accommodate load cell (adjustable in height) and horizontal LVDT (Linear Variable Deformation Transformer);
- LVDT's for both horizontal and vertical displacement measurements;
- Load cell (max 5 kN);
- Modified loading bracket with increased width (220 mm);
- Additional earthing connection.

The design and performance of the 'phase-1' set-up are taken into account for the design of the 'phase-2' set-up. This mainly applies to the design of the shear boxes and the sample preparation procedure. The 'phase-1' set-up allows the simultaneous preparation of 4 samples, outside the direct-shear machine. This means that the direct-shear machine itself can be used for other purposes during sample preparation. Another advantage of the 'phase-1' set-up is the large slurry volume available for filtration due to the use of a standpipe. However, apart from the small scale the 'phase-1' set-up also provided some difficulties in sample preparation and during shearing:

1. Filtration pressure is applied through a standpipe. Regular refilling is required to more or less maintain a constant pressure;

2. Concrete curing increases friction with sample container with ongoing hydration:

    2.1. Sample container friction reduces the effective consolidation load, depending on the speed of applying load increments;

    2.2. During shearing, part of the normal load is transferred through the sample container directly to the bottom shear box, since the top and bottom shear box make direct contact.

3. Interface friction between shear boxes influences direct-shear results:

    3.1. Locking of shear boxes sometimes causes multiple smaller peaks towards main peak;

    3.2. Post-peak behaviour sometimes shows rough patterns with multiple peaks.

The development of the new direct-shear set-up offers the possibility to mitigate the encountered difficulties with the 'phase 1' equipment. Considering the list above, the reduction of interface friction between the shear boxes is considered to be the most important design improvement. By incorporating an interface spacing in between the shear boxes 2 problems are solved:

1. During shearing no normal load is 'lost' through wall friction in the shear box, since the shear boxes do not make contact;

2. The measured shear force is only a result of the transfer of shear stress through the sample and is not influenced by interface friction of the shear boxes.

Lam et al. (2014) applied an interface spacing of 20 mm to allow for the use of 20 mm concrete aggregates. The interface spacing reduces the risk of the concrete aggregates to lock behind the bottom shear box. In addition, the location of the shear plane is less predefined. However, as stated in the literature review, it is thought that the presence of such a wide interface spacing causes a reduction in interface shear strength, since the horizontal confining stress around the shear plane is reduced. Therefore, in this research the interface spacing is kept as small as possible, accepting the risk of concrete aggregates locking behind the bottom shear box, but maintaining the horizontal confining stress, whilst preventing friction between the shear box interface. As for Lam et al. (2014), the shear boxes are not placed inside a water container during shearing, which limits the shear rate due to the risk of drying of the filter cake. Table 5.2 presents an overview of the main dimensions of the shear boxes.

Table 5.2: Characteristics new shear boxes

Property	**Dimension** [mm]
Internal plan dimensions	170 x 170
External plan dimensions	200 x 200
Wall thickness	15
Height bottom box (internal)	52
Height top box	100
Interface spacing	2 (adjustable)

5.2. Sample preparation procedure

In this section the design of the shear boxes with respect to the sample preparation process is presented. As stated in the above, starting point of the development of the modified direct-shear set-up has been to perform the sample preparation in the shear boxes outside the direct-shear set-up. As for the ’phase-1’ tests, the sample preparation procedure consists of 3 stages; *filtration stage*, *consolidation stage* and *transfer to direct-shear set-up*.

5.2.1. Filtration stage

The first step of the sample preparation procedure is to place the top shear box on top of the bottom shear box, with a rubber seal in between. Connection rods provide a tight sealing. The thickness of the rubber seal determines the eventual interface spacing during shearing. By choosing a certain seal thickness, the interface spacing can be controlled. As described in the above, in this research the interface spacing is kept as small as possible. Therefore, a rubber seal of 2 mm thickness is applied, which eventually leads to an interface spacing just under 2 mm due to the compressibility of the rubber to create a watertight sealing.

Figure 5.2 presents an overview of the 2 steps in the filtration stage. Before applying the sand layer in the bottom shear box, a filtration layer is placed on the bottom of the bottom shear box. This filtration layer (felt) prevents blocking of the 9 1 mm holes in the bottom and accommodates even drainage through the sand layer. Along the outside perimeter of the filtration layer, a clay ring is applied to prevent slurry leaking in between the shear box wall and the sides of the filtration layer. On top of the filtration layer, filter paper is placed to prevent the filtration layer from clogging. Subsequently the sand is applied to the desired density with a tamping method. The sand layer surface is aligned with the top of the rubber seal. In this way, the top of the sand layer will fall within the interface margin, even after some compression of the filtration layer underneath. The sand layer is saturated by placing the shear boxes in a water container, which is filled with water upto the sand level. When saturation is complete, the bentonite suspension is carefully placed on the sand, whilst preventing any disturbance of the sand surface. Before placing the lid, a rubber seal is placed on top of the top shear box. Finally, the valve is attached to a pressure regulator and the filtration pressure is gradually applied. The ’phase 1’ experimental set-up involved a standpipe to apply the filtration pressure. As described in the above, the main advantage of applying air pressure is that no refilling is required. In addition, the filtration pressure is constant. Based on the filtration volume results of ’phase 1’, the height of the top shear box is chosen such that the slurry volume is sufficient for at least 168 hours of filtration time. The applied parameter configurations are discussed in the next chapter, in which experimental results are presented.

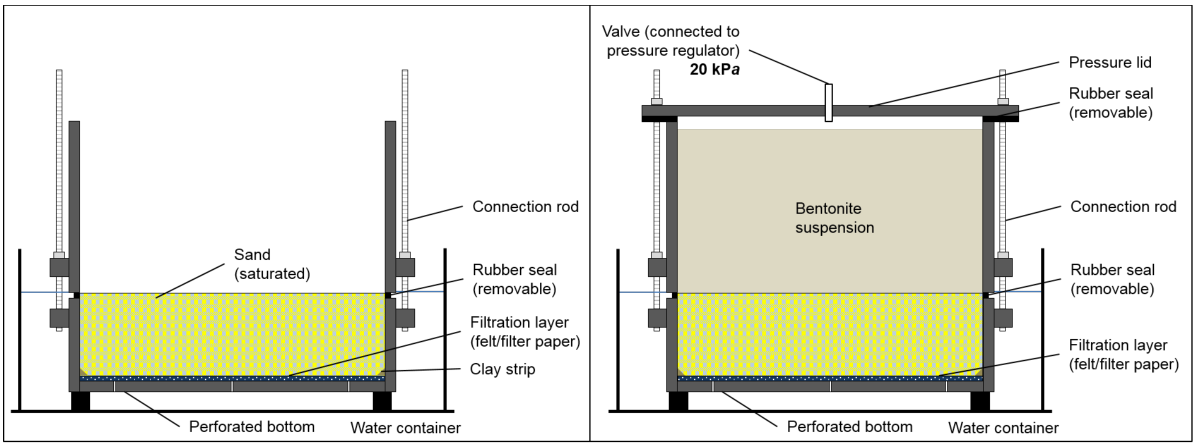

Figure 5.2: Left: saturation of sand layer. Right: bentonite suspension and filtration pressure.

5.2.2. Consolidation stage

When the filtration stage is complete, the air pressure is disconnected and the lid is removed. Depending on the filtration time, a certain volume of slurry is still present on top of the formed filter cake. This slurry is carefully removed using a syringe to expose the filter cake (Figure 5.3, left). Unlike in the 'phase 1' procedure, the top shear box is not removed to remove excess slurry. The thickness of the filter cake is measured with respect to the topside of the top shear box. Subsequently, diaphragm wall concrete is carefully placed on top of the filter cake, with 0 falling height, to initially ensure filter cake integrity. More details on the applied concrete are provided in the next chapter. A concrete layer with 50 mm thickness is applied. On top of the concrete layer a pressure plate is placed. Next, 2 rubber seals are placed on the top shear box, with a latex membrane in between. The lid is finally placed very tightly on the top of this system (Figure 5.3, right).

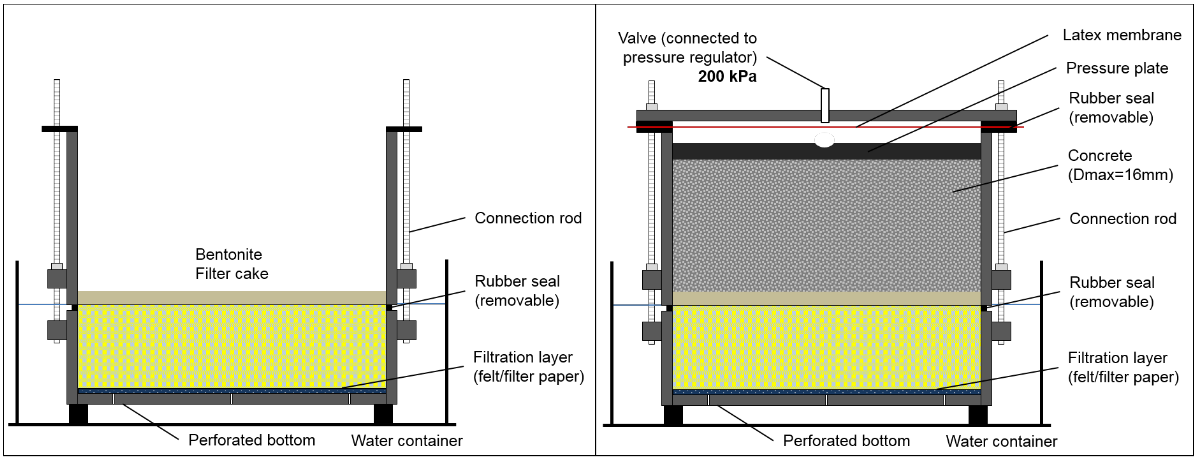

Figure 5.3: Left: exposed filter cake. Right: concrete, pressure plate, latex membrane and lid.

As for the filtration pressure, the consolidation pressure is applied by means of air pressure, unlike in phase 1 where the consolidation pressure was mechanically induced (oedometer). Preliminary tests have shown that directly applying air pressure on a wet concrete mixture does not lead to compression of the total grain skeleton, but only drains the water out. Therefore, the latex membrane is applied, which acts as pressure vessel and transfers the air pressure to the pressure plate, which in turn transfers the pressure to the sample underneath, causing filter cake consolidation. When the pressure chamber between the latex membrane and the lid is pressurized, the membrane will deform and completely fill the square cross-section. However, to reach this state, the present air is displaced through the sample. To reduce this displaced volume of air, in between the pressure plate and the latex membrane rubber plates are placed to reduce the volume of the pressure chamber.

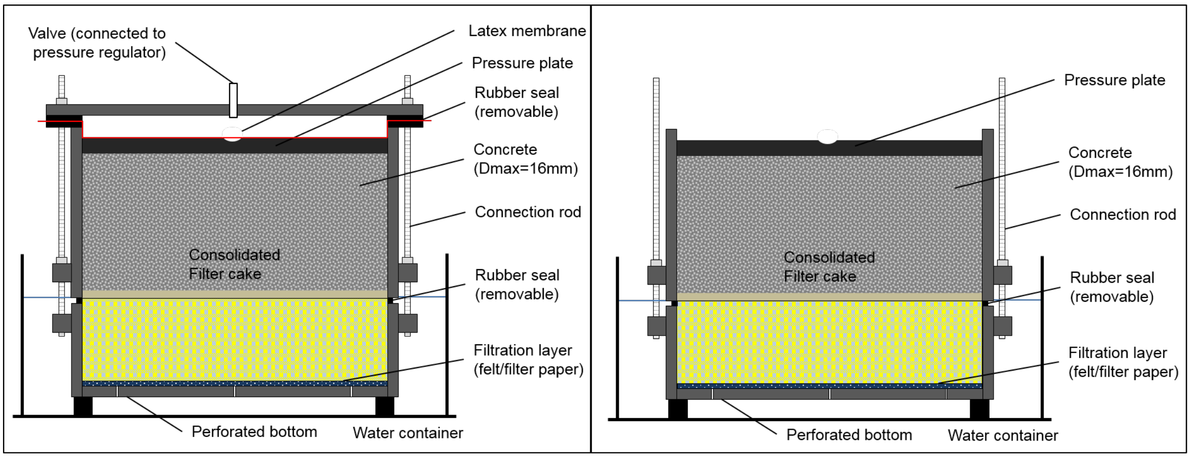

Figure 5.4: Left: consolidated filter cake. Right: removed lid and latex membrane.

5.2.3. Transfer to direct-shear machine

After the consolidation stage (when complete filter cake consolidation and sufficient concrete strength are reached), the air pressure is disconnected and the lid and latex membrane are removed (Figure 5.3). Next, the shear boxes are taken out of the water container and the rubber seal is removed from the shear box interface. Finally, the shear boxes are placed in the direct-shear machine and the connection rods are removed (Figure 5.5, left). After applying the normal pressure through the lever arm, equal reloading time is included prior to shearing (Figure 5.5, right).

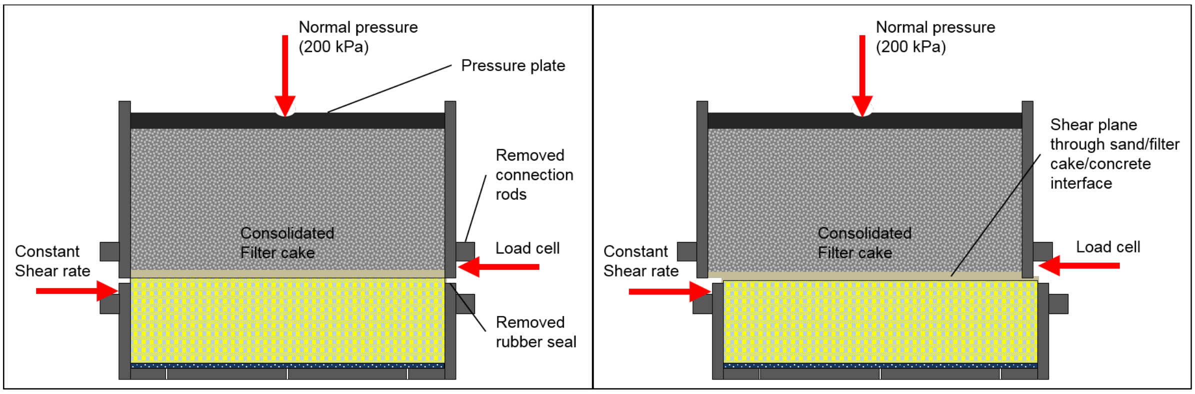

Figure 5.5: Left: placed in direct-shear machine, connection rods removed. Right: shearing under normal load.

During the filtration and consolidation stages the shear boxes are placed in a water container, whilst connected to a pressure regulator (Figure 5.6). Figure 5.7 shows the shear boxes out of the water container. In between the shear boxes the rubber seal is visible. In addition, the seals and latex membrane are visible in between the top shear box and lid. The rubber seal is dimensioned such that it can be removed with pliers (Figure 5.8). For this purpose, the rubber seal is pre-cut over half its thickness at the middle of each side. In this way, the rubber seal can be pulled out in 4 parts from the corners (Figure 5.9). To accommodate the removal of the seal, the screws at the concerning corner are slightly loosened to locally release some pressure of the seal. Pressure release on all sides simultaneously is prevented, since the rebound of the rubber seal might cause vertical deformation of the top shear box, disrupting the sample within. Since the rubber seal is destroyed in the removal process, a new seal needs to be cut prior to each test.

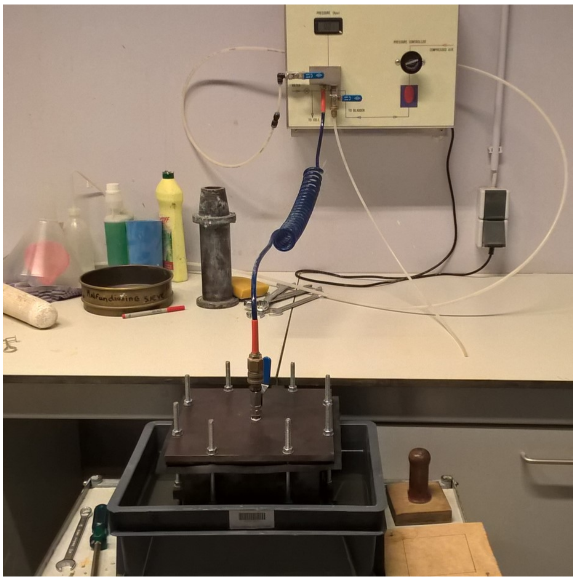

Figure 5.6: Shear boxes during filtration/consolidation process

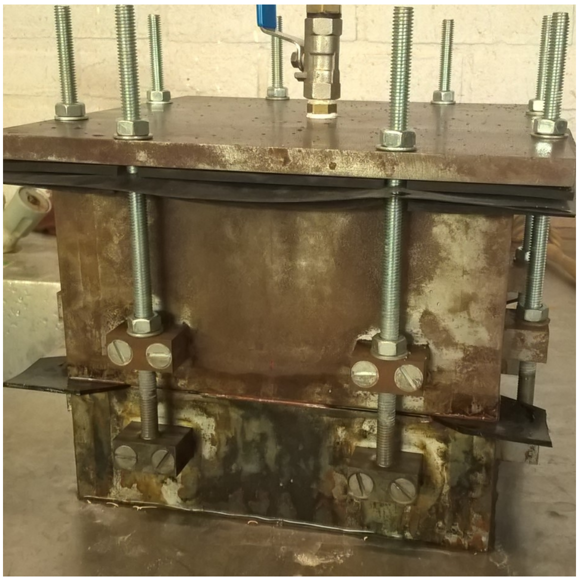

Figure 5.7: Shear boxes disconnected from pressure regulator and outside water container

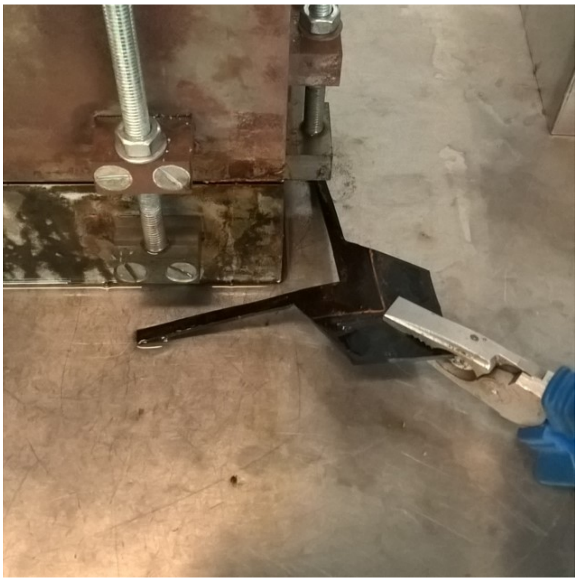

Figure 5.8: Removal of interface spacing

Figure 5.9: Remains of interface spacing after removal

In the 'phase 1' set-up, a latex membrane was placed in between the sample tube and cement-mortar to reduce friction. In the new set-up the friction between concrete and shear box is used to keep the top shear box in its vertical position after removal of the interface seal to maintain the interface spacing. In turn, this interface spacing mitigates the loss of normal pressure through friction, since the shear boxes do not make contact. When placed in the direct-shear set-up, the top side of the bottom shear box aligns with the pressure rod (Figure 5.10), which is connected to the electric motor and induces the constant shear rate. The bottom side of the top shear box aligns with a pressure rod, which is connected to the load cell (Figure 5.11). The load cell is adjustable in height to accommodate the application of wider interface spacings if desired. During shearing the driving shear force and resulting force in the load cell generate a force couple, which influences the distribution of normal pressure over the sample. In this respect, a small interface spacing is beneficial, since the arm of the force couple is reduced.

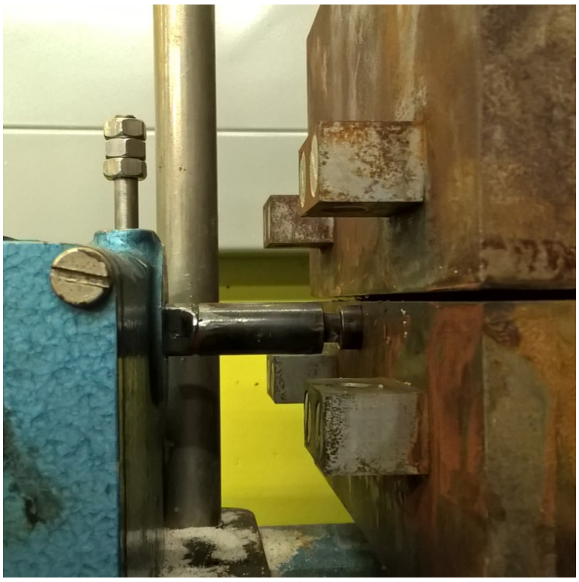

Figure 5.10: Pressure rod: Motor and bottom shear box

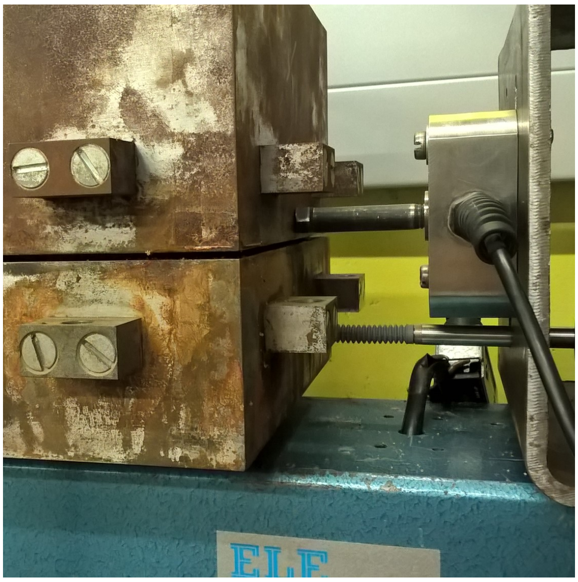

Figure 5.11: Pressure rod: Top shear box and load cell

5.3. Conclusion

Based on a comparison of direct-shear geometries in previous research, shear box dimensions of 170 mm x 170 mm are thought to be of sufficient scale for the modelling of a maximum concrete aggregate size of 16 mm. In The Netherlands, this value is often applied in concrete mix design for diaphragm wall construction (CUR/COB, 2010). In between the shear boxes an interface spacing of 2 mm is applied to mitigate the issue of shear box friction, which causes problems with the small-scale set-up in the direct-shear test series on the filter cake shear strength. With such small interface spacing, the risk of concrete aggregates interlocking behind the shear box side during shearing is accepted. To prevent this, an interface spacing of a minimum height of 16 mm should be applied. However, it is thought that such a wide interface spacing causes a reduction of the confining pressure around the shear plane, causing a reduction of measured interface shear strength. The relatively low values of filter cake shear strength found by Lam et al. (2014), who applied an interface spacing of 20 mm, are an indication of this negative effect of a large interface spacing. The shear box dimension of 170 mm x 170 mm allow for the mechanical application of 200 kPa normal pressure during shearing by means of the existing lever arm of the direct-shear machine. The filtration- and consolidation pressure is applied by air pressure. For the consolidation pressure, directly applying air pressure onto a wet concrete mix causing the extrusion of the water out of the concrete in stead of an even compression of the concrete skeleton. Therefore, a latex membrane is applied between the air pressure and concrete mix to transfer the air pressure onto the complete concrete mixture. For an even pressure distribution, in between the latex membrane and concrete mixture a steel pressure plate is applied. This plate also acts as pressure plate during the direct-shear test.

6

Experimental Phase 2: Interface shear strength as a function of filtration time

This chapter describes the experimental analysis of the development of interface shear strength as a function of filtration time. For this purpose, a new direct-shear set-up (170 mm x 170 mm) has been developed to enable the modelling of diaphragm wall concrete (max. aggregate size 16 mm), which has been explained in the previous chapter. In this chapter, first, the methodology is explained. Next, the experimental results of a series of direct-shear tests on sand/filter cake/concrete samples are presented, together with data from the sample preparation. A comparison is made between the surface roughness of the concrete samples in this research and in-situ concrete roughness data (in both cases based on 3D laser scans). Finally, conclusions are presented.

6.1. Methodology

To investigate the development of interface shear strength as a function of filtration time, a series of direct-shear tests on sand/filter cake/concrete is performed, in which the filtration time and filter cake composition are the main parameters. The experimental results are applied to test previously proposed conceptual model (Section 2.4). To realistically model the influence of filtration time (and the directly related filter cake thickness) on the interface shear strength, a realistic concrete surface should be incorporated in the sample layering (sand/filter cake/concrete). For this purpose, a new direct-shear set-up has been developed (170 mm x 170 mm) to allow for the modelling of diaphragm wall concrete with a maximum aggregate size of 16 mm. In the previous chapter, the design considerations have been addressed, as well as a global explanation of the experimental procedure, which is similar to the 'phase 1' set-up. Therefore, in this section only the applied materials and parameter configurations are explained.

6.1.1. Applied materials

In preparation of the layered sand/filter cake/concrete samples, the applied materials are equal to the 'phase 1' samples, except for the applied concrete mix instead of the cement-mortar. The sieve curve of the applied sand is presented in Figure 4.6. The sand is placed by dry tamping to the desired Relative Density (more details in the next section). The applied bentonite suspensions are based on Cebogel Trenchcontrol AT. The applied concrete mix recipe is presented in Table 6.1. For each test, the concrete mix is prepared in a batch of 10 L and mixed with a concrete hand mixer. The same method of concrete placement has been applied in the small-scale experimental procedure, in which the wet concrete mix is placed gently on top of the filter cake with 0 falling height to prevent initial filter cake disturbance.

6.1.2. Parameter configurations

To test the hypothesis on the development of interface shear strength of contaminated filter cakes compared to clean filter cakes (Section 2.4), the filtration time and filter cake composition are the main variables in experimental phase 2. In addition, an important difference with the small-scale tests is the application of diaphragm wall concrete with maximum aggregate size of 16 mm and workability class

F5. Table 6.2 presents an overview of the general test parameters. To be able to compare results, the applied filtration-, consolidation- and normal pressures and the shear rate correspond to 'phase-1' tests. To allow for efficient planning, the consolidation time is kept as short as possible. This shortening is justified by experimental results from phase-1, which indicate that no chemical strengthening of the filter cake takes place with progressing cement hydration. In addition, the phase-1 oedometer results indicate that filter cake consolidation reaches the creep phase within 48 hours. As shown in Table 6.2, the consolidation time varies between 2 and 3 days for planning purposes. Table 6.3 presents the applied combinations of filtration time and filter cake composition in order to test the hypothesis regarding the development of interface shear strength for contaminated filter cakes compared to clean filter cakes (Section 2.4). To analyse the proposed trends of interface shear strength development, the applied filtration times for the contaminated filter cakes have deliberately been chosen shorter compared to the clean filter cakes, since it is expected that due to the higher filter cake growth rate the decrease of interface shear strength will commence earlier compared to clean filter cakes.

Table 6.1: Diaphragm wall concrete recipe

Constituent	**Quantity** [kg/m^3]
CEM III/B 42,5	340
Fly ash	70
Aggregate 0-4 mm	820
Aggregate 4-16 mm	1004
Water	175

Table 6.2: Overview of general test parameters for experimental phase 2

Parameter	**Value**
Relative Density sand layer	89 %
Bentonite concentration in slurry	4 %
Sand/silt concentration in contaminated slurry	**Variable**
Filtration time	**Variable**
Filtration pressure	20 kPa
Maximum aggregate size	16 mm
Consolidation time	2-3 days
Consolidation pressure	200 kPa
Normal pressure in direct-shear test	200 kPa
Shear rate	1,2 mm/min

Table 6.3: Parameter configurations of filtration time and filter cake composition

Sample	**Filtration time**	**Filter cake composition**
P2.1 (REF)*	0	-
P2.2	48	clean
P2.3	23	clean
P2.4	12	clean
P2.5	12	contaminated**
P2.6	3	contaminated
P2.7	1	contaminated

**: Reference test ($\delta/\phi = 1.0$)*
***: According to Table 4.10, Mixture 2*

6.2. Analysis of interface shear strength development

Table 6.4 presents an overview of experimental results, for both the sample preparation stage as for the direct-shear tests. Since filter cake consolidation is achieved by air pressure in stead of the oedometer, no consolidation data is available. Some aspects of the sample preparation procedure have developed over the course of testing. First of all, during the first 2 tests involving clean filter cakes (tests P2.2 and P2.3, Tabel 6.4), high slurry loss was observed during the filtration stage, which was caused by leakage of slurry along the perimeter of the bottom shear box and along the outer perimeter of the filtration layer. This issue has been mitigated in later tests by applying a strip of clay along the outer perimeter of the filtration layer to block this flow path (Figure 5.2). Figure 6.1 presents an overview of filter cake thickness results for both the small-scale and large-scale tests, showing the average growth rate values for clean and contaminated filter cakes of 0,201 $mm/\sqrt{min}$ and 0,338 $mm/\sqrt{min}$ respectively.

Table 6.4: Experimental results experimental phase 2: sample preparation and direct-shear test

Sample	**Slurry density** [g/cm^3]	**Filtration time** [hours]	**Filter cake* thickness** [mm]	**Filter cake growth rate** [$mm/\sqrt{min}$]	**Shear strength** [kPa]	**Strain at peak** [%]	**Friction angle** [°]
P2.1 (REF)	-	0	0	-	155,5	1,1	38,0
P2.2	1,03	48	12,0**	0,22	67,2	0,57	18,7
P2.3	1,03	23	6,3**	0,17	88,5	0,98	24,0
P2.4	1,03	12	5,3	0,20	138,4	2,20	34,5
P2.5	1,25	12	9,5	0,35	77,0	0,75	21,2
P2.6	1,25	3	4,0	0,30	88,4	0,39	24,1
P2.7	1,25	1	2,5	0,33	140,0	2,76	34,7

**: Average value of filter cake thickness at filter cake midpoint and around the outer perimeter*
***: High slurry loss caused by leakage around filtration layer, mitigated in later tests*

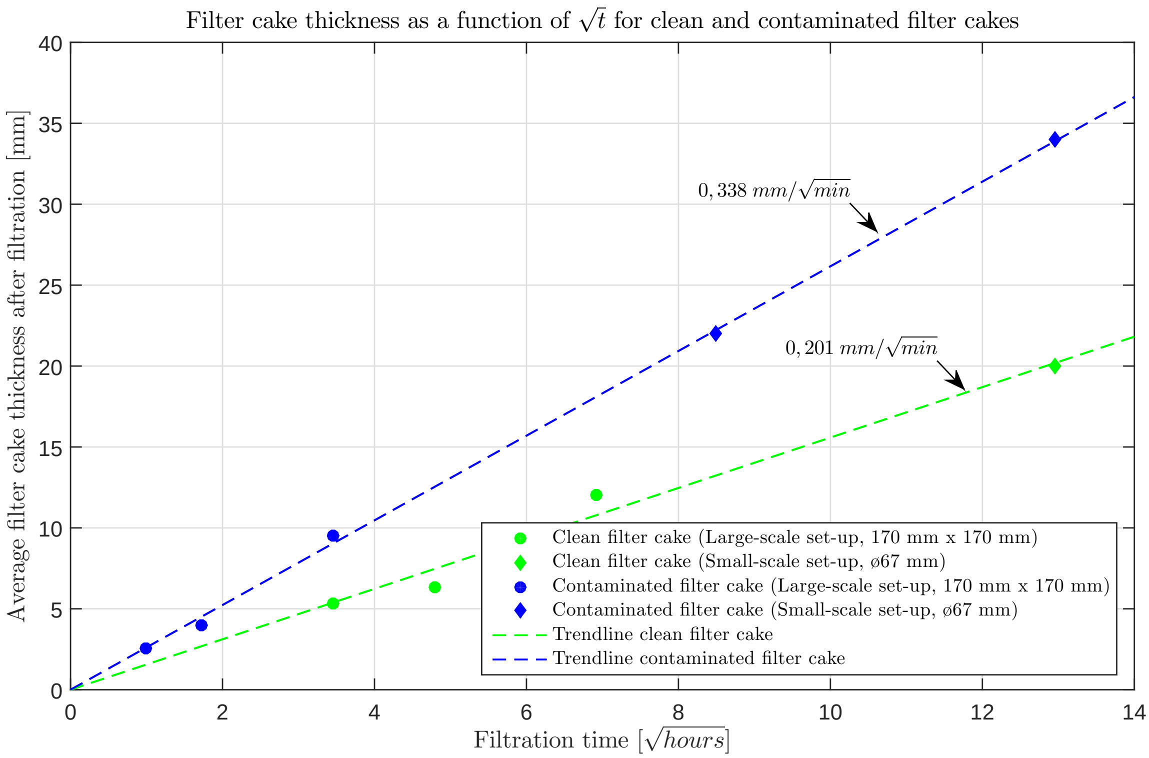

Figure 6.1: Filter cake thickness as a function of filtration time (20 kPa filtration pressure) for clean and contaminated filter cakes (results from small-scale and large-scale tests combined)

By combining the filter cake thickness observations for both the small-scale experiments (7 days filtration time) and the large-scale experiments with varying filtration time (Table 6.4), a clear linear trend with $\sqrt{t}$ is observed (Figure 6.1). The direct-shear test results performed on the layered interface samples are presented in Figure 6.2 (stress-strain) and Figure 6.3 (horizontal and vertical displacement). In addition, the results of the preliminary test with a sand/cement-mortar configuration are added. A comparison of the direct-shear results of test P2.1 (sand/diaphragm wall concrete) and the sand/cement-mortar test indicates that for the applied concrete-pouring method (no falling height), the maximum aggregate size of the concrete mix does not influence the interface shear strength. These results also provide an indication that the application method of the sand layer leads to consistent packing of the sand (dry tamping, R.D. 89 %, constant for all tests).

With decreasing filtration time (and subsequent filter cake thickness) an increase of peak shear strength is observed, for both the clean and contaminated filter cake samples. However, for all tests on sand/filter cake/concrete samples (P2.2 to P2.7), an increasing post-peak shear strength is observed. Direct-shear results by Arwanitaki et al. (2007) and Lam et al. (2014) also showed this development for layered interface samples including filter cakes. Lam et al. (2014) attribute this phenomenon to the sand shear strength being mobilised at increasing horizontal strain. The shear stress values interpreted as peak shear strength values in this research (Table 6.4) are taken at values of horizontal strain where a clear peak or deflection towards a plateau is observed. It should be noted that 'aggregate interlocking' has caused some disturbance for tests P2.3 and P2.4, resulting in additional peaks (Figure 6.2). By keeping the interface spacing between the shear boxes as small as possible (2 mm), the risk of concrete aggregates interlocking behind the bottom shear box during shearing was known on forehand. However, the 'unrealistic' peaks caused by aggregate interlocking could be clearly identified, since they were accompanied by a cracking noise during shearing. In addition, an examination of the concrete/filter cake surfaces after shearing shows the location of the interlocked concrete aggregates (Figures 6.5 and 6.4). For test P2.3 (23 hours filtration time), the aggregate interlocking occured at a higher horizontal strain compared to test P2.4 (12 hours filtration time), which corresponds with the larger distance between the interlocked aggregate and the shear box side for test P2.3.

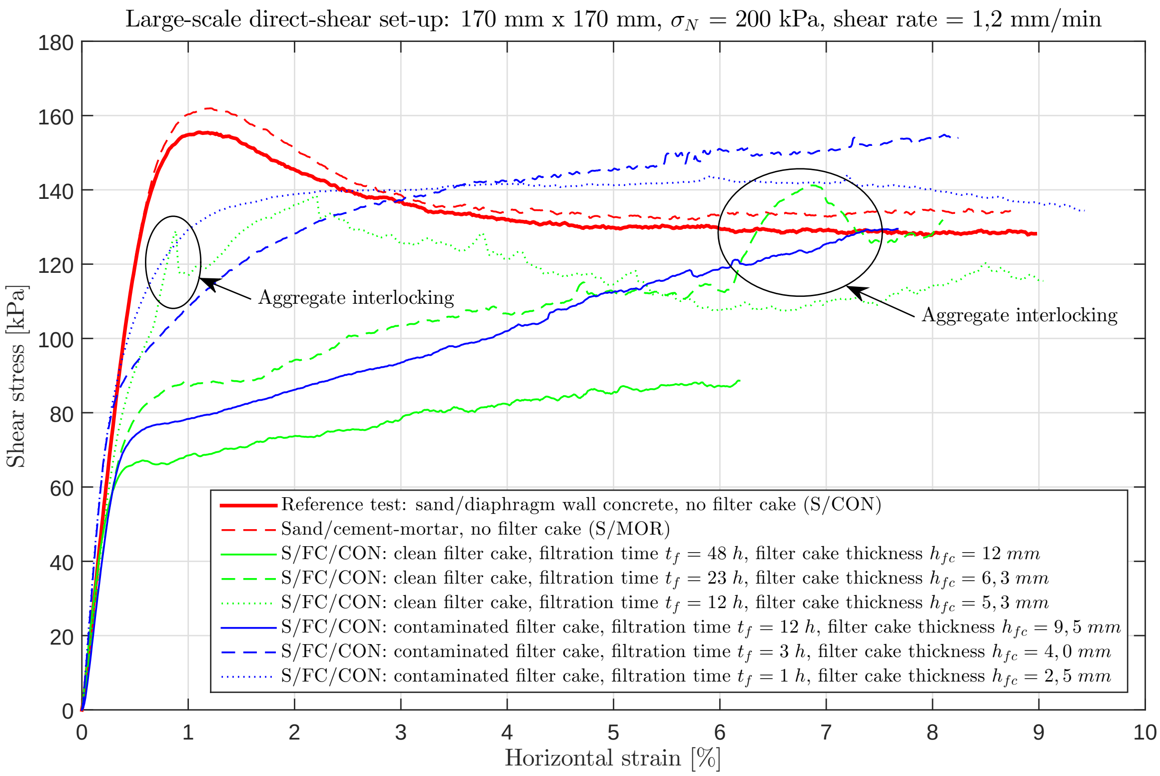

Figure 6.2: Stress-Strain results direct-shear tests Phase 2

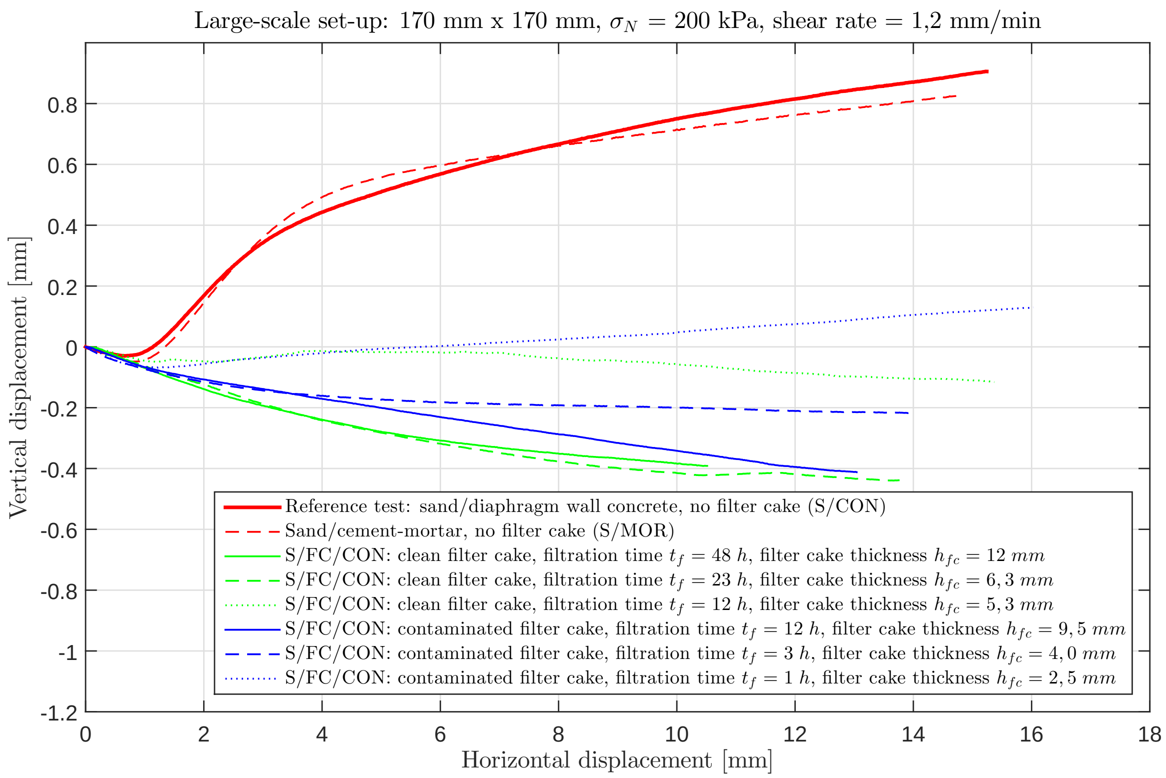

Figure 6.3: Horizontal-Vertical displacement results direct-shear tests Phase 2

For the clean filter cake tests (P2.2 to P2.4), the stress-strain curves shift towards the sand/concrete test curve (P2.1) with decreasing filtration time. Lam et al. (2014) showed that the influence of 'aggregate protrusion' increases with decreasing filter cake thickness for a constant maximum concrete aggregate size. The influence of aggregate protrusion is highest between tests P2.3 and P2.4 (filtration times of 23 and 12 hours respectively), since the largest increase of interface shear strength is observed (Figure 6.2). This clear increase of interface shear strength corresponds to the increased surface ratio of direct sand/concrete contact, based on a visual inspection of the samples after removal of the sand layer (Figures 6.5 and 6.6). The development of vertical deformation is also an indication of increased aggregate protrusion. As observed in the small-scale tests, filter cake shows contractant behaviour. Figure 6.3 shows that the increased direct sand/concrete contact between tests P2.3 and P2.4 causes increased dilatant behaviour, indicating increased mobilisation of the sand shear strength.

Figure 6.4: Concrete/filter cake surface test P2.2, clean filter cake, 48 hours filtration time

Figure 6.5: Concrete/filter cake surface test P2.3, clean filter cake, 23 hours filtration time (arrow: aggregate interlocking)

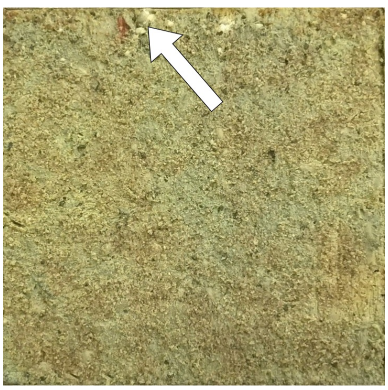

Figure 6.6: Concrete/filter cake surface test P2.4, clean filter cake, 12 hours filtration time (arrow: aggregate interlocking)

Figure 6.7: Concrete/filter cake surface test P2.5, contaminated filter cake, 12 hours filtration time

Figure 6.8: Concrete/filter cake surface test P2.6, contaminated filter cake, 3 hours filtration time

Figure 6.9: Concrete/filter cake surface test P2.7, contaminated filter cake, 1 hour filtration time

Concerning the contaminated filter cake tests (P2.5, P2.6, P2.7), the largest increase of interface shear strength occurs between tests P2.6 and P2.7. However, an increase of the surface ratio of direct sand/concrete contact is not clearly visible (Figures 6.7 to 6.9). On the other hand, an increase of dilatant behaviour for decreasing filtration time is clearly observed for the contaminated filter cake samples (Figure 6.3), indicating an increased mobilisation of the shear strength of the sand layer. It should be noted that prior to tests P2.6 and P2.7 (latest tests performed), additional strengthening of the load cell support frame was applied to ensure a rigid support of the load cell.

Figure 6.10 presents the observed peak shear strength values for tests P2.1 to P2.7 (Table 6.4), expressed relatively to the peak shear strength of test P2.1 (no filter cake) as the 'Interface shear strength reduction factor δ/ϕ. For test P2.1, $\delta/\phi = 1,0$. The δ/ϕ values are plotted versus $\sqrt{t}$ (filtration time). Filter cake shear strength results from phase 1 are added as well (σ_N equals 200 kPa).

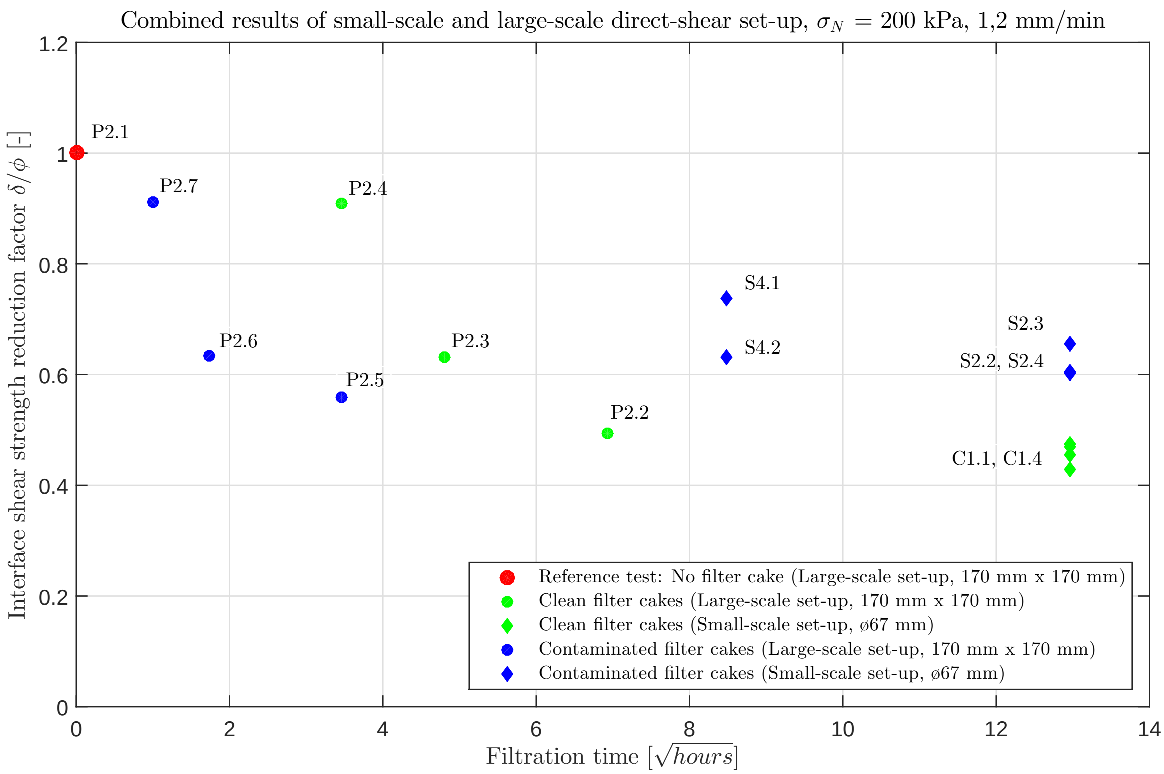

Figure 6.10: Interface Reduction δ/ϕ as a function of the square root of filtration time

The test results of the different direct-shear set-ups presented in Figure 6.10 can not be compared directly due to differences in test geometry, although the applied normal stress and shear rate are equal. In addition, the large-scale tests have not been repeated. However, Figure 6.10 clearly indicates that the decrease of interface shear strength starts after a shorter filtration time for contaminated filter cakes compared to clean filter cakes, which confirms the hypothesis proposed in Section 2.4. For the clean filter cake tests, the shear strength of test P2.2 approaches the range of shear strength values from tests C1.1 to C1.4 (performed with the small-scale direct-shear set-up), which modelled the filter cake shear strength (around 168 hours filtration time). This is an indication that for the case of clean filter cakes and a filtration pressure of 20 kPa, the lower boundary interface shear strength is reached after 24 hours. For the case of contaminated filter cakes, the shear strength results of tests P2.5 and P2.6 roughly correspond to the shear strength results of tests S4.1, S4.2 and S2.2 - S2.4 (small-scale set-up, 72 hours and 168 hours filtration time respectively). This indicates that for the applied contaminated slurry composition, the lower boundary interface shear strength is at least reached after 12 hours. Test result S4.1 deviates from this trend, which is probably caused by shear box interface friction.

Figure 6.10 presents the development of interface shear strength as a function of the square root of filtration time. For a certain slurry composition, the filtration time and filtration pressure (constant in this research at 20 kPa) mainly control the filter cake thickness prior to concrete pouring. However, as observed in experimental phase 1, the consolidation pressure causes filter cake compression, which leads to a reduced filter cake thickness prior to shearing. This filter cake thickness reduction is a function of trench depth, since the lateral concrete pressure acting on the filter cake increases with depth. This is confirmed by Cernak et al. (1973), who observed a reduced filter cake thickness with depth. For the experimental results presented in Figure 6.10, a constant consolidation pressure has been applied (200 kPa). Therefore, the indicated development of interface shear strength is only applicable for a certain trench depth, corresponding to a lateral concrete pressure of 200 kPa. For increased consolidation pressures, additional filter cake compression is expected, leading to a reduced final filter cake thickness for equal filtration time. Therefore, for increasing trench depth, the decrease of interface shear strength and the lower boundary shear strength are expected to be reached after a longer filtration time for both clean and contaminated filter cakes.

Lam et al. (2014) also found that the filter cake shear strength is reached after a filtration time of 24 hours, although their filtration pressure of 230 kPa lead to higher filter cake growth rate. The faster filter cake growth might be compensated by additional filter cake compression, since the consolidation pressure applied by Lam et al. (2014) is higher (360 kPa) compared to this research (200 kPa). Another factor could be the method of concrete pouring. In this research, the concrete is applied carefully on top of the bentonite filter cake with 0 falling height. It is believed that Lam et al. (2014) applied a similar concrete placement method, since they mention that scouring of the filter cake by the rising concrete has deliberately been avoided. Arwanitaki et al. (2007) simulated the in-situ concrete pouring conditions by injecting a cement-mortar mix adjacent to a vertically placed filter cake in upward direction, thereby expelling the liquid slurry from the top shear box. Arwanitaki et al. (2007) reported some filter cake scouring near the injection point, which is most probably an experimental effect.

6.3. Analysis of concrete surface roughness

Lam et al. (2014) observed that the degree of concrete aggregate protrusion through the filter cake depends on both the filter cake thickness and the maximum aggregate size of the concrete. Their results indicate that when applying a concrete mixture on a bentonite filter cake with 0 falling height, an increased maximum aggregate size results in a higher concrete surface roughness, causing a larger amount of discontinuities in the filter cake, resulting in an increase of interface shear strength. In this research, tests P2.1 to P2.7 involve the application of diaphragm wall concrete mixture (max 16 mm). The concrete pooring method was similar to Lam et al. (2014), applying 0 falling height to avoid initial filter cake disturbance prior to application of the consolidation load. In this section, the concrete surface roughness of the sand/filter cake/concrete samples is analysed. First, the differences in surface roughness of the laboratory samples are investigated. Next, the roughness results of the laboratory samples are compared to in-situ roughness data of a diaphragm wall panel constructed at the Spoorzone Delft project in the context of the PhD research projects of Spruit (2015) and Van Dalen (2016).

6.3.1. Surface roughness of laboratory concrete samples

To analyse the surface roughness, 3D laser scans have been performed on 6 concrete samples (sample P2.2 failed during extraction of the top shear box). For this purpose, a Leica C10 laser scanner has been used, to obtain 1 mm resolution point cloud data. Surface roughness is defined as the "repetitive or random deviation from the nominal surface that forms the three-dimensional topography of the surface" (Bushan, 2001). For each sample, the reference plane is fitted through the 3D laser point cloud data by using hyperplanar fitting by orthogonal regression. More details on this fitting method can be found in Eberly (2008).

Figure 6.11 presents 2D plots of the z-values relative to the fitted reference plane for all analysed concrete samples. The presented colour scale is equal for all samples. Visual inspection of Figure 6.11 indicates that the sample P2.1 has the 'smoothest' concrete surface. Samples P2.3, P2.4, P2.5 and P2.6 clearly show a rougher surface compared to P2.1. Sample P2.7 shows a comparable surface texture with sample P2.1. These observations indicate that for the applied method of concrete placement, the concrete surface roughness increases when it is poured on a bentonite filter cake, which corresponds to observations by Wates and Knight (1975), who observed increased concrete roughness for a model pile in the presence of bentonite filter cake. This is explained by the low shear strength of the bentonite filter cake prior to consolidation, which provides more freedom for the wet concrete mix to take a rougher shape compared to the sand layer (in the case of no filter cake, P2.1). Figure 6.12 presents the Histograms of the z-values for the 6 samples. Sample P2.1 shows the sharpest peak in the Histogram. For the contaminated filter cake samples (P2.5, P2.6, P2.7), increased filtration time results in increased widening of the Histogram curve. The fact that the mean z-values are not 0 is most probably a result of the applied fitting method of the reference plane. Figure 6.11 shows different surface texture patterns. First of all, sample P2.6 clearly shows increased surface elevation towards the center of the sample. A similar pattern can be observed for samples P2.4 and P2.5, but to a lower extent. This pattern might be caused by a reduced consolidation pressure towards the shear box sides by friction between the concrete and the shear box sides, causing filter cake compression towards the sample centre. Samples P2.1, P2.3 and P2.7 show a more even spreading.

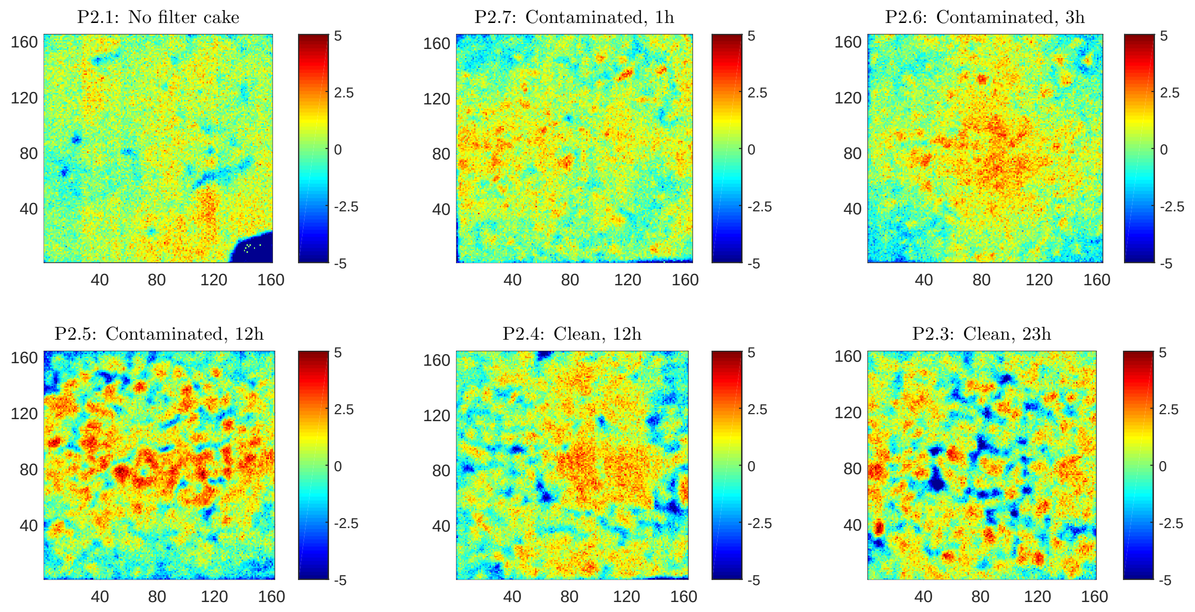

Figure 6.11: Surface roughness of laboratory concrete samples (height relative to 0-plane)

Visual inspection of the surface elevation plots (Figure 6.11) and the distribution of z-values (Figure 6.12) are suited for a comparison of the laboratory samples and to investigate the influence of the presence of a filter cake on the surface texture. However, to be able to compare the laboratory surface textures with in-situ data, the surface roughness must be quantified in a more robust way. The roughness of the laboratory surface textures has been expressed in terms of R_a and R_{max}. R_a is the arithmetic mean of the absolute values of the vertical deviation from the mean line along a scan line of a certain length (Bushan, 2001) (Equation 6.1). Due to the applied fitting method of the reference plane, for all samples the mean z-value does not necessarily equals 0.

$$R_a = \frac{1}{L}\int_0^L | z - m | \, dx \tag{6.1}$$

R_{max} is defined as the difference between the highest and lowest peak along a scan line of a certain length L. Table 6.5 presents average values for R_a and R_{max} over all scan lines in x and y direction. For samples P2.5 and P2.7 it is observed that $R_{a;avg;y}$ and $R_{max;avg;y}$ are relatively high compared to $R_{a;avg;x}$ and $R_{max;avg;x}$ respectively. This can be explained by the observed surface texture patterns, which show a ridge shape along the surface in x-direction. This is best visible for sample P2.5 (Figure 6.11).

Table 6.5: Surface roughness data of laboratory concrete samples

Sample	**Slurry density** [g/cm^3]	**Filtration time** [hours]	**Filter cake* thickness** [mm]	$R_{a;avg;x}$ [mm]	$R_{a;avg;y}$ [mm]	$R_{max;avg;x}$ [mm]	$R_{max;avg;y}$ [mm]
P2.1 (REF)	-	0	0	0,62	0,62	4,19	4,33
P2.3	1,03	23	6,3	1,03	1,02	7,25	7,04
P2.4	1,03	12	5,3	0,95	0,85	6,05	6,12
P2.5	1,25	12	9,5	0,88	1,10	5,88	6,90
P2.6	1,25	3	4,0	0,75	0,72	4,81	4,80
P2.7	1,25	1	2,5	0,66	0,72	4,66	5,55

**: Average value of filter cake thickness at filter cake midpoint and around the outer perimeter*

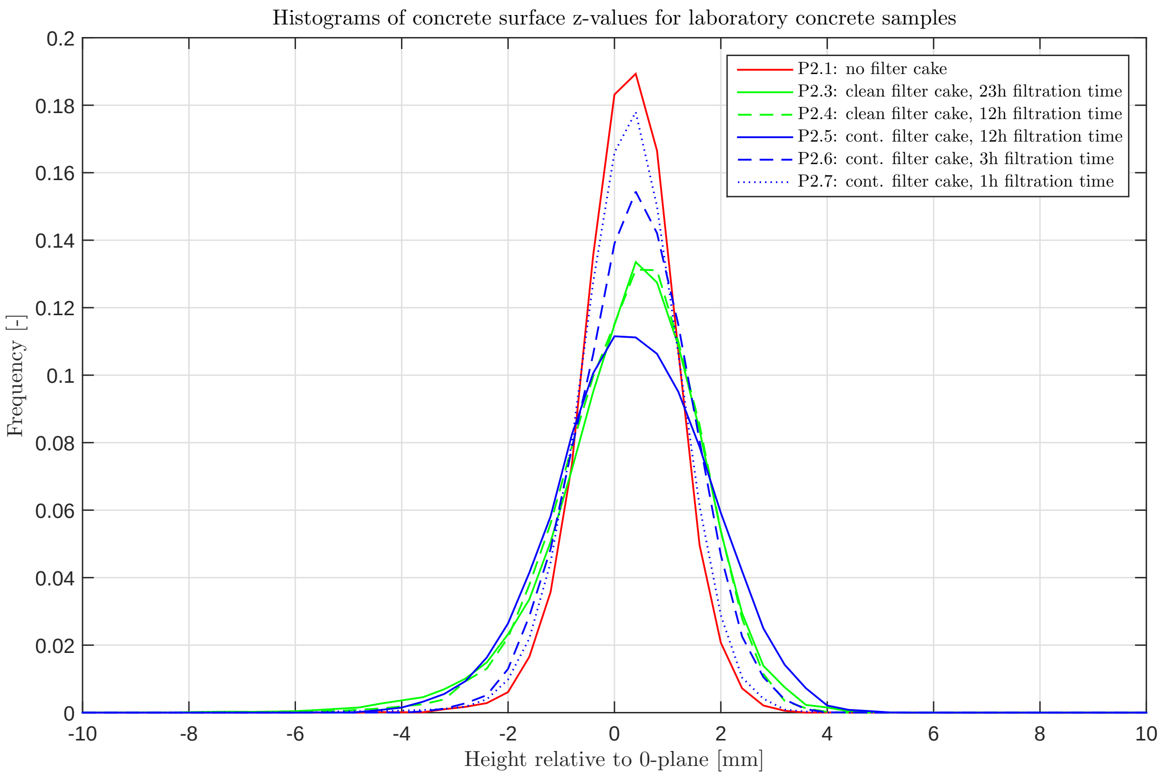

Figure 6.12: Histograms of surface z-values of laboratory concrete samples

6.3.2. Comparison with in-situ concrete roughness

To investigate if the concrete surface textures of the laboratory samples are a realistic simulation of in-situ conditions, a comparison is made with in-situ surface roughness data. Arwanitaki et al. (2007) analysed the in-situ concrete surface roughness of a diaphragm wall at a construction site in Rotterdam. They made laser scans on gypsum casts of the concrete surface texture along a number of grid lines. Arwanitaki et al. (2007) quantified the concrete roughness by means of R_{max}, which is, as explained before, the difference between the highest and lowest peak along a certain profile. Arwanitaki et al. (2007) observed R_{max} values ranging from 3,3 mm to 6,4 mm for samples of 150 mm x 150 mm. Their sample size is comparable to the dimensions of concrete samples analysed in this research (around 160 mm x 160 mm). However, their applied measuring resolution is unknown. The average R_{max} values observed in this research are in the range of 4,19 mm to 7,25 mm (Table 6.5). This range lies above the range found by Arwanitaki et al. (2007). However, part of the increased R_{max} values might be attributed to the larger sample size. In addition, the resolution of Arwanitaki et al. (2007) is unknown.

As mentioned before, in the context of the PhD research projects of Spruit (2015) and Van Dalen (2016) 2 test diaphragm wall panels have been constructed at the Spoorzone Delft project. 3D laser scans (5 mm resolution) have been performed of both sides of the test panels, resulting in 4 scanned concrete surfaces. The concrete surface texture of 1 panel is analysed and compared to the laboratory samples to further investigate whether these samples are representative for in-situ conditions. Figures 6.13 and 6.14 present the surface textures of the north- and south side of the considered diaphragm wall panel. Macro patterns are clearly visible, which are most probably caused by the excavation process. For a meaningful comparison of the concrete surface texture, sub-samples are extracted from the in-situ data of similar size compared to the laboratory samples (160 mm x 160 mm). In this way, the roughness parameters R_a and R_{max} are evaluated at similar scale as the laboratory samples. The evaluation of R_a and R_{max} based on sub-samples is performed for the complete panels and for selected zones to investigate the influence of the observed macro-roughness patterns. It should be noted that for the analysis of the 'complete' panels, the raw data has been trimmed to a rectangular shape, which is required for the sub-sampling method. Table 6.6 presents the main results of the roughness analysis.

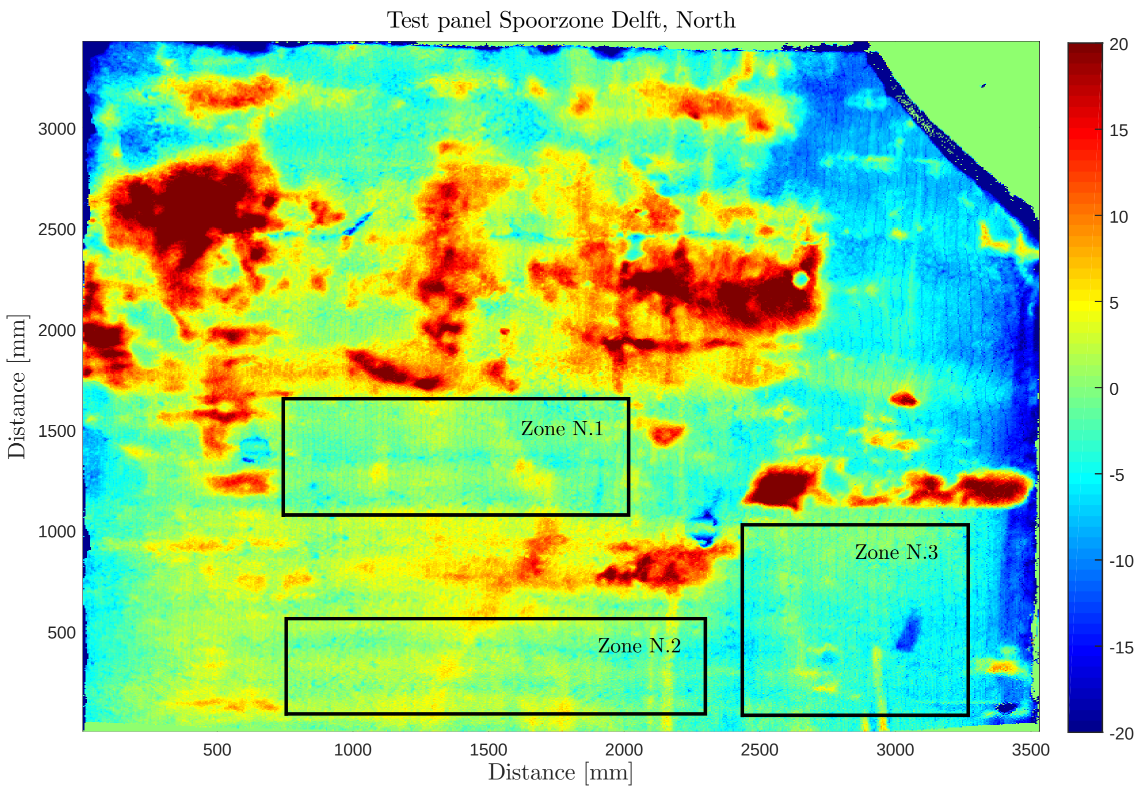

Figure 6.13: Analysed zones of concrete panel, north-side

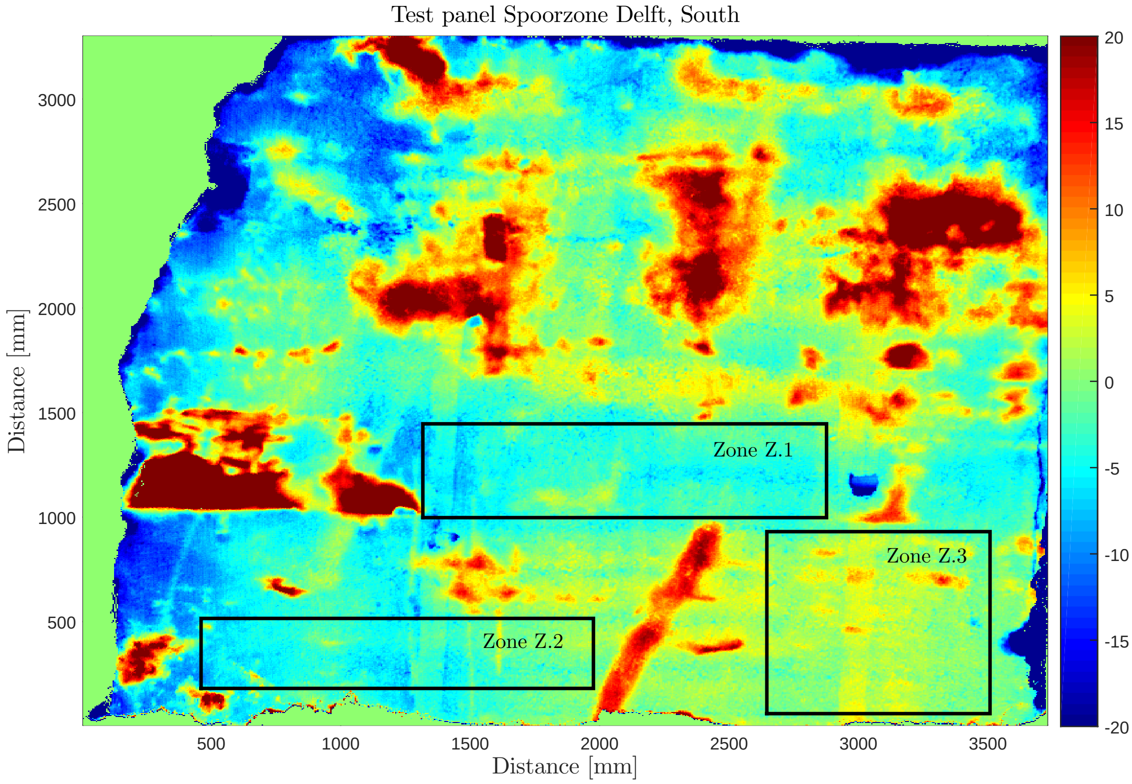

Figure 6.14: Analysed zones of concrete panel, south-side

Table 6.6: Surface roughness analysis results of in-situ data from Spoorzone Delft project

Zone	Dimensions of zone [m]	Number of samples* [-]	$R_{a;avg;x}$ (160 mm)** [mm]	$R_{a;avg;y}$ (160 mm) [mm]	$R_{max;avg;x}$ (160 mm)*** [mm]	$R_{max;avg;y}$ (160 mm) [mm]
N.total****	2,85 x 3,25	333022	1,83	1,94	8,33	8,43
Z.total	2,80 x 3,07	308407	1,95	2,11	8,41	8,99
N.1	1,32 x 0,55	18560	0,96	0,97	4,83	4,74
N.2	1,75 x 0,32	10176	0,96	0,97	4,93	5,00
N.3	0,82 x 0,93	20174	1,18	1,04	6,17	5,39
Z.1	1,62 x 0,43	15768	0,87	0,90	4,36	4,37
Z.2	1,53 x 0,33	9042	0,96	0,88	4,99	4,53
Z.3	0,86 x 0,86	19460	0,97	1,02	4,75	4,99

**: Number of samples (160 mm x 160 mm) extracted from the considered zone*
***: Average R_a of profiles in x-direction for scan line length of 160 mm (extracted samples)*
****: Average R_{max} of profiles in x-direction for scan line length of 160 mm (extracted samples)*
*****: Raw data is trimmed to a rectangular shape*

The surface roughness results in Table 6.6 show that the average R_a and R_{max} values are clearly higher for the 'complete' panels (trimmed to rectangular shape) compared to the smaller zones, although the sub-sample size is equal (160 mm x 160 mm). This increased surface roughness is caused by the macro-roughness patterns, which have been avoided by the selected zones (Figures 6.13, 6.14). For the selected zones, R_a and R_{max} values are observed in the range of 0,87 mm - 1,18 mm and 4,36 mm - 6,17 mm respectively. These results are comparable to the R_a and R_{max} values observed for the laboratory samples, which lie in the range of 0,62 mm - 1,10 mm and 4,19 mm - 7,25 mm respectively. However, as stated before, the laboratory laser scan data has a higher resolution (1 mm) compared to the in-situ data (5 mm). Therefore, for a final comparison with the in-situ data, the laboratory data resolution is reduced to 5 mm. The general applied method of resolution reduction is to represent each cell of 25 data points by one single value. As an example, Figure 6.15 presents the histograms of z-values for sample P2.3 for the original and reduced resolution. It is clear that when reducing the resolution by taking the average value of each cell of 25 data points, a sharper distribution is obtained compared to taking a single cell value from each set of 25 data points. For the laboratory samples, the resolution is reduced by taking the middle data point of each cell (of 25 data points) and the average value of the data points in each cell. Table 6.7 presents the values of R_a and R_{max} for each laboratory sample for the 2 explained resolution methods (midpoint values, indicated by 'M' and average values, indicated by 'A'). Both methods lead to generally lower values for R_a and R_{max} compared to the original resolution, for which R_a and R_{max} values of 0,62 mm - 1,10 mm and 4,19 mm - 7,25 mm were observed respectively (Table 6.5). The resolution reduction by midpoint values leads to the smallest decrease of R_a and R_{max} values, for which a range of 0,63 mm - 1,08 mm and 3,21 mm - 5,97 mm is observed respectively. The results also provide an indication that the parameter R_a is less sensitive to an alteration of the resolution compared to R_{max}.

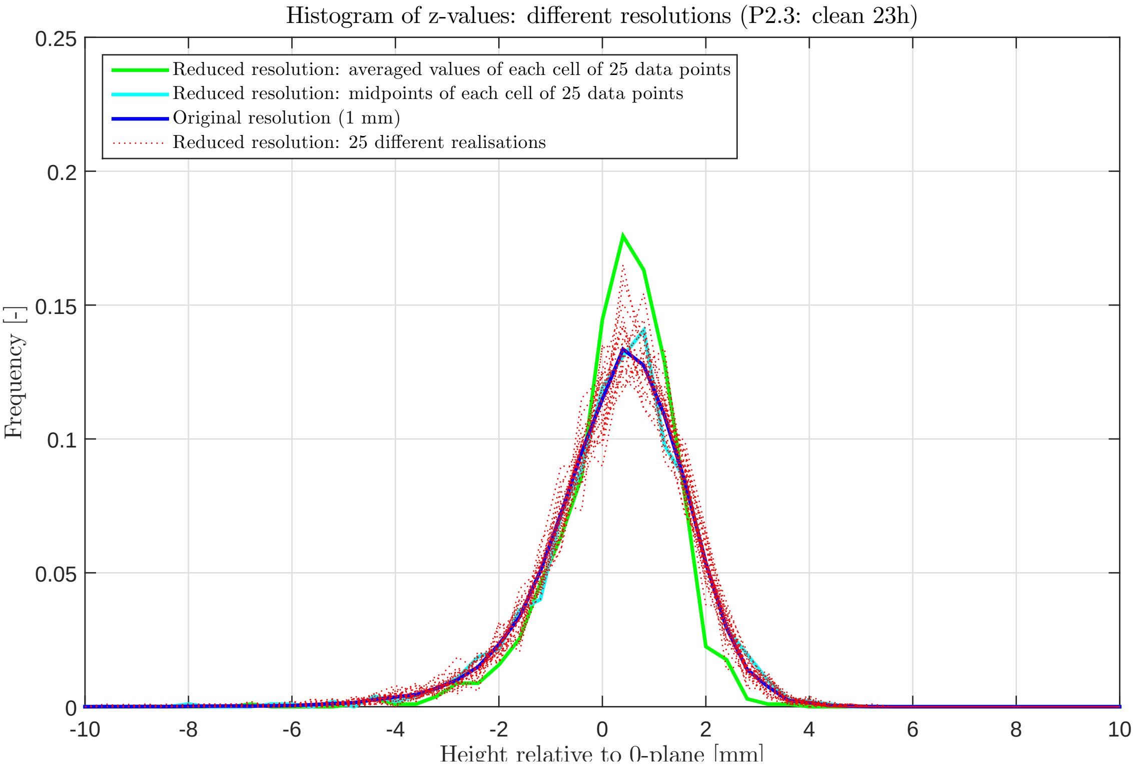

Figure 6.15: Resolution reduction: original and reduced resolution for P2.3 (averaged and midpoint values)

Table 6.7: Surface roughness results of laboratory concrete samples (reduced resolution)

Sample	$R_{a;x;M}$ * [mm]	$R_{a;y;M}$ [mm]	$R_{max;x;M}$ [mm]	$R_{max;y;M}$ [mm]	$R_{a;x;A}$ ** [mm]	$R_{a;y;A}$ [mm]	$R_{max;x;A}$ [mm]	$R_{max;y;A}$ [mm]
P2.1	0,63	0,63	3,21	3,39	0,37	0,36	1,98	2,00
P2.3	1,04	1,03	5,97	5,96	0,80	0,78	4,58	4,53
P2.4	0,92	0,81	4,91	4,52	0,76	0,62	3,76	3,38
P2.5	0,88	1,08	4,75	5,57	0,64	0,89	3,47	4,46
P2.6	0,74	0,70	3,74	3,69	0,56	0,51	2,47	2,56
P2.7	0,65	0,71	3,46	3,77	0,41	0,49	2,14	2,74

*: *Average* R_a *in x-direction for reduced resolution based on midpoint values*
**: *Average* R_a *in x-direction for reduced resolution based on averaged values*

When considering the resolution reduction method by midpoint values, the ranges of R_a and R_{max} values of the laboratory samples (0,63 mm - 1,08 mm and 3,21 mm - 5,97 mm respectively) are of similar magnitude compared to the observed ranges for R_a and R_{max} of the selected zones (Figure 6.13, 6.14) of the Spoorzone Delft in-situ data (0,87 mm - 1,18 mm and 4,36 mm - 6,17 mm respectively). The macro-roughness effects result in increased R_a and R_{max} values for the in-situ data at the considered sub-sample size of 160 mm x 160 mm (Table 6.6). This is an indication that the applied sample size is not sufficient to model these macro-roughness effects. Another limitation of this research with respect to the concrete surface texture is the method of concrete pouring, in which 0 falling height is applied to prevent initial filter cake disturbance. In addition, in the performed tests the sand surface, which models the excavation face, is perfectly horizontal prior to filter cake formation or concrete pouring (in the case of no filter cake). This is not realistic for in-situ conditions, since the excavation process is expected to lead to some irregularities of the excavation face, which will have some contribution in the formation of the eventual concrete surface texture.

6.4. Conclusion

To analyse the influence of filtration time on the interface shear strength for clean and contaminated filter cakes, a total of 7 direct-shear tests have been performed on layered sand/filter cake/concrete samples (170 mm x 170 mm, max. concrete aggregate size 16 mm) with varying filter cake thickness (controlled by the filtration time) and slurry compositions. The development of the applied modified direct-shear set-up has been discussed in the previous chapter. The direct-shear results (consolidation- and normal pressure of 200 kPa, 1,2 mm/min shear rate) show that for both the clean and contaminated filter cake samples a decrease of interface shear strength is observed with increased filtration time towards the filter cake shear strength (lower boundary interface shear strength), which has been analysed in experimental phase 1. However, the test results show that for the contaminated filter cakes, this lower boundary shear strength is reached after a shorter filtration time (around 12 hours) compared to the samples containing clean filter cakes (around 24 hours). This observation confirms the hypothesis (Section 2.4). The increase of interface shear strength with decreasing filter cake thickness is caused by aggregate protrusion, which is a function of both filter cake thickness and concrete surface roughness Lam et al. (2014). An analysis of the concrete surface roughness by means of 3D laser scan data shows that the concrete surface roughness is a function of the filter cake thickness. Given the applied concrete placement method (0 falling height), concrete directly placed on the sand bed (no filter cake presents) leads to the 'smoothest' surface, while an increased surface roughness is observed for increasing filter cake thickness. To compare the laboratory concrete surface roughness with in-situ data, the roughness is expressed as R_a and R_{max}. R_a is the arithmetic mean and R_{max} is the difference between the highest peak and deepest value along a certain profile. The range of R_{max} for the laboratory samples (4,19 mm to 7,25 mm, profile length around 160 mm, 1 mm resolution) is higher compared to the R_{max} range observed by Arwanitaki et al. (2007) for a profile length of 150 mm (3,3 mm to 6,4 mm). It should be noted that the applied data resolution of Arwanitaki et al. (2007) is unknown. In addition, an analysis of in-situ laser scan data from Spoorzone Delft test panels has been performed, showing a range of R_a and R_{max} values of 0,87 mm - 1,18 mm and 4,36 mm - 6,17 mm respectively for selected zones based on a sub-sample size of 160 mm x 160 mm at 1 mm resolution. An analysis of the complete panels at equal sub-sample size resulted in increased values of R_a and R_{max}, which is caused by macro-roughness patterns. To compare the laboratory data with the in-situ data, the resolution of the laboratory data (1 mm) is reduced to match the in-situ resolution (5 mm). For this purpose, 2 methods are applied; representing a cell of 25 data points by the midpoint value and the average value. Both methods of resolution reduction cause a decrease of R_a and R_{max}. However, the 'midpoint method' causes a smaller decrease of R_a and R_{max}. In addition, R_a seems to be least sensitive to the resolution reduction. A comparison of the observed range of R_a and R_{max} values for the selected zones in the in-situ data (thereby ignoring the macro-roughness patterns) with the laboratory roughness data (resolution reduction by midpoint values) indicates that the achieved concrete surface textures for the laboratory samples are comparable to in-situ conditions. However, as stated before, the effect of macro-roughness patterns has not been modelled in the direct-shear tests, given the shear box dimensions (170 mm x 170 mm). These large-scale surface texture patterns might cause an increased window of filtration time during which the sand shear strength is (partially) mobilised.

7 Conclusion and Recommendations

In this chapter, an answer to the main research question is formulated based on the results presented in the previous chapters. The goal of this thesis is to analyse the conservatism of the current CUR 231 recommendations on the external friction angle of diaphragm walls by means of an experimental test program. Therefore, the main research question has been formulated as follows:

How conservative are the current Dutch recommendations on the external friction angle δ of diaphragm walls?

To establish an experimental methodology, first a literature review has been performed. The literature review reveals that support fluid contamination by excavated soil material during trench excavation has a large influence on the formation and shear strength of the soil/structure interface of diaphragm walls. The soil/structure interface of a diaphragm wall is characterized by the presence of a bentonite filter cake, which is formed by filtration of the support fluid in non-cohesive soils. For different existing filtration criteria, see Walz et al. (1983), Sherard et al. (1984) and Henry et al. (1998). Soil material suspended in the support fluid contributes to the formation of the filter cake, thereby increasing the filter cake growth rate (Arwanitaki et al., 2007). In addition, the presence of the excavated soil material in the filter cake leads to an increased filter cake shear strength (Scott, 1978; Day et al., 1981; Henry et al., 1998; Arwanitaki et al., 2007; Deltares, 2008). In previous research, the filter cake shear strength has mainly been analysed by means of direct-shear tests on layered sand/filter cake/cement-mortar samples. Previous research on clean filter cake shear strength indicates a range of friction angle values around 20° (Henry et al., 1998; Deltares, 2008; Arwanitaki et al., 2007). However, for the case of filter cake contamination, friction angle values have been found ranging from 22,5° (Deltares, 2008) to around 30° (Henry et al., 1998; Arwanitaki et al., 2007).

The filter cake shear strength (clean or contaminated) is only governing if a continuous shear plane through the filter cake can be formed. Depending on the filter cake thickness and concrete surface texture, discontinuities in the filter cake can be present, caused by the phenomenon of 'aggregate protrusion' (Lam et al., 2014). Aggregate protrusion involves the penetration of the bentonite filter cake by individual concrete aggregates, thereby making direct contact with the sand layer. Direct-shear tests on layered sand/filter cake/concrete samples by Cernak et al. (1973) and Lam et al. (2014) show a decreased interface shear strength with increasing filtration time (and subsequent filter cake thickness) towards the filter cake shear strength, which forms the lower boundary interface shear strength.

Given the fact that the current CUR 231 recommendations on δ are based on an experimental investigation on the shear strength of clean bentonite filter cakes (Deltares, 2008), the following 2 sources of conservatism of the current recommendations have been identified in the Literature Review:

- Filter cake contamination by excavated soil particles is not taken into account;
- Continuous shear plane through filter cake is assumed (influence of concrete roughness and filter cake thickness is ignored).

Both aspects are captured in the proposed conceptual model (Section 2.4), which predicts the development of interface shear strength as a function of filtration time for clean and contaminated filter cakes. For filter cakes contaminated with excavated soil material, the filter cake shear strength (which is the lower boundary interface shear strength) is higher compared to clean filter cakes (Henry et al., 1998; Arwanitaki et al., 2007). However, due to the higher filter cake growth rate caused by slurry contamination (Arwanitaki et al., 2007), it is expected that for the case of contaminated filter cakes the lower boundary shear strength is reached after a shorter filtration time. This conceptual model forms the hypothesis for the experimental investigation of this research.

7.1. Experimental research questions

The experimental investigation of this research is divided into 2 phases to test the previously discussed hypothesis. The first experimental phase focusses on the filter cake shear strength, applying an existing experimental set-up developed by Van Dalen (2016), which involves direct-shear tests on layered sand/filter cake/cement-mortar samples (Ø 67 mm). The second experimental phase has focussed on the development of interface shear strength as a function of filtration time. For this purpose, a new direct-shear set-up has been developed (170 mm x 170 mm), which enables the analysis of layered sand/filter cake/concrete samples. For the first experimental phase, 2 research questions have been formulated, which are answered below.

1. *What is the influence of filter cake consolidation on the filter cake shear strength?*

Test series C1 to C3 show a friction angle of 18,3° for normally-consolidated clean filter cakes ($\gamma_{slurry} = 1,03 - 1,04 g/cm^3$) at a shear rate of 1,2 mm/min for consolidation- and normal pressures in the range of 200 kPa - 400 kPa. This value corresponds to the underlying experimental research of the current CUR 231 recommendations, in which a friction angle of 19,5° has been observed. Test series C4 and C5 show that for over-consolidated filter cakes (OCR = 4,0) at a shear rate of 1,2 mm/min and normal pressures of 50 kPa and 100 kPa (200 kPa and 400 kPa consolidation pressures resp.), the shear strength of the sand layer is governing ($\delta = \phi$). These results indicate that for conditions where the lateral concrete pressure exceeds the normal soil pressure (expected for the case of active soil pressure), an increased filter cake shear strength can be taken into account. However, part of the observed increased filter cake shear strength is caused by the presence of pore water under pressure prior to shearing due to the short reloading time. For further research it is therefore recommended to apply a longer reloading time to ensure complete pore water dissipation prior to shearing, which better models in-situ conditions, since building pit excavation is a slow process.

Tests C6.1 and C6.2 show an increased friction angle of around 23° for normally-consolidated clean filter cakes at a shear rate of 0,0072 mm/min (200 kPa normal pressure), which is a clear increase compared to test series C1 to C3 at 1,2 mm/min (18,3°). The increased shear strength of tests C6.1 and C6.2 is accompanied by additional vertical deformation during shearing compared to C1 to C3, which indicates additional filter cake consolidation during shearing (dissipation of pore water pressures). Although test series C1 to C3 show contractant behaviour, the shear rate of 1,2 mm/min did not allow for complete consolidation during shearing, causing a decrease of shear strength. It should be noted that only 2 tests have been performed at 0,0072 mm/min on clean filter cakes. Finally, the results of test C6.3 indicate that an increased consolidation time, leading to an increased exposure time to hydrating cement (35 days in stead of 6 days for all other tests) does not influence the shear strength of clean filter cakes. This is supported by Cernak et al. (1973) and Arwanitaki et al. (2007), who observed no chemical strengthening of the filter cake in the presence of hydrating cement.

2. *What is the influence of the filter cake composition on the filter cake shear strength?*

Results from test series S1 to S4 generally show an increased filter cake shear strength due to the presence of excavated soil material in the filter cake. The applied slurry composition in test series S1 to S4 is based on the analysis of an in-situ slurry sample from the Spoorzone Delft project. Based on the results of test series S1, an increase from $\gamma_{slurry} = 1,03 - 1,04 g/cm^3$ to $\gamma_{slurry} = 1,06 g/cm^3$ causes an increase of filter cake growth rate (from 0,20 $mm/\sqrt{min}$ for clean filter cakes to 0,24 $mm/\sqrt{min}$), but the filter cake shear strength corresponds to the 18,3° friction angle observed for the clean filter cakes. Replicating the complete in-situ sieve curve by addition of a sand/silt mixture (test series S2 and S3, $\gamma_{slurry} = 1,26 g/cm^3$) leads to a friction angle of 25,6° at a shear rate of 1,2 mm/min for normal pressures in the range of 200 kPa - 400 kPa. This is a clear increase compared to 18,3° for clean filter cakes at equal shear rate and normal pressure range. In the replication of the in-situ sieve-curve, the organic- and clay content has not been taken into account, since only a sand/silt mixture is added to a clean bentonite slurry, similar to Arwanitaki et al. (2007). The observed increase in shear strength by filter cake contamination in tests S2 and S3 is lower compared to Henry et al. (1998) and Arwanitaki et al. (2007), who observed friction angles around 30°.

However, as for test series C1 to C3 on clean filter cakes, the shear rate of 1,2 mm/min has lead to (partially) undrained shearing for tests S1 to S3. The higher filter cake thickness in tests S1 to S3, due to the increased filter cake growth rate at equal filtration time, causes an increase of the hydrodynamic period of the filter cake, decreasing the ability of excess pore water pressures to dissipate during shearing. A reduced filter cake thickness does not lead to a clear increase of filter cake shear strength, based on the results of tests S4.1 and S4.2, although increased volumetric deformation is observed during shearing, indicating additional filter cake consolidation during shearing. However, based on tests S4.3 and S4.4, the reduced filter cake thickness combined with a shear rate of 0,0072 mm/min does show a clearly increased friction angle of around 30°, which is of the same order as results by Henry et al. (1998) and Arwanitaki et al. (2007).

In general, the experimental procedure applied in the first experimental phase showed a number of problems and limitations. First of all, the measured shear resistance is disturbed by friction between the shear box- and sample tube interfaces. The direct-shear results indicate that mainly the post-peak behaviour is influenced. However, in some tests multiple peaks occur towards peak shear strength. Prior to each test, the sample tube interface is checked for irregularities and sanded down as good as possible. Another issue is the friction between the sample tube and cement-mortar, despite the presence of a latex membrane over the complete height of the cement-mortar. This friction influences both the filter cake compression results as the effective normal load acting on the filter cake during shearing. Given these issues, the experimental results on the filter cake shear strength should be interpreted with some caution. The mitigation of these issues is part of experimental phase 2.

3. *How can a direct-shear set-up be developed which enables the modelling of sand/filter cake/-concrete samples?*

To analyse the influence of filtration time (and subsequent filter cake thickness) on the interface shear strength, a realistic concrete mixture should be applied in sample preparation, since the phenomenon of aggregate protrusion is a function of both filter cake thickness and maximum aggregate size (Lam et al., 2014). In The Netherlands, a maximum aggregate size of 16 mm is often applied in diaphragm wall construction (CUR/COB, 2010). Based on the shear box geometry applied by Lam et al. (2014) compared to their applied concrete mixture (max. 20 mm), a desired minimum length and width of at least 10 times the maximum aggregate size has been established, leading to plan dimensions of 170 mm x 170 mm. In the development of the new direct-shear set-up, an attempt is made to mitigate the issues encountered with the small-scale set-up. First of all, the issue of shear box friction has been mitigated by the application of an interface spacing, for which a width of 2 mm is deemed sufficient. The possibility of concrete aggregates (max. 16 mm) interlocking behind the bottom shear box is accepted, since reducing this risk by the application of a wide interface spacing is expected to cause a reduction of shear strength due to the reduction of horizontal confining pressure around the shear plane. This is indicated by the relatively low values of filter cake shear strength by Lam et al. (2014), who applied an interface spacing of 20 mm to prevent concrete aggregate interlocking during shearing. In the sample preparation procedure, air pressure is applied for both filtration- and consolidation pressure. A latex membrane is applied as air vessel to apply the air pressure onto the wet concrete mix. The normal load during shearing is applied mechanically by a lever arm, present on the existing direct-shear machine frame.

4. *What is the influence of filter cake thickness on the interface shear strength for clean and contaminated filter cakes?*

The results of a series of large-scale direct-shear tests (170 mm x 170 mm, 200 kPa, 1,2 mm/min) show that for layered interface samples (sand/filter cake/concrete) containing a contaminated filter cake ($\gamma_{slurry} = 1,26 g/cm^3$), a decrease of interface shear strength is observed at lower filtration time values than is the case for clean filter cake samples. Together with the experimental results obtained with the small-scale direct-shear set-up (Ø 67 mm), which showed a higher filter cake shear strength for contaminated filter cakes ($\gamma_{slurry} = 1,26 g/cm^3$), the hypothesis (Section 2.4) is confirmed, which predicted the development of interface shear strength for an interface layering containing a contaminated filter cake compared to a clean filter cake. In addition, 3D laser scans of the concrete surface indicate that given the applied concrete pouring method (applying the concrete with 0 falling height on the bentonite filter cake), the concrete surface roughness is a function of the filter cake thickness (based on a comparison of z-value histograms). Concrete placed directly on the sand bed (no filter cake) creates the smoothest surface, whilst the surface roughness increases with increasing filter cake thickness. Since the phenomenon of aggregate protrusion is a function of both filter cake thickness and concrete surface roughness (Lam et al., 2014), the achieved concrete roughness of the laboratory samples is compared to in-situ data. The range of observed surface roughness expressed in terms of R_{max} is comparable to the observed R_{max} values by Arwanitaki et al. (2007). In addition, the laboratory roughness is comparable to in-situ data from the Spoorzone Delft project, based on a comparison of R_a and R_{max} at similar sample size and resolution, ignoring macro-roughness patterns. The influence of macro-roughness patterns (caused by excavation process) has not been modelled in this research. However, these macro-roughness might cause an increased window of filtration time during which the sand shear strength is (partially) mobilised, causing an increased interface shear strength.

7.2. Final conclusion

Based on literature and the experimental results of this research, omitting the influence of filter cake contamination on the filter cake shear strength is the main source of conservatism in the current recommendations on the external friction angle δ of diaphragm walls. In addition, as predicted in the conceptual model and observed in the large-scale experimental results, an additional optimisation of δ might be obtained when limiting the filtration time, thereby utilizing the mobilisation of the sand shear strength at low filter cake thickness. However, due to the high filter cake growth rate in the case of slurry contamination, the time frame of increased interface shear strength for contaminated filter cakes is limited (around 12 hours in this research). Previous research has shown even higher filter cake growth rates (Arwanitaki et al., 2007) for a contaminated slurry, which would lead to an even shorter time frame towards the lower boundary shear strength. Hence, it is expected that including the time effect into recommendations on δ would not be of practical use. It is therefore advised that when taking account of filter cake contamination, the recommended δ value(s) should be representing the filter cake shear strength, omitting the time effect (Figure 7.1, horizontal cut-off at $[t_{a2}, r_a]$). However, it can not be ruled out that macro-roughness effects do not cause an extended time effect.

7.3. Recommendations

The experimental results of this thesis show that by taking account of filter cake contamination, the current recommendations on δ of diaphragm walls can be optimized. However, in this research filter cake contamination has only been investigated by means of a replicated slurry mixture, omitting the organic- and clay content. It is therefore recommended that future research should focus on the shear strength of in-situ filter cakes, to get a better insight into the spreading of contaminated filter cake shear strength and its relation with the soil profile in which excavation takes place. For this purpose, the developed modified direct-shear equipment is suited, by applying in-situ slurry samples in filter cake formation. In further analyses of in-situ filter cake shear strength, attention should be paid to the applied shear rate, since the experimental results of this research show a dependency of filter cake shear strength to the applied shear rate. In addition, further research is recommended with respect to the influence of over-consolidation on filter cake shear strength, thereby applying sufficient reloading time to ensure complete dissipation of pore water pressures prior to shearing. The large-scale direct-shear test results show a limited window of filtration time (trench stand-open time) during which the sand shear strength is (partially) mobilised. The influence of consolidation pressure on the length of this time frame should be investigated in further testing. It is expected that increased consolidation pressure (increased trench depth) causes an extended time frame of increased interface shear strength. In addition, additional research on the influence of macro-roughness patterns on the interface shear strength is advised, which also might show an increased time effect. Furthermore, it is advised to investigate the sensitivity of diaphragm wall performance to the external friction angle δ for different building pit geometries. From theory it is known that δ directly influences the magnitude of K_p. Preliminary calculations indicate that the sensitivity of diaphragm wall performance with respect to δ is limited in the case of the application of an underwater concrete floor, since the passive soil resistance is mobilised to a limited extent. Finally, the developed modified direct-shear set-up can be applied to investigate the influence of polymer-based support fluids on the interface shear strength.

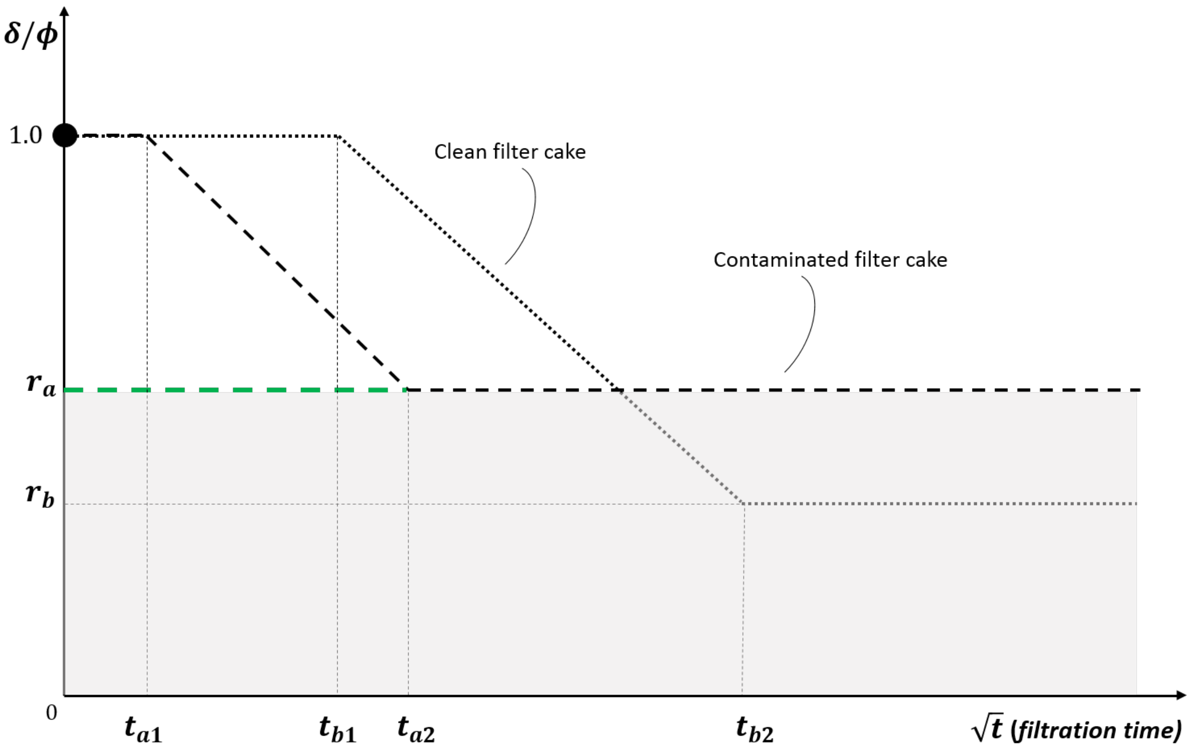

Figure 7.1: Recommendation on omitting the influence of filtration time on interface shear strength in future recommendations, thereby focussing on contaminated filter cake shear strength (lower boundary shear strength)

Bibliography

Anaraki, K. Hypoplasticity Investigated - Parameter Determination and Numerical Simulation. Master's thesis, Delft University of Technology, 2008.

Arwanitaki, A., König, D., and Triantafyllidis, T. Zum kontaktverhalten zwischen suspensionsgestützten ortbetonwänden und dem anstehenden boden. *Bautechnik*, 84(11):781–792, 2007.

Boskalis. Aanvullend grondonderzoek bemaling fietstunnel N209, September 2015.

BS. 1377-2:1990 Methods of test for soils for civil engineering purposes. Classification tests. British Standards Institution, 1990.

Bushan, B. *Modern Tribology Handbook, Volume One, Principles of Tribology*. CRC Press LLC, Boca Raton, 2001.

Buykx, S. M., Delfgaauw, S., and Bosch, J. W. Probabilistic analysis of soil - diaphragm wall friction used for value engineering of deep excavation, North/South metro Amsterdam. In *Safe Tunneling for the City and Environment: ITA-AITES World Tunnel Congress, 23-28 May 2009, Budapest, Hungary*. Hungarian Tunneling Association, 2009.

Cernak, B., Dvorak, A., Hlavacek, J., Klein, K., and Petrasek, J. New approaches to problems of bearing capacity and settlement of piles. In *Proceedings of the 8th international conference on soil mechanics and foundation engineering, Moscow*, volume 2, pages 67–74, 1973.

COB. *Handboek Ondergronds Bouwen, Deel 1: Ondergronds Bouwen In Breed Perspectief*. A.A. Balkema, Rotterdam, 1997.

Craig, R. F. *Soil Mechanics*. E & FN SPON, London, Sixth edition, 1997.

CUR. *Publicatie 166: Damwandconstructies*. Stichting CURNET, Gouda, Fifth edition, 2008.

CUR/COB. *Rapport 231: Handboek diepwanden - Ontwerp en uitvoering*. Stichting CURNET, Gouda, 2010.

Day, P., Knight, K., and Wates, J. Skin friction on underslurry piles. In *Proceedings of the Tenth International Conference on Soil Mechanics and Foundation Engineering, Stockholm*, 1981.

Deltares. Onderzoek naar wrijving tussen grond en diepwand. Advies diepe stations, Noord-Zuidlijn, 2008.

Diao, Y. and Zheng, G. Numerical analysis of effect of friction between diaphragm wall and soil on braced excavation. *Journal of Central South University*, 15(2):81–86, 2008.

DIN. 4126: Cast-in-situ concrete diaphragm walls, Design and construction. Deutsches Institut für Normung, 1986.

Eberly, D. Least Squares Fitting Of Data, Geometric Tools LLC, 2008.

Filz, G., Boyer, R., and Davidson, R. Bentonite-water slurry rheology and cutoff wall trench stability. *In Situ Remediation of the Geoenvironment, Geotechnical Special Publication*, (71):139 – 152, 1997.

Hamparuthi, K. and Kumar, V. Effect of filtercake on interfacial friction - an experimental study. In *Proceedings of Indian Geotechnical Conference December 15-17, 2011, Kochi*, pages 183 – 186, 2011.

Henry, L. B., Filz, G. M., and Davidson, R. R. Formation and properties of bentonite filter cakes. In *Proceedings of the ASCE annual convention: Filtration and drainage in geotechnical/geoenvironmental engineering, Boston. ASCE Geotechnical Special Publication*, volume 78, pages 69–88. ASCE, 1998.

Hutchinson, M. T., Daw, G. P., Shotton, P. G., and James, A. N. The properties of bentonite slurries used in diaphragm walling and their control. In *Proceedings of conference on diaphragm walls and anchorages, London*, pages 33–39. Institution of Civil Engineers, 1975.

Khayat, K. H., Bonen, D., Shah, S., and Taylor, P. SCC formwork pressure, task 1: Capturing existing knowledge on formwork pressure exerted by SCC, 2007.

Kishida, H. and Uesugi, M. Frictional resistance at yield between dry sand and mild steel. *Soils and Foundations*, 26(4):139–149, 1986. As cited in Paikowsky et al. (1995).

Lam, C., Jefferis, S. A., and Martin, C. M. Effects of polymer and bentonite support fluids on concrete–sand interface shear strength. *Géotechnique*, 64(1):28–39, 2014.

Lings, M. L., Ng, C. W. W., and Nash, D. F. T. The lateral pressure of wet concrete in diaphragm wall panels cast under bentonite. In *Proceedings of the Institution of Civil Engineers: Geotechnical Engineering*, pages 163–172, 1994.

Lubach, A. Bentonite cavities in diaphragm walls; case studies, process decomposition, scenario analysis and laboratory experiments. Master's thesis, Delft University of Technology, 2010.

Müller-Kirchbauer, H. Stability of slurry trenches. In *Proceedings of the 5th European Conference on Soil Mechanics and Foundation Engineering, Madrid*, pages 543–553, 1972.

Nash, K. L. Stability of trenches filled with fluids. *Journal of the Construction Division: ASCE*, 100(4): 533–542, 1974.

NEN. 1538: Execution of special geotechnical work - Diaphragm walls. Nederlands Normalisatie Instituut, 2010.

NEN. 15935: Sludge, treated biowaste, soil and waste - Determination of loss on ignition. Nederlands Normalisatie Instituut, 2012.

Olson, R. E. and Lai, J. Direct shear testing. Technical report, Chaoyang University of Technology, Department of Construction Engineering, Advanced Geotechnical Laboratory, 2004.

Paikowsky, S. G., Player, C. M., and Connors, P. J. A dual interface apparatus for testing unrestricted friction of soil along solid surface. *Geological Engineering*, 2:168–193, 1995.

Scott, H. The shear strength of a bentonite layer in a pile foundation. Master's thesis, University of Natal, 1978. As cited in Day et al. (1981).

Shakir, R. and Zhu, J. An examination of the mechanical interaction of drilling slurries at the soil-concrete contact. *Journal of Zhejiang University-Science A*, 11(4):294–304, 2010.

Sherard, J. L., Dunnigan, L. P., and Talbot, J. R. Filters for silts and clays. *Journal of Geotechnical Engineering*, 110(6):701–718, 1984.

Spruit, R. *To detect anomalies in diaphragm walls*. PhD thesis, Delft University of Technology, 2015.

Thasnanipan, N., Baskaran, G., and Anwar, M. A. Effect of construction time and bentonite viscosity on shaft capacity of bored piles. In *Deep foundations on bored and auger piles: Proceedings of the 3rd international geotechnical seminar on bored and auger piles, Ghent, Belgium*, 1998.

Tucker, K. and Reese, L. The effect of bentonitic slurry on drilled shafts. Technical report, Center for Transportation Research, The University of Texas at Austin, Texas, 1984.

Van Dalen, J. H. *Diaphragm walls, optimization of the production process with 3D FEM simulation of flow processes*. PhD thesis, Delft University of Technology, 2016.

Van Tol, A. F. and Everts, H. J. *Funderingstechnieken, Uitvoeringsaspecten*. VSSD, Delft, 2008.

Van Weele, A. F. *Moderne Funderingstechnieken*. Waltman, Delft, 1981.

Verruijt, A. *Soil Mechanics*. Delft University of Technology, 2012.

Verruijt, A. and Van Baars, S. *Grondmechanica*. VSSD, Delft, 2009.

Walz, B., Gerlach, J., and Pulsfort, M. Schlitzwandbauweise, Konstruktion, Berechnung und Ausführung. Bergische Universität Gesamthochschule Wuppertal, 1983.

Wates, J. A. and Knight, K. The effect of bentonite on the skin friction in cast-in-place piles and diaphragm walls. In *Proceedings of the 6th Regional Conference for Africa on Soil Mechanics and Foundation Engineering, Durban*, volume 1, pages 183–188, 1975.

A

Sample preparation experimental phase 1: description

A.1. Filtration stage

Figures A.1 and A.2 show the process of filter cake exposure. First the standpipe is drained through a valve. Next, the sample tubes are disconnected from the manifold. The slurry in the separated sample tubes is removed with a syringe, whilst taking care not to disturb the filter cake surface. Finally, the top sample tube is carefully pulled upwards using a pulley tool (Figure A.1) to allow the remaining slurry to flow off the filter cake (Figure A.2).

Figure A.1: Uplifting of sleeve joint to remove top sample tube, using a pulley removal tool

Figure A.2: Exposed filter cake on bottom sample tube and removed top sample tube with sleeve joint

A.2. Consolidation stage

A latex membrane is placed on the inside of the top sample tube (coated with vaseline) and carefully slided down until it just makes contact with the top of the bentonite filter cake (Figure A.3). Next, cement-mortar is gently placed on top of the filter cake with 0 falling height using a small spoon. In this way, an effort is made to avoid initial disturbance of the filter cake. After filling the top sample tube to the top of the latex membrane, a pressure plate is placed on top of the cement-mortar and the sample tube is placed in an oedometer to apply a consolidation pressure (Figure A.4).

Figure A.3: Applying cement mortar inside top sample tube on top of filter cake

Figure A.4: Sample container placed in oedometer to apply curing pressure

A.3. Transfer to direct-shear test

Prior to shearing the connection sleeve is removed using a pulley tool (Figure A.5). Next, the sample tubes are placed within the existing shear boxes, a normal load is applied and the sample is sheared after reloading is finished (Figure A.6).

Figure A.5: Sleeve joint removed with pulley tool prior to direct-shear test

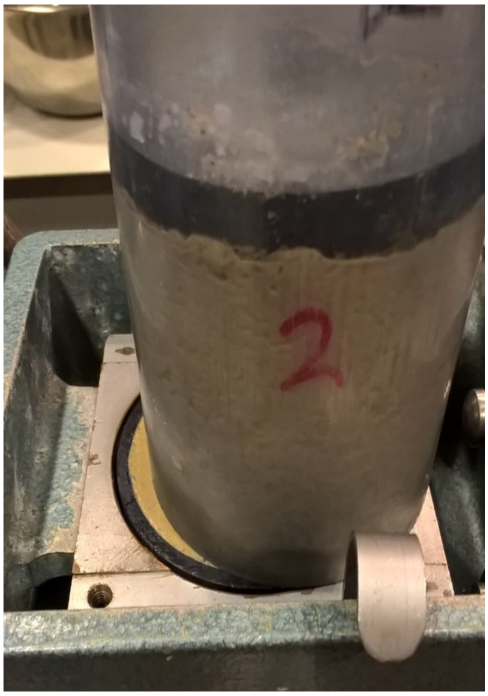

Figure A.6: Sample containers after direct-shear test: shear-plane through filter cake

A.4. Points of attention

For further application of the small-scale set-up and procedure, the following aspects require special attention:

- The sample tube interfaces should be polished prior to each new test series to reduce the interface friction as much as possible;
- When placing the top sample tube on the bottom sample tube after filter cake exposure, any sand grains should be removed to prevent them to end up in between the sample tubes, causing additional interface friction;
- The latex membrane must be placed such that it reaches to the top of the filter cake, to avoid any direct contact between the cement-mortar and sample tube which would obstruct the vertical movement of the sample within the sample tubes;
- To avoid upward squeezing of the top sample tube due to the consolidation load, fix the top sample tube to the oedometer frame (by means of a rope) to prevent any vertical movement of the sample tube (Figure A.7).

Figure A.7: Consolidation stage: prevention of vertical movement by rope attached to oedometer frame

B Sample preparation experimental phase 1: test results

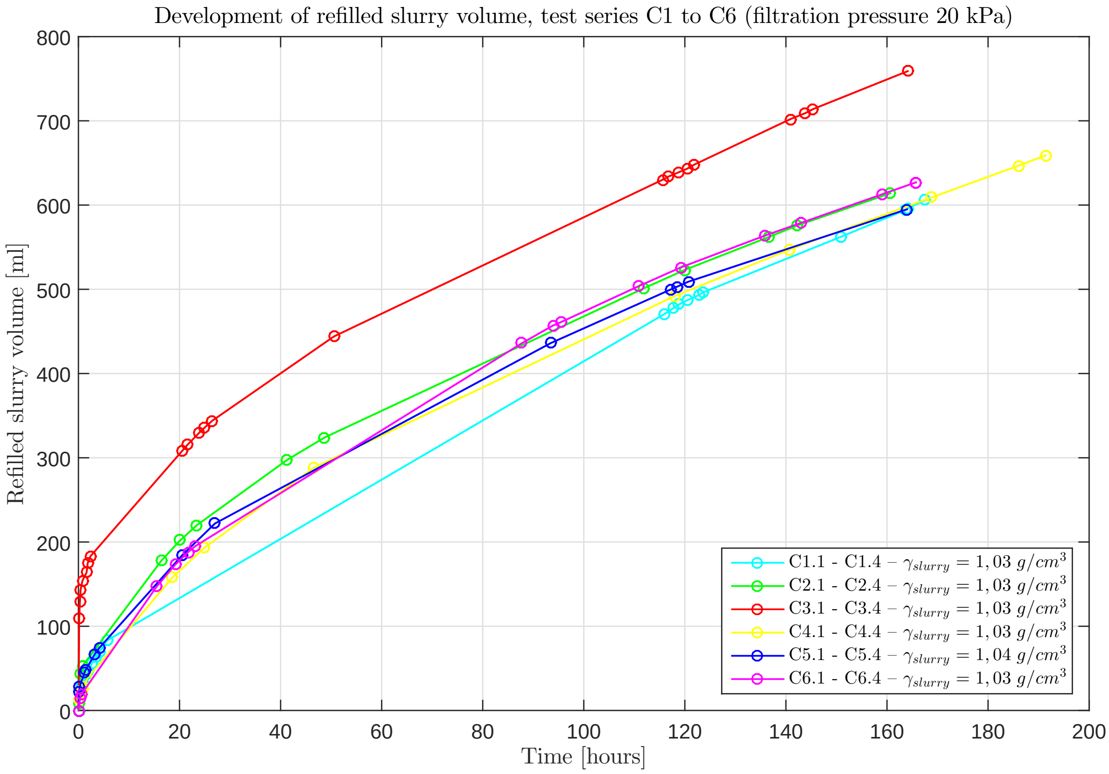

Figure B.1: Refilled slurry volume as a function of time (series C1 to C6, clean bentonite slurry)

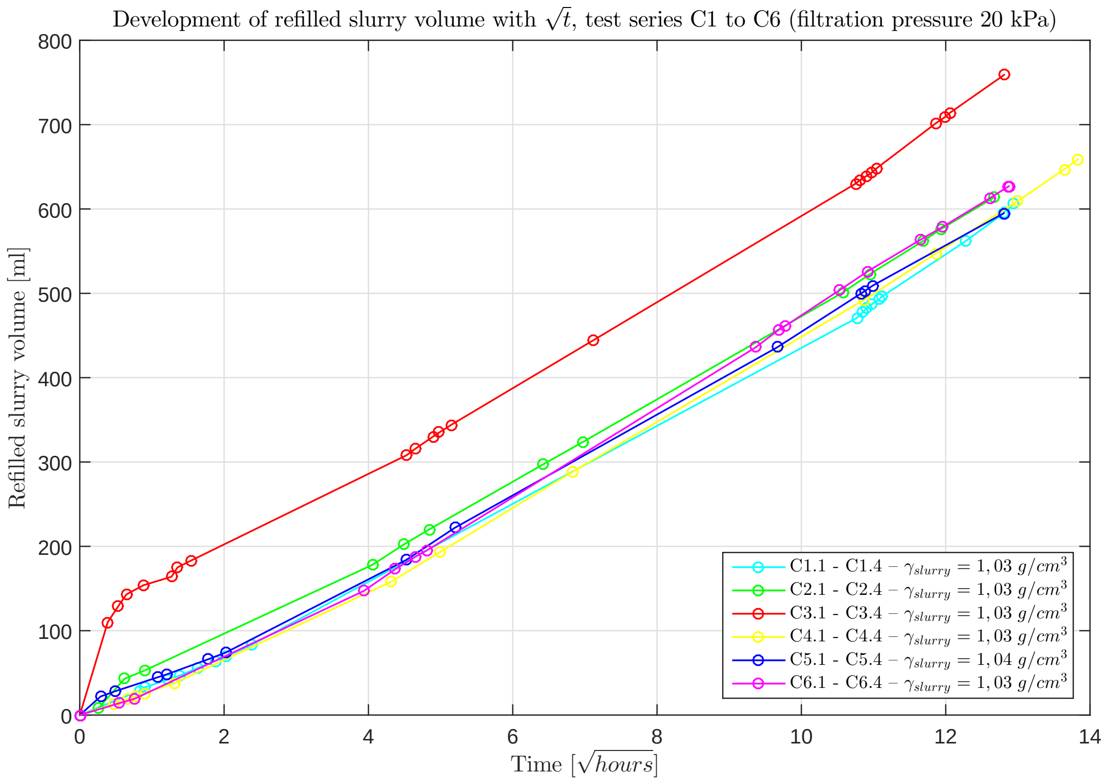

Figure B.2: Refilled slurry volume as a function of the square root of time (series C1 to C6, clean bentonite slurry)

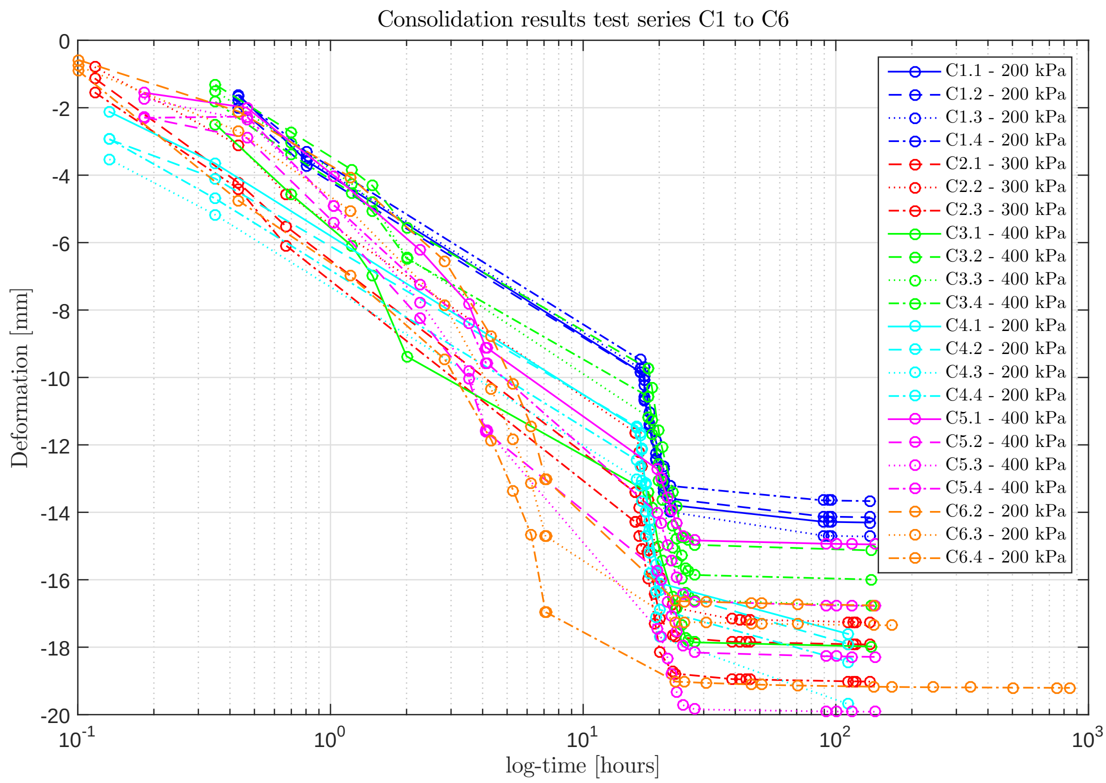

Figure B.3: Filter cake consolidation results for test series C1 to C6

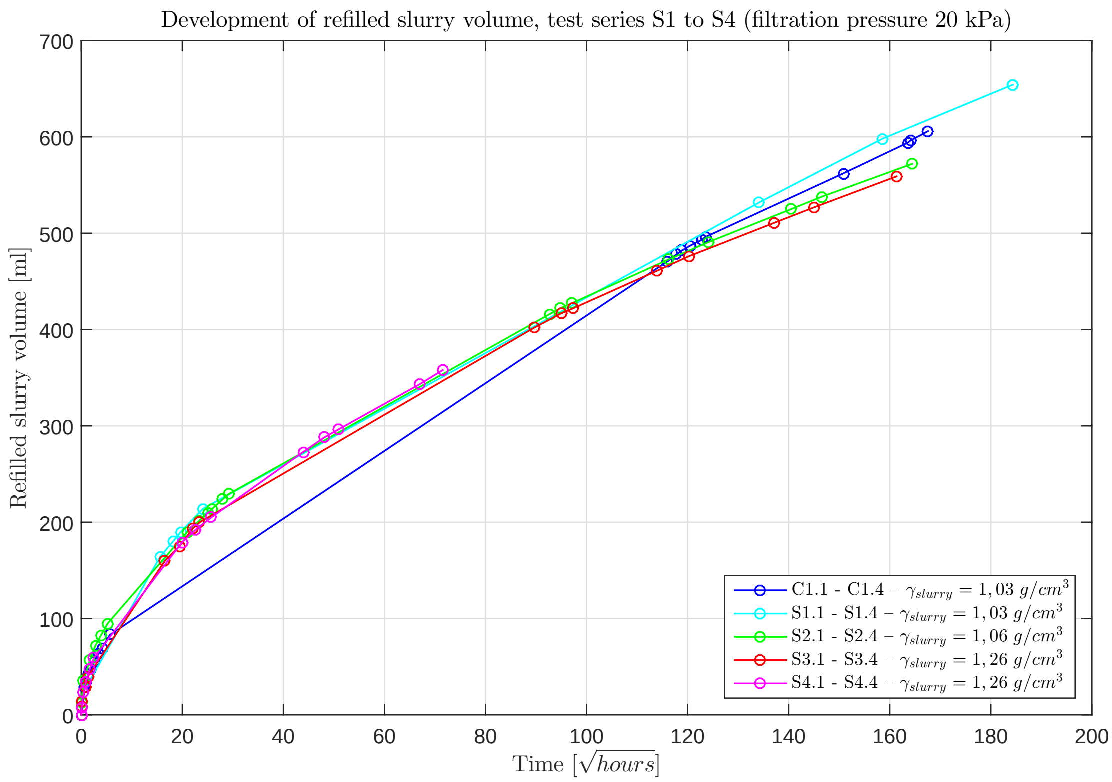

Figure B.4: Refilled slurry volume as a function of time (S1 to S4 and C1 as reference)

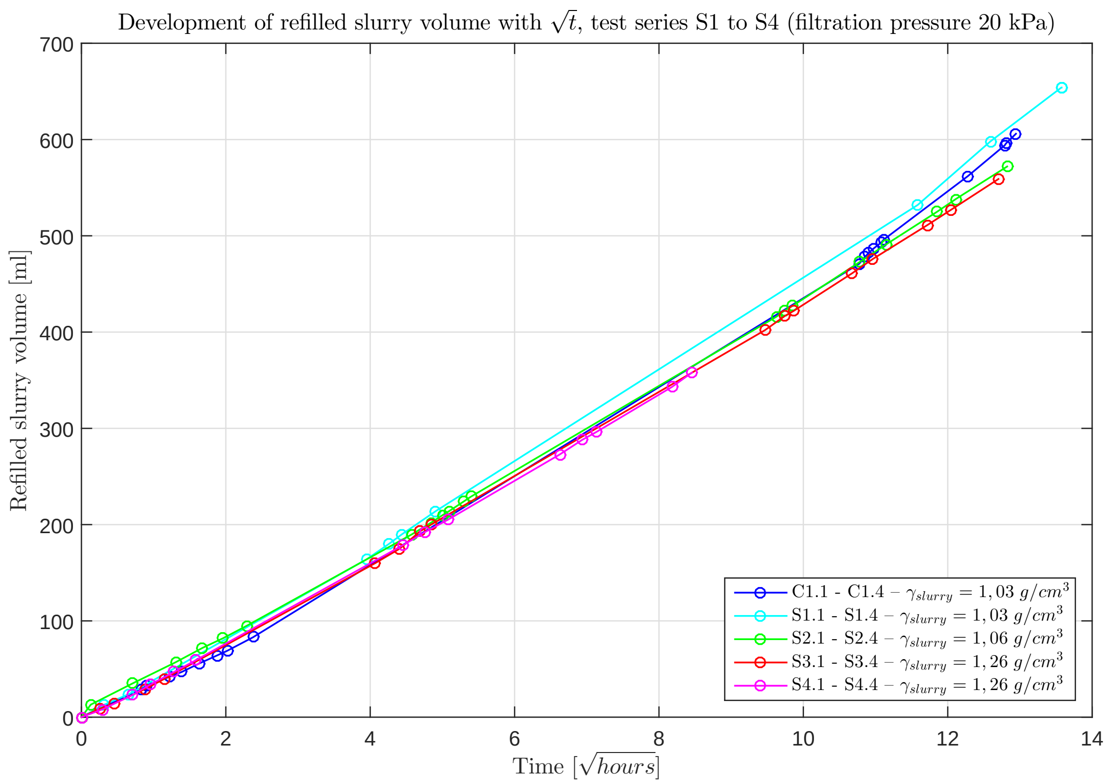

Figure B.5: Refilled slurry volume as a function of the square root of time (S1 to S4 and C1 as reference)

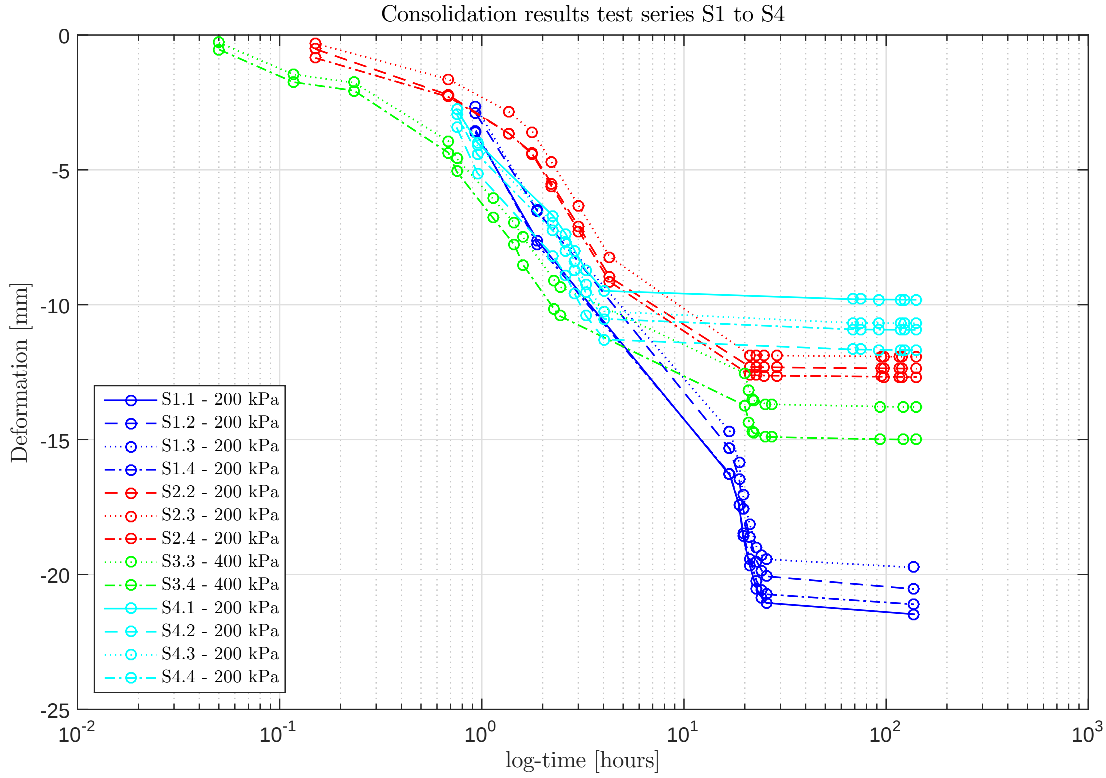

Figure B.6: Filter cake consolidation results for test series S1 to S4

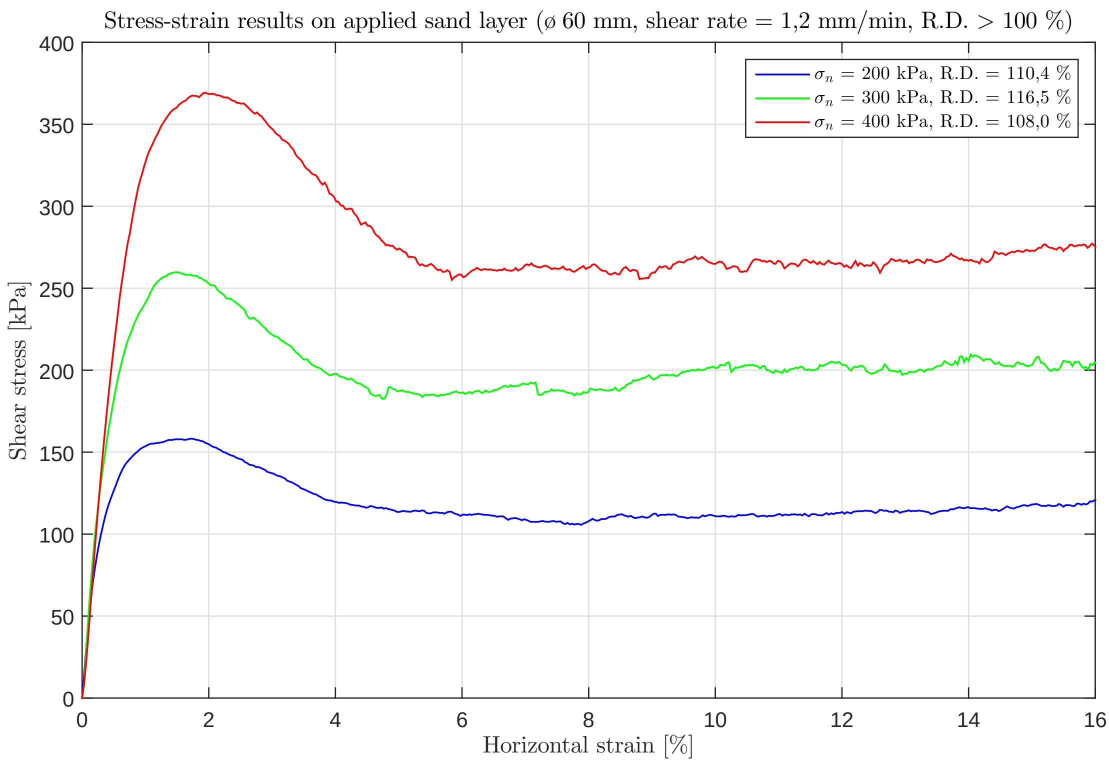

Figure B.7: Stress-strain results of direct-shear tests on the applied sand layer

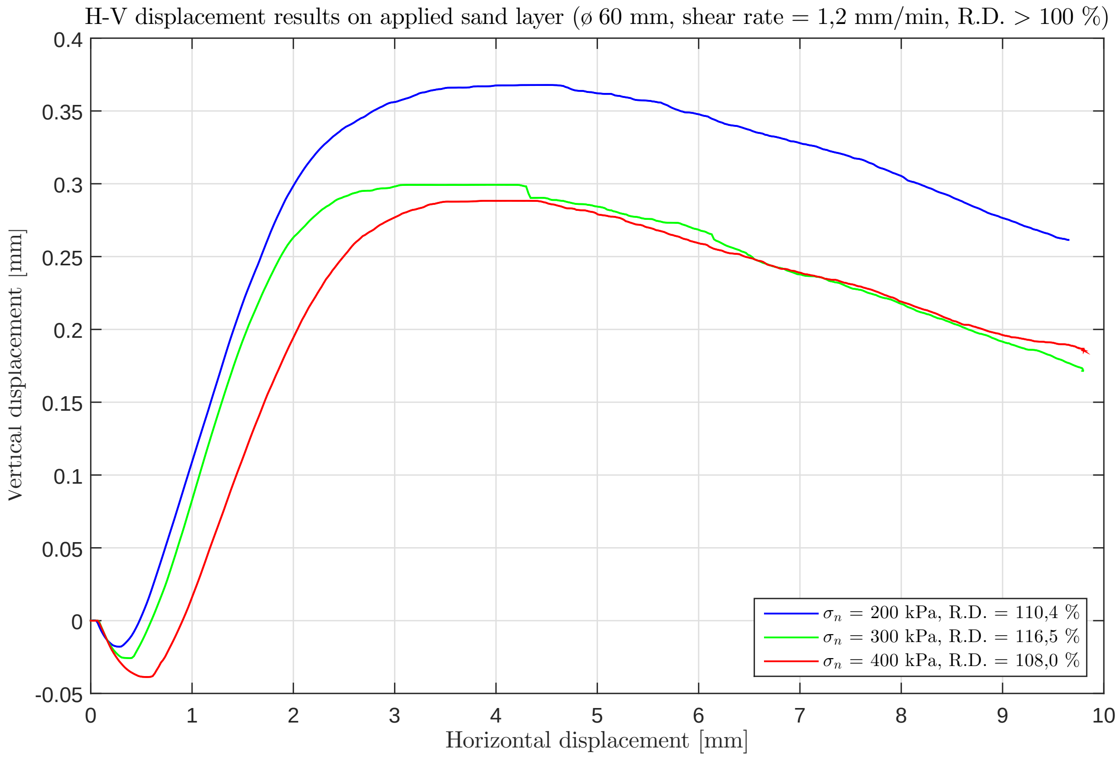

Figure B.8: Horizontal/vertical displacement results of direct-shear tests on the applied sand layer

C

Product specification Cebogel Trenchcontrol AT (Cebo Holland)

Product Data Blad

Cebogel Trenchcontrol AT

Toepassing **Diepwanden**

Omschrijving

Cebogel Trenchcontrol AT is een 100% geactiveerde natrium bentoniet welke zich kenmerkt door snelle afdichting van de sleufwanden en een laag filtraatwaterverlies. Het lage filtraatverlies van **Cebogel Trenchcontrol AT** maakt hem zeer effectief in zanderige formaties waar gevaren voor spoelingsverliezen aanwezig zijn. **Cebogel Trenchcontrol AT** voldoet aan de eisen gesteld in CUR 231* Handboek Diepwanden.

Eigenschappen

Cebogel Trenchcontrol AT heeft de volgende eigenschappen;

Laag filtraatverlies
Cebogel Trenchcontrol AT heeft goede stabiliserende eigenschappen door een lager filtraatverlies en een snelle afpleistering van de sleufwanden. Een laag filtraatwaterverlies zorgt voor een geringe indringing in de formatie en is essentieel voor de sleufstabiliteit.

Lager meerverbruik
De uitstekende afpleisterings- en stabilisatie-eigenschappen zorgen voor een lager bentoniet- en betonverbruik, wat een positieve bijdrage levert aan de kostenbeperking van het project.

Cebogel Trenchcontrol AT heeft de volgende typische waarden;

Typische waarden Cebogel Trenchcontrol AT			
Parameter	**Test methode**	**Eis**	**Typische waarde**
Korrelgrootte	-	Min. 95% door 125 micron (µm) zeef	**96%**
Vochtgehalte	Volgens DIN 18121-1	≤ 13% (m/m)	**8%**
Soortelijk gewicht	-	-	**2300 kg / m^3 $^{+/-}$ 10%**
Stort gewicht	-	-	**900 kg / m^3 $^{+/-}$ 10%**

Cebogel Trenchcontrol AT heeft de volgende chemische en fysische eigenschappen;

Chemische en fysische eigenschappen Cebogel Trenchcontrol AT	
Samenstelling	**Hoogwaardige geactiveerde natrium bentoniet**
Kleur	**Beige**
Vorm	**Poeder**

Cebo Holland

Industrial Minerals, Powerful Logistics

Cebo Holland BV, Westerduinweg 1, 1976 BV IJmuiden, The Netherlands
Tel. +31(0)255-546262, Fax +31-(0)255-546202, info@cebo.com, www.cebo.com

Cebogel Trenchcontrol AT

Product Data Blad

Aanbevolen gebruik

De eigenschappen van Cebogel Trenchcontrol AT worden het best benut als het aanmaakwater de volgende eigenschappen bezit;

- Geleidbaarheid : < 1000 µS/cm
- pH : 7.5 – 10
- Hardheid : < 100 ppm

Langzaam en gelijkmatig toevoegen aan een hoog circulatie mixer. Blijf de slurry rond circuleren totdat de bentoniet volledig is gedispergeerd. Aanbevolen wordt de suspensie minimaal 4 uur te laten rijpen.

Cebogel Trenchcontrol AT in suspensie van 40kg/m³ heeft de volgende typische waarden (na 24 uur);

Typische waarden van de 4% Cebogel Trenchcontrol AT suspensie (vers)			
Parameter	**Test methode**	**Eis***	**Typische waarde**
Dichtheid	Fann Mud Balance	-	**1,03 g/ml**
Viscositeit	Fann Marsh Funnel	32 - 60 sec.	**34 sec.**
Waterafscheiding	-	0% na 24 uur	**0%**
Vloeigrens kogelnummer	Kugelharfengerät	-	**1 kogel - 6,9 N/m²**
Filtraatwaterverlies	Fann API Filter Press	≤ 15 ml (7,5 min)	**≤ 10 ml**

Verpakking

Cebogel Trenchcontrol AT is verkrijgbaar in de volgende verpakkingen;

- 1000 kg verpakt in 25 kg zakken op een pallet met krimpfolie
- 1000 kg big bag
- bulk

Revisie datum : 29.08.2013
Document nummer : 100602NL

Voor zover wij kunnen beoordelen is bovengenoemde informatie correct. Wij kunnen u echter geen garanties geven over de resultaten die u hiermee zult bereiken. Deze beschrijving wordt u aangeboden op voorwaarde dat u zelf bepaalt in hoeverre zij geschikt is voor uw doeleinden.

Cebo Holland

Industrial Minerals, Powerful Logistics

Cebo Holland BV, Westerduinweg 1, 1976 BV IJmuiden, The Netherlands
Tel. +31(0)255-546262, Fax +31-(0)255-546202, info@cebo.com, www.cebo.com

D

Product specification Millisil M6 (Sibelco)

M6.pdf M6.bb

SIBELCO

MILLISIL® M6 - M6.1 - M10

MILLISIL® is produced by iron-free grinding and accurate sieving by means of air-separators.
A selected silica sand with a SiO_2 content of over 99 % is used as raw material. The purity, controlled particle size distribution, chemical inertness, optical properties and hardness make **MILLISIL®** the performance standard in ceramics, tile-glues, special mortars and coatings.

GRANULOMETRIC DATA AND PHYSICAL CHARACTERISTICS

		M6	M6.1	M10		Method
control-sieve > 63 µm		14	14	2	%	Alpine
D50		37	37	23	µm	Malvern Laser diffr.
> 160 µm		1	1		%	"
> 100 µm		9	9	2	%	"
> 63 µm		26	26	11	%	"
> 40 µm		47	47	28	%	"
> 30 µm		57	57	40	%	"
> 20 µm		68	68	54	%	"
> 15 µm		74	74	63	%	"
> 10 µm		80	80	72	%	"
> 5 µm		88	88	81	%	"
> 2 µm		95	95	90	%	"
> 1 µm		99	99	95	%	"
density		2.65	2.65	2.65	kg/dm³	
bulk density		1	1	0.9	kg/dm³	
specific surface		0.8	0.8	0.5	m²/g	BET
		2400	2400	3600	cm²/g	Blaine
oil absorption		16.5	16.5	17.5	g/100 g	
hardness		7	7	7	Mohs	
pH		7	7	7		
loss on ignition		0.12	0.08	0.12	%	
colour	L*	90	91	91		Minolta CM-3610d
	a*	0.87	0.98	0.74		D65/10°
	b*	4.13	3.50	3.57		
refractive index		1.55	1.55	1.55		

CHEMICAL ANALYSIS (XRF) %

	M6	M6.1	M10
SiO_2	99.5	99.8	99.5
Fe_2O_3	0.03	0.01	0.03
Al_2O_3	0.20	0.05	0.20
TiO_2	0.03	0.02	0.03
K_2O	0.04	0.01	0.04
CaO	0.02	0.01	0.02

The above given information is based on mean values. The typical properties and chemical analyses are intended as examples and are not to be considered as substitutes for actual testing and analyses in those situations where properties and chemical compositions are critical factors.
Sales and supplies will always be according to our general sales conditions.

CAS-Nr.: 14808-60-7 EINECS-Nr.: 238-878-4 MSDS available on request

ed.06 TDS.03.05.32 17/12/04 1/1

S.C.R.-Sibelco N.V. • De Zate 1 • BE-2480 DESSEL • Tel. int. + 32 14 83 72 31 • Fax int. + 32 14 83 72 32
www.sibelco.be • H.R.A. 612 • BTW. BE 404 679 941 • BBL 320-0004270-72 • sales@sibelco.be

E

Results triaxial tests on sand/silt mixture

Table E.1: Summary of triaxial test parameters and results

Test ID	$\gamma_{mixture}$ [kg/dm^3]	σ_1 [kPa]	σ_3 [kPa]	ϕ' [°]
T1	1,32	217	50	38,7
T2	1,40	484	100	41,1
T3	1,42	450	100	39,5
T4	1,61	398	50	51,0
T5	1,57	498	75	47,6

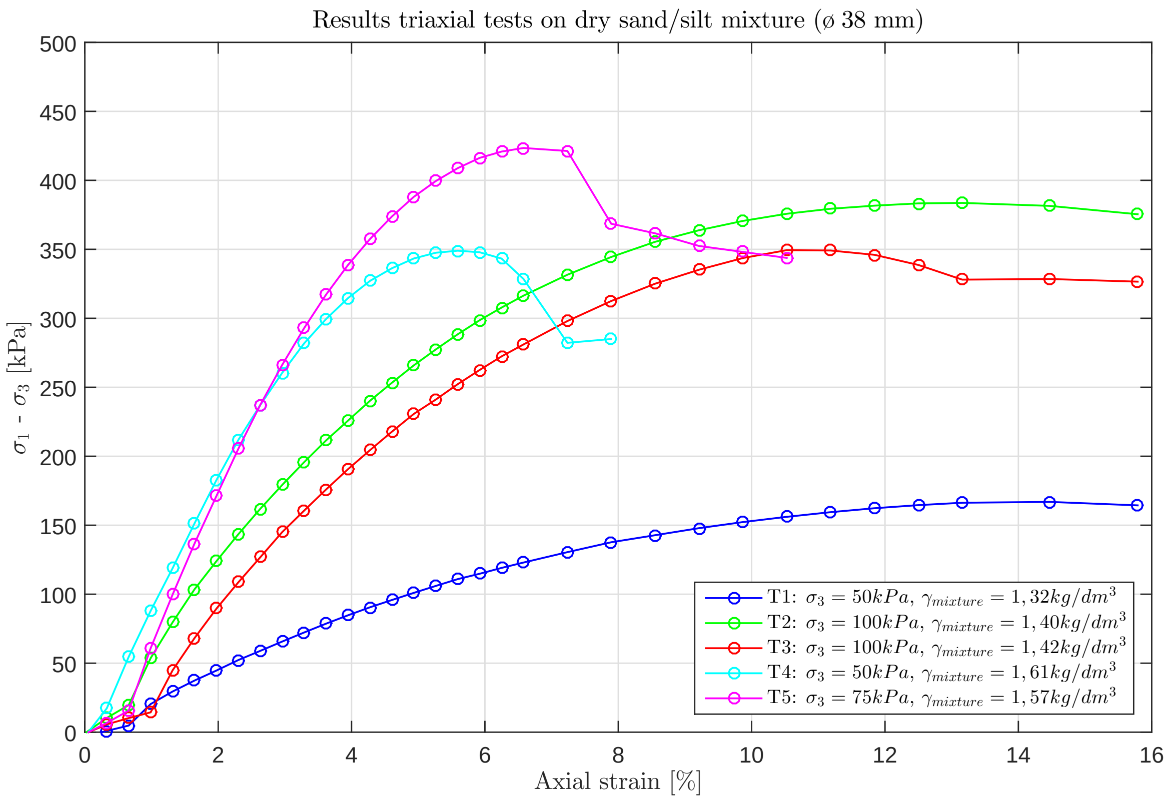

Figure E.1: Results triaxial tests on dry sand/silt mixture for different densities and cell pressures